Abstract

The vast eastern-Tethyan oceanic domain that throughout the Mesozoic extended between Gondwana and Eurasia was a puzzle of larger and smaller microcontinents separated by larger and smaller oceans, the paleogeographic reconstruction of which poses major challenging problems. This review article summarizes the available stratigraphic, sedimentological, petrological, geochronological, geochemical, tectonic, and paleomagnetic evidence on the Bangong-Nujiang suture zone and adjacent geological domains now at the heart of the Tibetan Plateau, with the final aim to reconstruct the history of the Bangong-Nujiang Ocean from its birth to its growth and final demise. The vivid debate on these highly controversial geological issues touches on several key problems in plate tectonics, including the birth of an ocean, the nature of microcontinents and seamounts, the initiation of oceanic subduction, the implications of subduction polarity, and the timing of continental collision. Rifting between South Qiangtang and the Lhasa blocks took place in the Early to Middle Permian. The Bangong-Nujiang Ocean was still narrow in the Late Permian. The Triassic saw the rapid northward drift of South Qiangtang and active sea-floor-spreading in the Bangong-Nujiang Ocean, which reached a maximum north–south width of ~4000 km in about 50 million years. In the Early Jurassic (~190-180 Ma), Bangong-Nujiang oceanic lithosphere began to subduct northward. After some 30-40 million years of oceanic subduction, documented by arc magmatism and high-pressure metamorphic rocks, the Bangong-Nujiang Ocean closed its northern branch (the Dongqiao-Amdo ocean) in the latest Middle Jurassic (166-163 Ma), when the Amdo and Dongkacuo microcontinents collided with South Qiangtang. The southern oceanic branch (the Beila-Nagqu ocean) closed in the latest Jurassic (150-145 Ma) at the onset of collision between the Lhasa and Qiangtang blocks. Early Cretaceous (140-120 Ma) syncollisional arc-type magmatism was widely distributed in the Lhasa-Qiangtang collisional zone. At earliest Late Cretaceous times, the complete demise of seaways and the transition to widespread deposition of continental red beds along the Bangong-Nujiang suture zone marked the onset of intracontinental convergence leading to initial uplift of the Tibetan Plateau.

Figures 1-13 and Table 1

Click here to access/download;Figure;Revised Figs and table in one.pdf

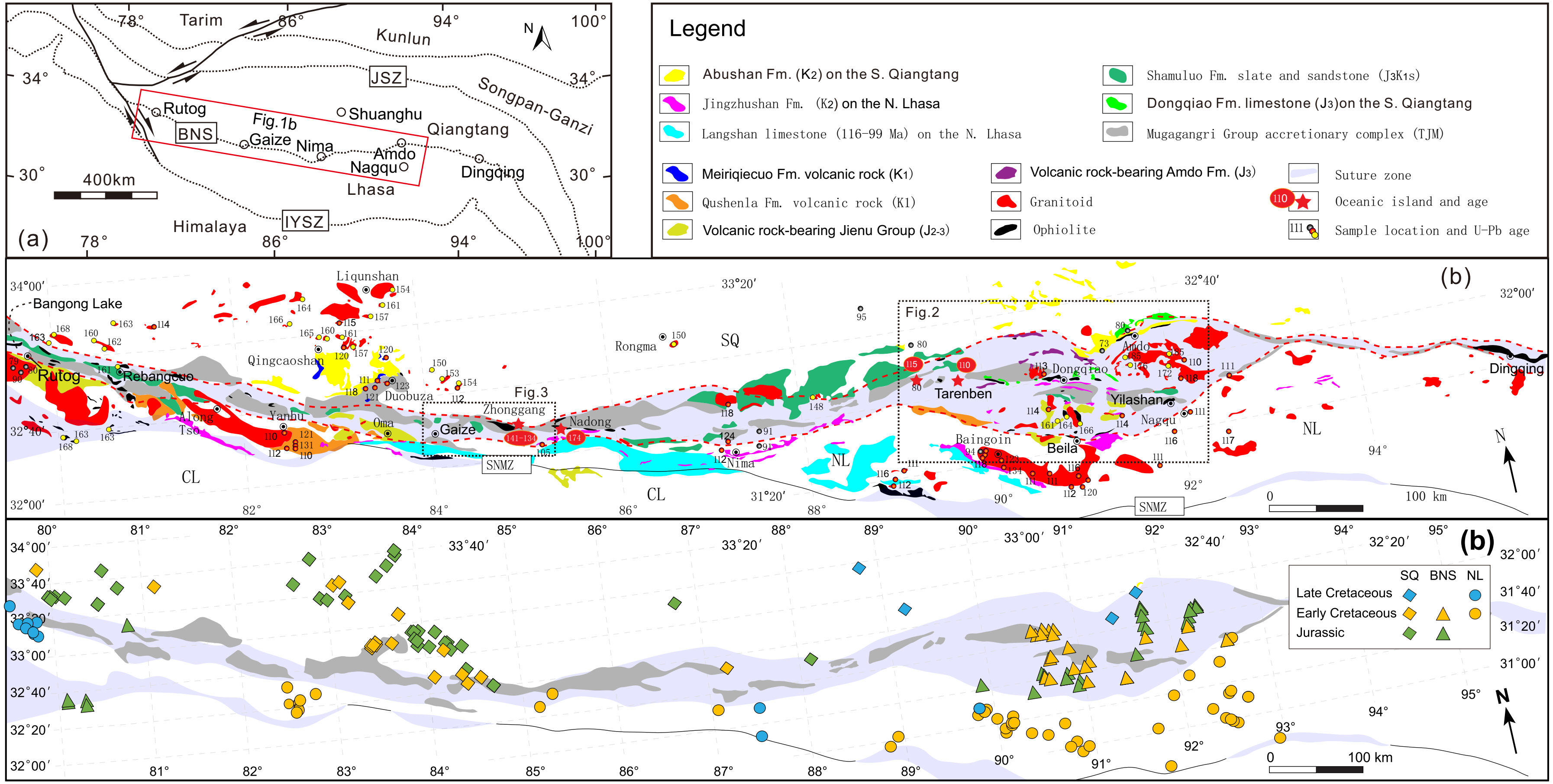

Fig. 1

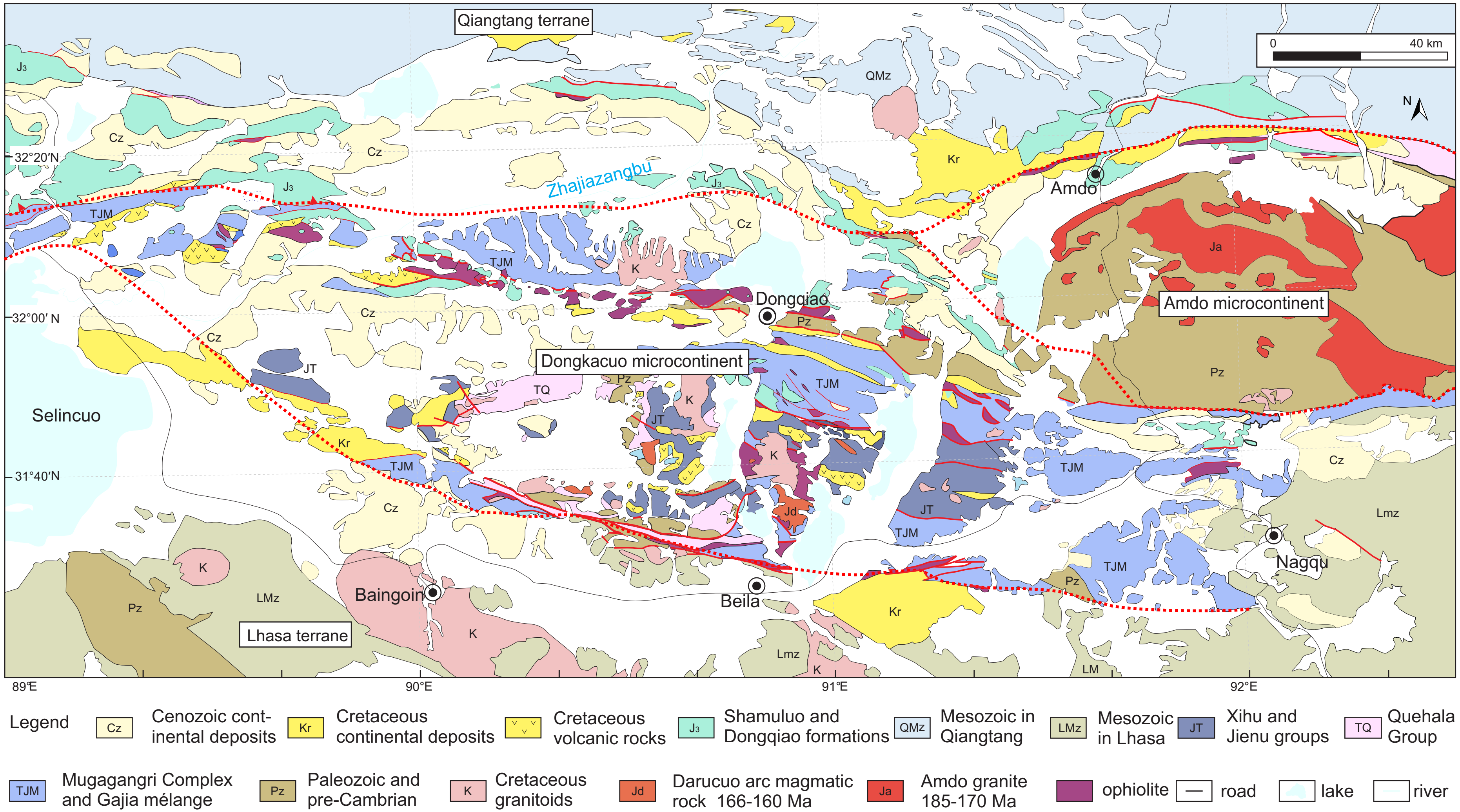
Qiangtang terrane
0
40 km
N
QMz
Kr
J3
Cz
32°20′N
Zhajiazangbu
Amdo
TJM
Ja
K
Dongqiao
Pz
Amdo microcontinent
32°00′ N
JT
Dongkacuo microcontinent
TQ
Selincuo
31°40′N
Jd
Lmz
LMz
Nagqu
Baingoin
Beila
Lhasa terrane
LM
89°E
90°E
91°E
92°E
Legend
Cz Cenozoic continental deposits
Kr Cretaceous continental deposits
Cretaceous volcanic rocks
J3 Shamuluo and Dongqiao formations
QMz Mesozoic in Qiangtang
LMz Mesozoic in Lhasa
JT Xihu and Jienu groups
TQ Quehala Group
TJM Mugagangri Complex and Gajia mélange
Pz Paleozoic and pre-Cambrian
K Cretaceous granitoids
Jd Darucuo arc magmatic rock 166-160 Ma
Ja Amdo granite 185-170 Ma
ophiolite
road
lake
river

Fig. 2

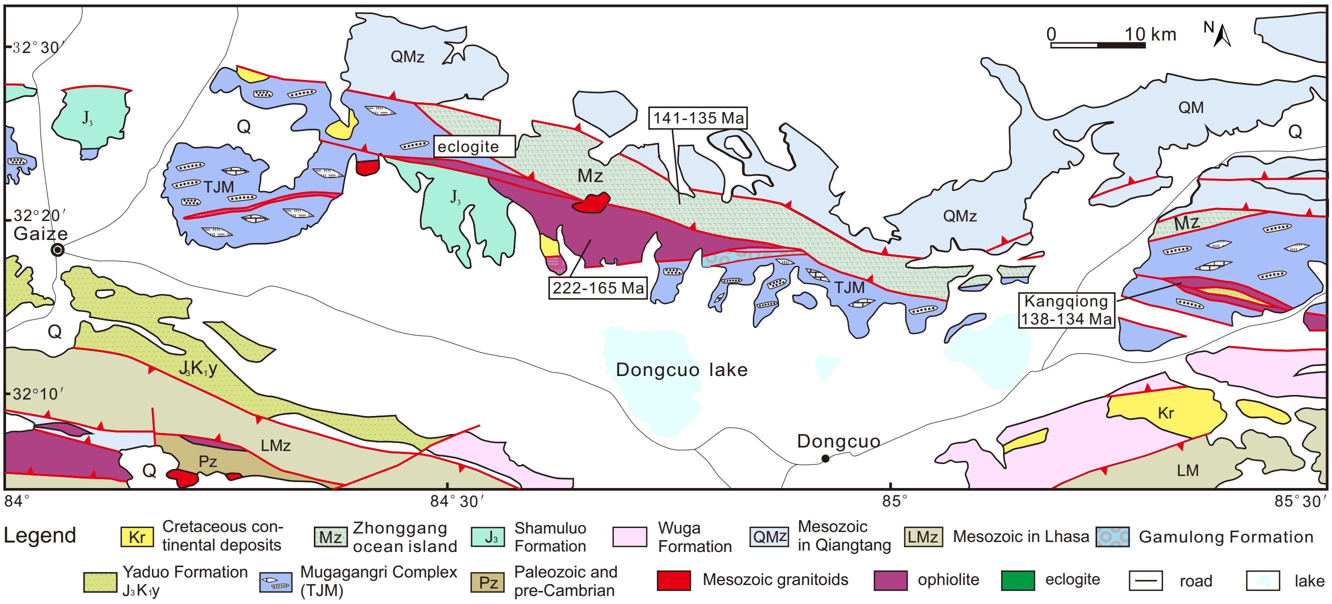

32°30′
32°20′
32°10′
84°
84°30′
85°
85°30′
0
10 km
N
Gaize
QMz
Q
J3
TJM
eclogite
141-135 Ma
Mz
222-165 Ma
QM
Kangqiong
138-134 Ma
Dongcuo lake
Dongcuo
J3K1y
LMz
Pz
Kr
LM
Legend
Kr Cretaceous continental deposits
Mz Zhonggang ocean island
J3 Shamuluo Formation
Wuga Formation
QMz Mesozoic in Qiangtang
LMz Mesozoic in Lhasa
Gamulong Formation
Yaduo Formation J3K1y
Mugagangri Complex (TJM)
Pz Paleozoic and pre-Cambrian
Mesozoic granitoids
ophiolite
eclogite
road
lake

Fig. 3

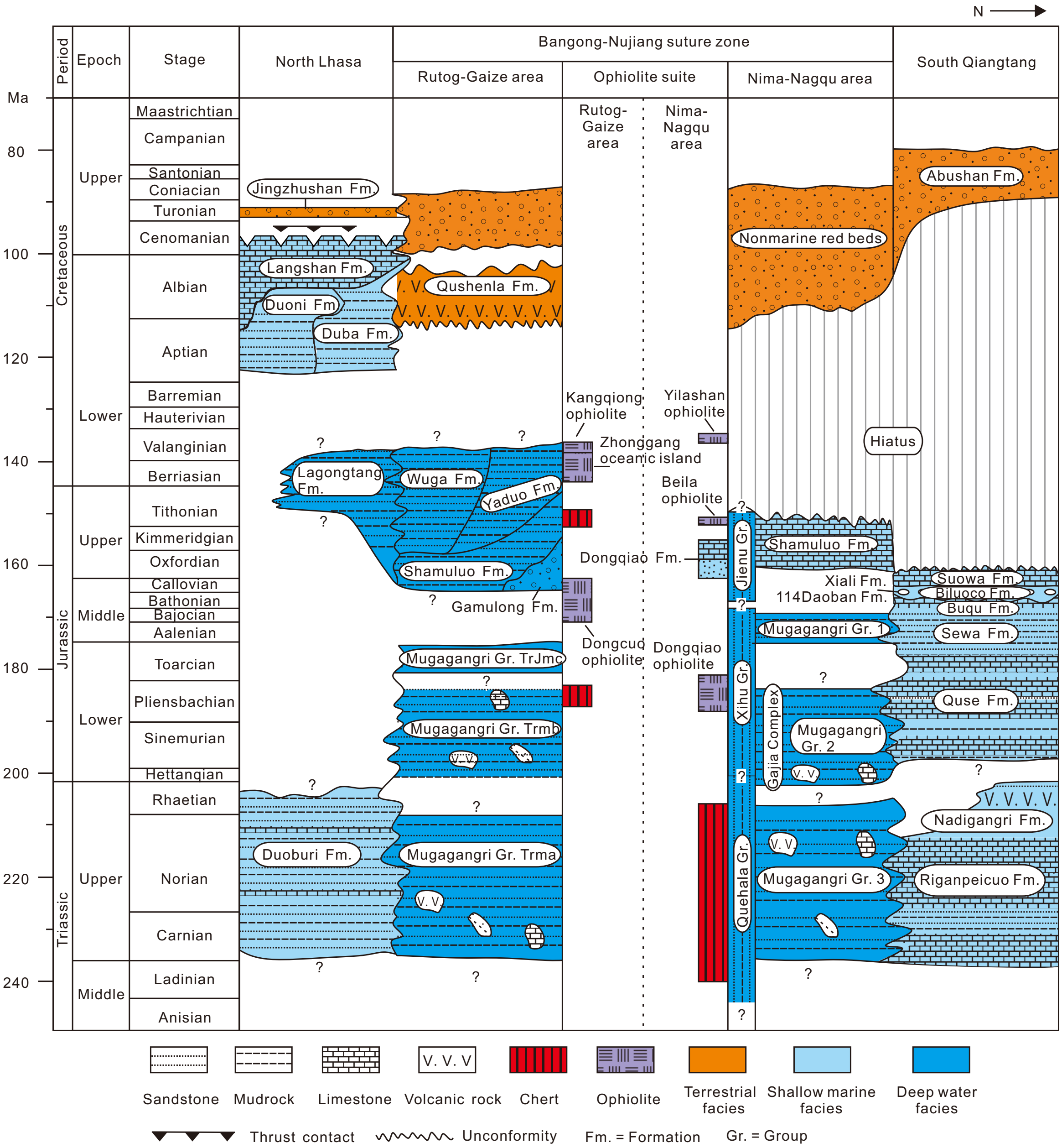
N
Period
Epoch
Stage
North Lhasa
Bangong-Nujiang suture zone
Rutog-Gaize area
Ophiolite suite
Nima-Nagqu area
South Qiangtang
Ma
80
100
120
140
160
180
200
220
240
Cretaceous
Jurassic
Triassic
Upper
Lower
Middle
Maastrichtian
Campanian
Santonian
Coniacian
Turonian
Cenomanian
Albian
Aptian
Barremian
Hauterivian
Valanginian
Berriasian
Tithonian
Kimmeridgian
Oxfordian
Callovian
Bathonian
Bajocian
Aalenian
Toarcian
Pliensbachian
Sinemurian
Hettangian
Rhaetian
Norian
Carnian
Ladinian
Anisian
Rutog-Gaize area
Nima-Nagqu area
Jingzhushan Fm.
Abushan Fm.
Nonmarine red beds
Langshan Fm.
Qushenla Fm.
Duoni Fm.
Duba Fm.
Kangqiong ophiolite
Yilashan ophiolite
Zhonggang oceanic island
Hiatus
Lagongtang Fm.
Wuga Fm.
Yaduo Fm.
Beila ophiolite
Shamuluo Fm.
Dongqiao Fm.
Jienu Gr.
Xiali Fm.
114Daoban Fm.
Suowa Fm.
Biluoco Fm.
Buqu Fm.
Gamulong Fm.
Mugagangri Gr. 1
Sewa Fm.
Dongcuo ophiolite
Dongqiao ophiolite
Mugagangri Gr. TrJmc
Xihu Gr.
Quse Fm.
Mugagangri Gr. Trmb
Gajia Complex
Mugagangri Gr. 2
Nadigangri Fm.
Duoburi Fm.
Mugagangri Gr. Trma
Quehala Gr.
Mugagangri Gr. 3
Riganpeicuo Fm.
V. V
Sandstone
Mudrock
Limestone
Volcanic rock
Chert
Ophiolite
Terrestrial facies
Shallow marine facies
Deep water facies
Thrust contact
Unconformity
Fm. = Formation
Gr. = Group

Fig. 4

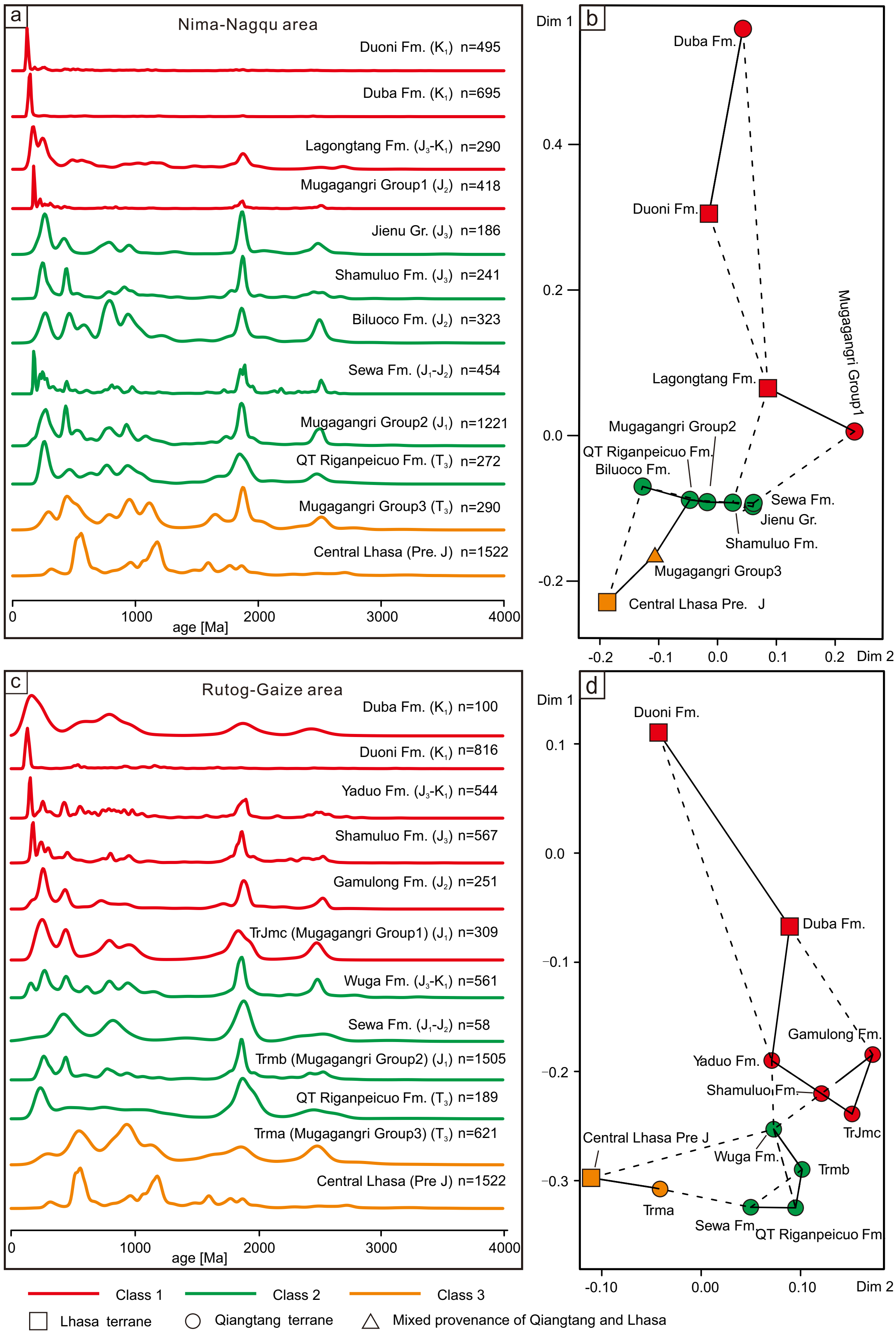
a
Nima-Nagqu area
Duoni Fm. (K1) n=495
Duba Fm. (K1) n=695
Lagongtang Fm. (J3-K1) n=290
Mugagangri Group1 (J2) n=418
Jienu Gr. (J3) n=186
Shamuluo Fm. (J3) n=241
Biluoco Fm. (J2) n=323
Sewa Fm. (J1-J2) n=454
Mugagangri Group2 (J1) n=1221
QT Riganpeicuo Fm. (T3) n=272
Mugagangri Group3 (T3) n=290
Central Lhasa (Pre. J) n=1522
0
1000
2000
3000
4000
age [Ma]
b
Dim 1
0.4
0.2
0.0
-0.2
-0.2
-0.1
0.0
0.1
0.2
Dim 2
Duba Fm.
Duoni Fm.
Lagongtang Fm.
Mugagangri Group1
Mugagangri Group2
QT Riganpeicuo Fm.
Biluoco Fm.
Sewa Fm.
Jienu Gr.
Shamuluo Fm.
Mugagangri Group3
Central Lhasa Pre. J
c
Rutog-Gaize area
Duba Fm. (K1) n=100
Duoni Fm. (K1) n=816
Yaduo Fm. (J3-K1) n=544
Shamuluo Fm. (J3) n=567
Gamulong Fm. (J2) n=251
TrJmc (Mugagangri Group1) (J1) n=309
Wuga Fm. (J3-K1) n=561
Sewa Fm. (J1-J2) n=58
Trmb (Mugagangri Group2) (J1) n=1505
QT Riganpeicuo Fm. (T3) n=189
Trma (Mugagangri Group3) (T3) n=621
Central Lhasa (Pre J) n=1522
0
1000
2000
3000
4000
age [Ma]
d
Dim 1
0.1
0.0
−0.1
−0.2
−0.3
-0.10
0.00
0.10
Dim 2
Duoni Fm.
Duba Fm.
Gamulong Fm.
Yaduo Fm.
Shamuluo Fm.
TrJmc
Central Lhasa Pre J
Wuga Fm.
Trmb
Trma
Sewa Fm
QT Riganpeicuo Fm
Class 1
Class 2
Class 3
Lhasa terrane
Qiangtang terrane
Mixed provenance of Qiangtang and Lhasa

Fig.5

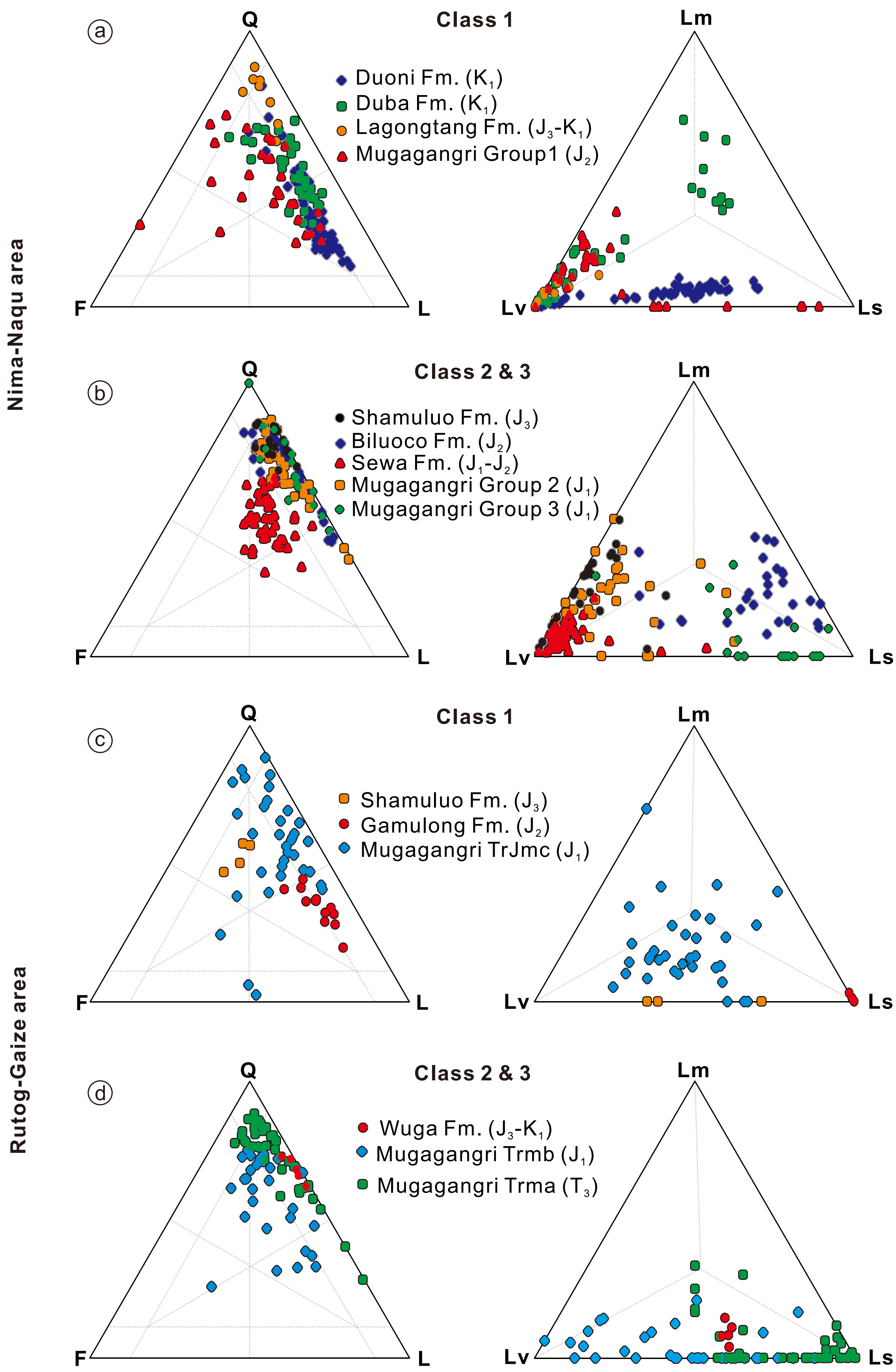

Nima-Naqu area
Rutog-Gaize area
a
Class 1
Q
F
L
Lm
Lv
Ls
Duoni Fm. (K1)
Duba Fm. (K1)
Lagongtang Fm. (J3-K1)
Mugagangri Group1 (J2)
b
Class 2 & 3
Shamuluo Fm. (J3)
Biluoco Fm. (J2)
Sewa Fm. (J1-J2)
Mugagangri Group 2 (J1)
Mugagangri Group 3 (J1)
c
Class 1
Shamuluo Fm. (J3)
Gamulong Fm. (J2)
Mugagangri TrJmc (J1)
d
Class 2 & 3
Wuga Fm. (J3-K1)
Mugagangri Trmb (J1)
Mugagangri Trma (T3)

Fig. 6

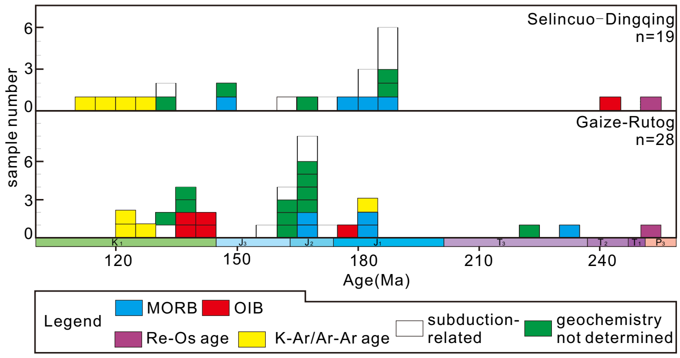
Selincuo–Dingqing
n=19
Gaize-Rutog
n=28
sample number
Age(Ma)
Legend
MORB
OIB
Re-Os age
K-Ar/Ar-Ar age
subduction-related
geochemistry not determined

Fig. 7

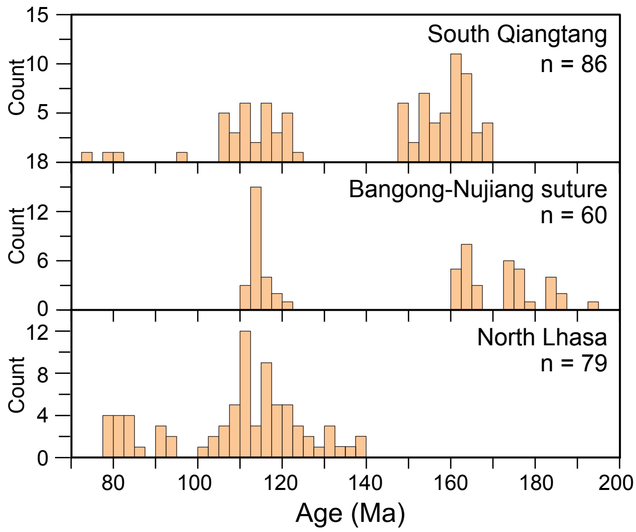
South Qiangtang
n = 86
Bangong-Nujiang suture
n = 60
North Lhasa
n = 79
Count
Count
Count
15
10
5
18
12
6
0
12
8
4
0
80
100
120
140
160
180
200
Age (Ma)

Fig. 8

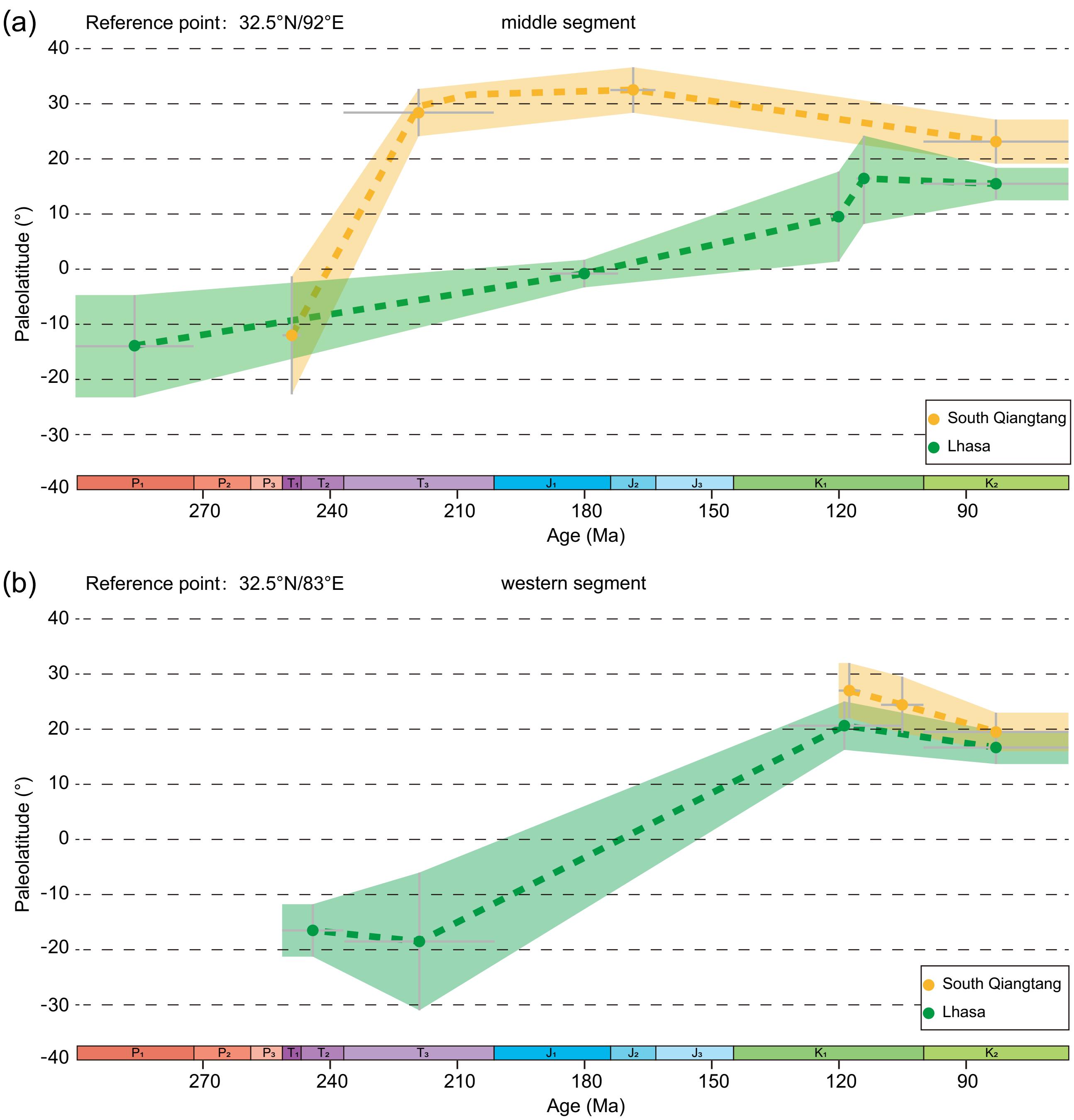
(a)
Reference point: 32.5°N/92°E
middle segment
Paleolatitude (°)
40
30
20
10
0
-10
-20
-30
-40
South Qiangtang
Lhasa
P₁ P₂ P₃ T₁ T₂ T₃ J₁ J₂ J₃ K₁ K₂
270
240
210
180
150
120
90
Age (Ma)
(b)
Reference point: 32.5°N/83°E
western segment
Paleolatitude (°)
40
30
20
10
0
-10
-20
-30
-40
South Qiangtang
Lhasa
P₁ P₂ P₃ T₁ T₂ T₃ J₁ J₂ J₃ K₁ K₂
270
240
210
180
150
120
90
Age (Ma)

Fig. 9

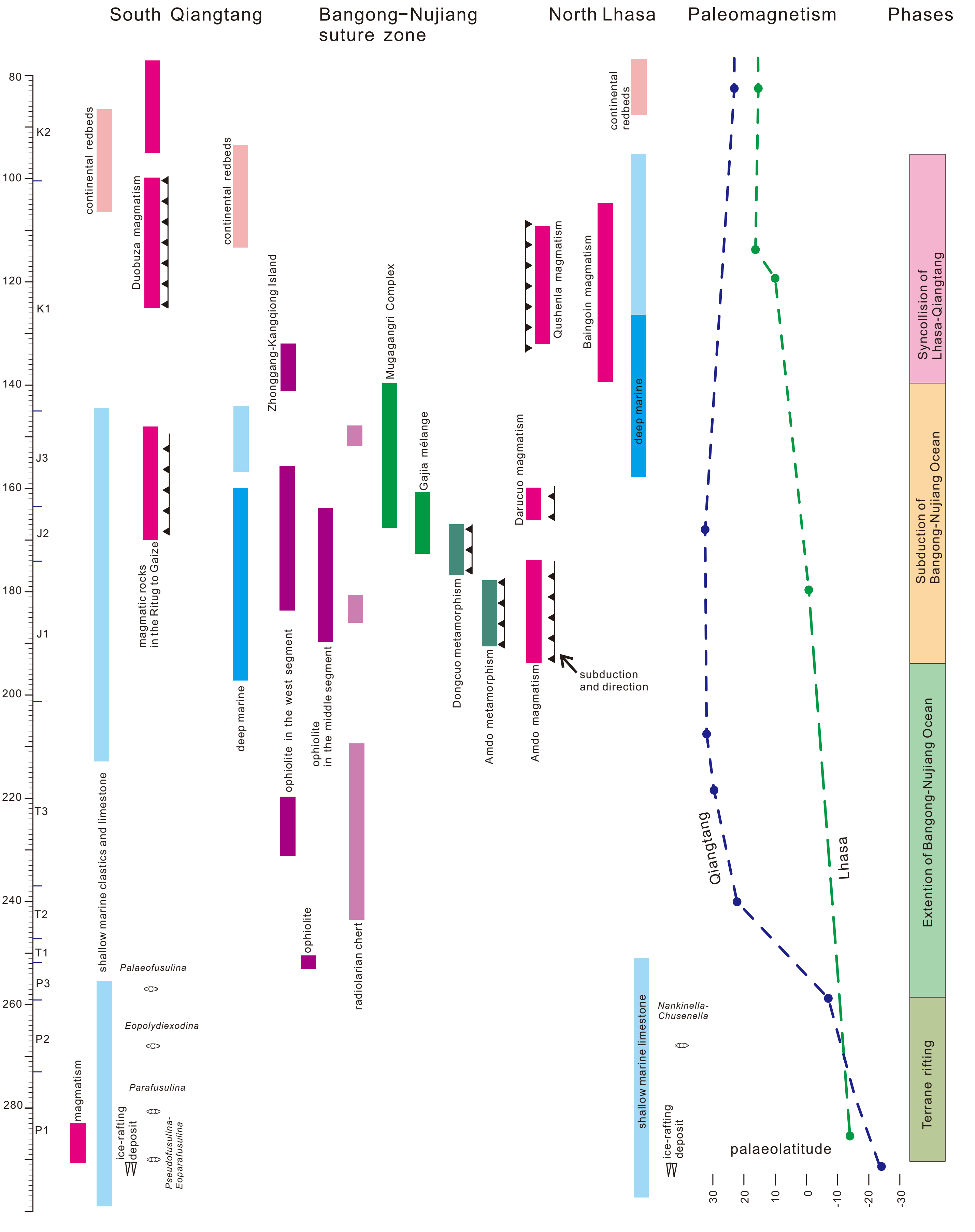

South Qiangtang
Bangong-Nujiang suture zone
North Lhasa
Paleomagnetism
Phases
K2
K1
J3
J2
J1
T3
T2
T1
P3
P2
P1
continental redbeds
Duobuza magmatism
magmatic rocks in the Ritug to Gaize
shallow marine clastics and limestone
magmatism
ice-rafting deposit
Palaeofusulina
Eopolydiexodina
Parafusulina
Pseudofusulina-Eoparafusulina
deep marine
Zhonggang-Kangqiong Island
ophiolite in the west segment
ophiolite in the middle segment
ophiolite
radiolarian chert
Mugagangri Complex
Gajia mélange
Dongcuo metamorphism
Amdo metamorphism
Amdo magmatism
Darucuo magmatism
Qushenla magmatism
Baingoin magmatism
subduction and direction
shallow marine limestone
Nankinella-Chusenella
Qiangtang
Lhasa
palaeolatitude
Syncollision of Lhasa-Qiangtang
Subduction of Bangong-Nujiang Ocean
Extention of Bangong-Nujiang Ocean
Terrane rifting

Fig. 10

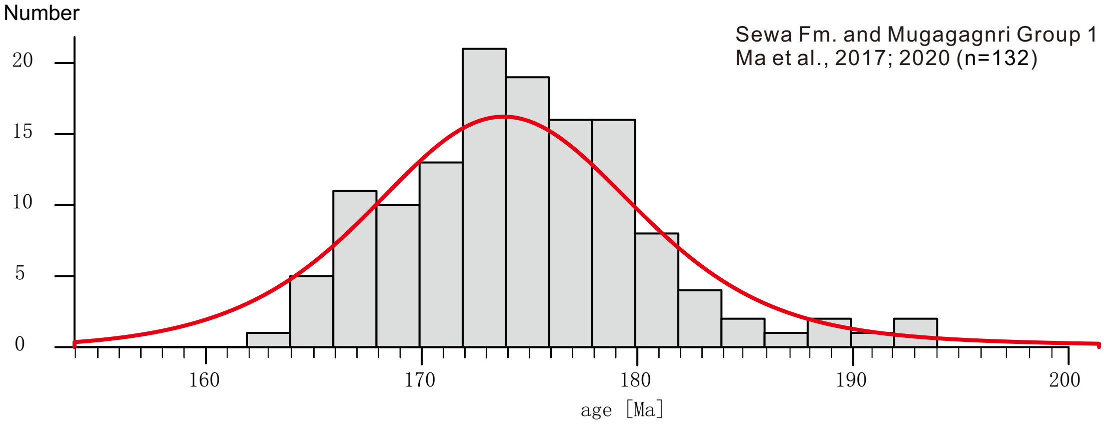
Number
Sewa Fm. and Mugagagnri Group 1
Ma et al., 2017; 2020 (n=132)
20
15
10
5
0
160
170
180
190
200
age [Ma]

Fig. 11

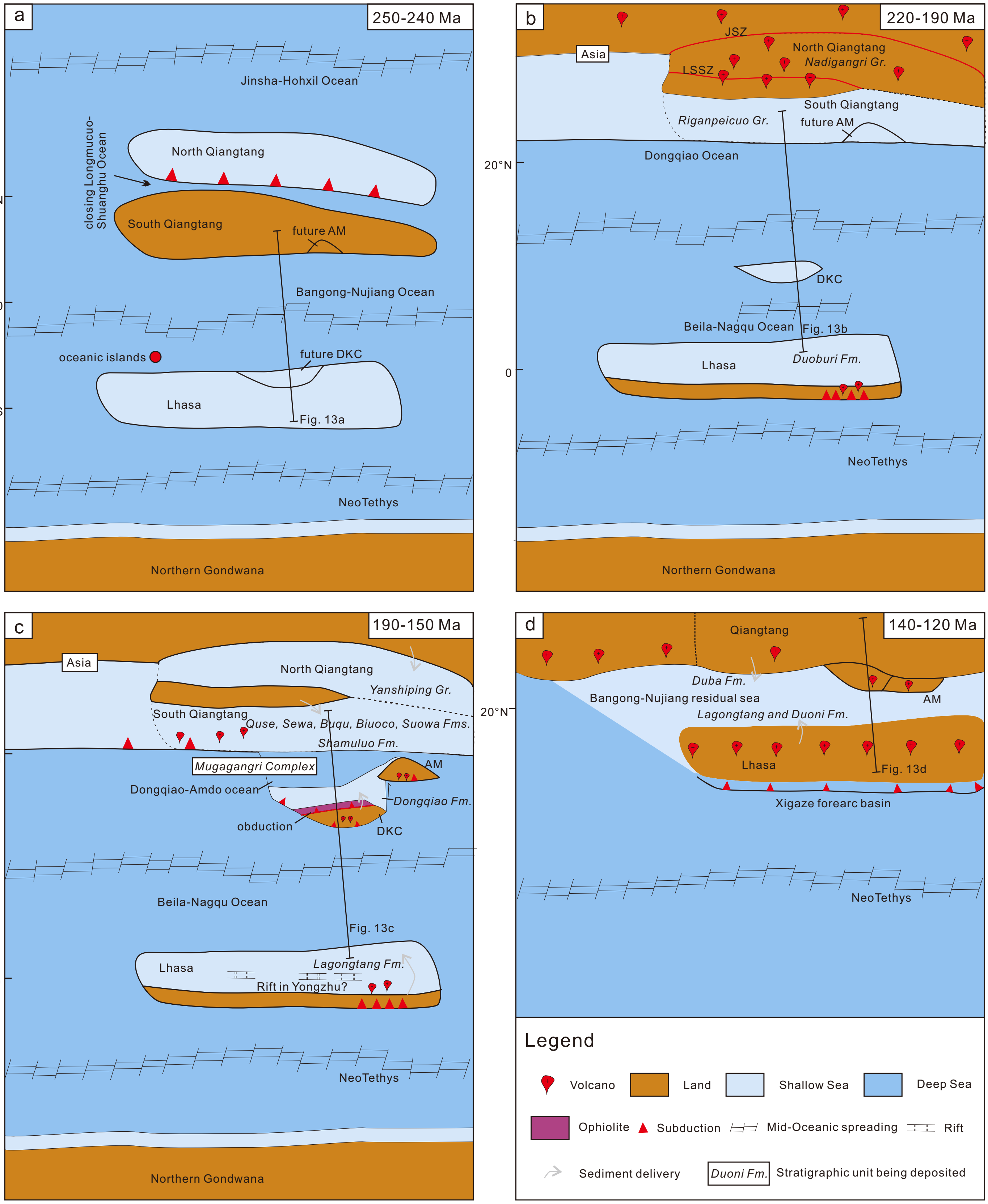

a
250-240 Ma
Jinsha-Hohxil Ocean
closing Longmucuo-Shuanghu Ocean
North Qiangtang
20°N
South Qiangtang
future AM
Bangong-Nujiang Ocean
0
oceanic islands
future DKC
Lhasa
20°S
Fig. 13a
NeoTethys
Northern Gondwana
b
220-190 Ma
Asia
JSZ
North Qiangtang
Nadigangri Gr.
LSSZ
South Qiangtang
Riganpeicuo Gr.
future AM
20°N
Dongqiao Ocean
DKC
Beila-Nagqu Ocean
Fig. 13b
0
Lhasa
Duoburi Fm.
NeoTethys
Northern Gondwana
c
190-150 Ma
Asia
North Qiangtang
Yanshiping Gr.
South Qiangtang
Quse, Sewa, Buqu, Biuoco, Suowa Fms.
Shamuluo Fm.
20°N
Mugagangri Complex
AM
Dongqiao-Amdo ocean
Dongqiao Fm.
obduction
DKC
Beila-Nagqu Ocean
Fig. 13c
0
Lhasa
Lagongtang Fm.
Rift in Yongzhu?
NeoTethys
Northern Gondwana
d
140-120 Ma
Qiangtang
Duba Fm.
Bangong-Nujiang residual sea
AM
20°N
Lagongtang and Duoni Fm.
Lhasa
Fig. 13d
Xigaze forearc basin
NeoTethys
Legend
Volcano
Land
Shallow Sea
Deep Sea
Ophiolite
Subduction
Mid-Oceanic spreading
Rift
Sediment delivery
Duoni Fm.
Stratigraphic unit being deposited

Fig. 12

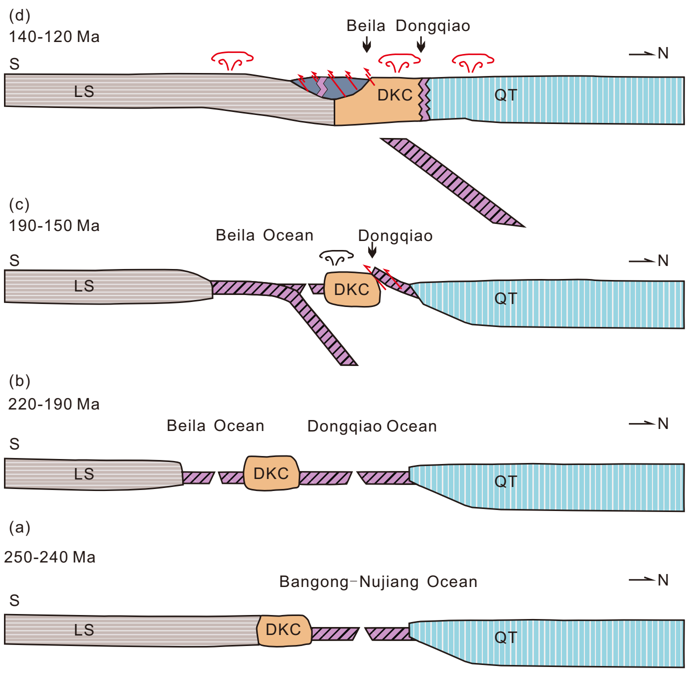

(d)
140-120 Ma
Beila Dongqiao
S
N
LS
DKC
QT
(c)
190-150 Ma
Beila Ocean
Dongqiao
S
N
LS
DKC
QT
(b)
220-190 Ma
Beila Ocean
Dongqiao Ocean
S
N
LS
DKC
QT
(a)
250-240 Ma
Bangong–Nujiang Ocean
S
N
LS
DKC
QT

Fig. 13

Table 1 Provenance samples and associated data information in the Bangong-Nujiang suture zone, North Lhasa, South Qiangtang.

Area	Lithostratigraphic unit	Point-counting samples	Analysis spots of detrital zircons	YC1σ (2+)	References
Selincuo-Amdo	Duoni Fm.	77	495	108 ± 1.2 (n=8)	Lai et al., 2019b; Zhu et al., 2019; Chen et al., 2020
	Duba Fm.	13	695	116.2 ± 0.8 (n=5)	Leier et al., 2007; Zhang et al., 2011; Lai et al., 2019b
	Lagongtang Fm.	8	290	136.3 ± 1.1 (n=3)	Lai et al., 2022
	Mugagangri Group 1	28	418	166.3 ± 0.4 (n=18)	Ma et al., 2017; Ma et al., 2020
	Jienu Gr.	/	186	169.5 ± 0.7 (n=2)	S Li et al., 2020
	Shamuluo Fm.	24	241	/	Ma et al., 2018；C Li et al., 2020
	Biluoco Fm.	29	323	211 ± 1.5 (n=4)	Ma et al., 2017
	Sewa Fm.	44	454	172.7 ± 0.7 (n=17)	Ma et al., 2017;
	Mugagangri Group 2	30	1012	204.5 ± 1.2 (n=4)	C Li et al., 2020; S M Li et al., 2020; Ma et al., 2020
	QT Riganpeicuo Fm.	/	272	224.1 ± 2.4 (n=2)	Ma et al., 2017; Wang et al., 2016; Gehrels et al., 2011
	Mugagangri Group 3	18	290	246 ± 2.8 (n=2)	Ma et al., 2017, 2020; C Li et al., 2020; C W Li et al., 2021
Gaize-Dongcuo	Duba Fm.	/	100	115.9 ± 3.3 (n=4)	Luo et al., 2020
	Duoni Fm.	/	816	106 ± 1.1 (n=13)	C Li et al., 2020; Sun et al., 2017
	Yaduo Fm.	7	544	144.1 ± 1.4 (n=8)	Huang et al., 2017; Luo et al., 2019；Luo et al., 2020
	Shamuluo Fm.	4	567	160 ± 1.3 (n=3)	S Li et al., 2017; Huang et al., 2017
	Gamulong Fm.	13	251	165 ± 1.7 (n=3)	Sun et al., 2019
	TrJmc - Mugagangri	34	309	190.7 ± 0.8 (n=10)	S Li et al., 2017; C W Li et al., 2021
	Wuga Fm.	5	561	147.7 ± 0.6 (n=4)	S Li et al., 2017
	Sewa Fm.	/	58	/	Huang et al., 2017
	Trmb - Mugagangri	33	1505	208 ± 1.2 (n=3)	C W Li et al., 2021
	QT Riganpeicuo Fm.	2	189	201.4 ± 3.1 (n=2)	Gehrels et al., 2011
	Trma - Mugagangri	40	621	219.8 ± 1.0 (n=2)	C W Li et al., 2021; S Li et al., 2017
Central Lhasa Pre. J		/	1522	/	Leier et al., 2007; G Li et al., 2014; Gehrels et al., 2011; Zhu, 2011

Declaration of Competing Interest

The authors declare that they have no known competing financial interests or personal relationships that could have appeared to influence the work reported in this paper.

2022-4-12 Revised version for Earth-Science Reviews

Exploring a lost ocean in the Tibetan Plateau: Birth, growth, and demise of the Bangong-Nujiang Ocean

Xiumian Hu [a*], Anlin Ma [a], Weiwei Xue [a], Eduardo Garzanti [b], Yong Cao [c], Shi-Min Li [d], Gaoyuan Sun [e], Wen Lai [f]

a. State Key Laboratory of Mineral Deposits Research, Institute of Continental Geodynamics, School of Earth Sciences and Engineering, Nanjing University, Nanjing 210023, China

b. Department of Earth and Environmental Sciences, Università di Milano-Bicocca, Milano 20126, Italy

c. Key Laboratory of Paleomagnetism and Tectonic Reconstruction of Ministry of Natural Resources, Institute of Geomechanics, Chinese Academy of Geological Sciences, Beijing, China

d. State Key Laboratory of Geological Processes and Mineral Resources, and School of Earth Science and Resources, China University of Geosciences, Beijing, China,

e. College of Oceanography, Hohai University, Nanjing 210098, China

f. School of Geography and Ocean Science, Nanjing University, Nanjing 210023, China

* Corresponding author: Xiumian Hu (huxm@nju.edu.cn)

Highlights

• Critical review of geological data related to the Bangong-Nujiang Ocean from its birth to its growth and demise.

• Bangong-Nujiang Ocean opened in the Early Permian and started to subduct northward in the Early Jurassic (~190-180 Ma).

• Dongqiao-Amdo and Beila-Nagqu oceans closed in the Middle Jurassic (166-163 Ma) and latest Jurassic (150-145 Ma), respectively.

Abstract

The vast eastern-Tethyan oceanic domain that throughout the Mesozoic extended between Gondwana and Eurasia was a puzzle of larger and smaller microcontinents separated by larger and smaller oceans, the paleogeographic reconstruction of which poses major challenging problems. This review article summarizes the available stratigraphic, sedimentological, petrological, geochronological, geochemical, tectonic, and paleomagnetic evidence on the Bangong-Nujiang suture zone and adjacent geological domains now at the heart of the Tibetan Plateau, with the final aim to reconstruct the history of the Bangong-Nujiang Ocean from its birth to its growth and final demise. The vivid debate on these highly controversial geological issues touches on several key problems in plate tectonics, including the birth of an ocean, the nature of microcontinents and seamounts, the initiation of oceanic subduction, the implications of subduction polarity, and the timing of continental collision. Rifting between South Qiangtang and the Lhasa blocks took place in the Early to Middle Permian. The Bangong-Nujiang Ocean was still narrow in the Late Permian. The Triassic saw the rapid northward drift of South Qiangtang and active sea-floor-spreading in the Bangong-Nujiang Ocean, which reached a maximum north–south width of ~4000 km in about 50 million years. In the Early Jurassic (~190-180 Ma), Bangong-Nujiang oceanic lithosphere began to subduct northward. After some 30-40 million years of oceanic subduction, documented by arc magmatism and high-pressure metamorphic rocks, the Bangong-Nujiang Ocean closed its northern branch (the Dongqiao-Amdo ocean) in the latest Middle Jurassic (166-163 Ma), when the Amdo and Dongkacuo microcontinents collided with South Qiangtang. The southern oceanic branch (the Beila-Nagqu ocean) closed in the latest Jurassic (150-145 Ma) at the onset of collision between the Lhasa and Qiangtang blocks. Early Cretaceous (140-120 Ma) syncollisional arc-type magmatism was widely distributed in the Lhasa-Qiangtang collisional zone. At earliest Late Cretaceous times, the complete demise of seaways and the transition to widespread deposition of continental red beds along the Bangong-Nujiang suture zone marked the onset of intracontinental convergence leading to initial uplift of the Tibetan Plateau.

Keywords：Tethys Ocean; Bangong-Nujiang Ocean; Lhasa Block; South Qiangtang Block; Mesozoic; Palaeogeography

1. Introduction

The Bangong-Nujiang suture zone (abbreviated as “BNS” throughout the article, Fig. 1) represents a major geological boundary within the Tibetan Plateau, separating the Lhasa Block to the south from the South Qiangtang block to the north and traced from Bangong Lake in the west, across the Gaize, Dongqiao, Nagqu, Dingqing and Baju areas, and finally southeastwards along the Nujiang River (Fig. 1a). The BNS was first considered in the light of modern plate-tectonic theory and identified as a "northward subduction suture" by Chang and Zheng (1973), a view widely accepted in subsequent publications (e.g., Dewey et al., 1988; Yin and Harrison, 2000; Kapp and DeCelles, 2019). Pan et al. (1983) systematically studied the structure and rock assemblage of the BNS consisting of ophiolitic mélange and flysch-type sediments and concluded that the Bangong-Nujiang oceanic lithosphere was subducted southward beneath the Lhasa Block (Zhu et al., 2013). Yu et al. (1991) argued that Jurassic strata in the BNS indicate segmentation, abrupt lithologic changes, rapid filling, short life span and recycling, pointing to deposition in a pull-apart basin, an opinion widely accepted thereafter (e.g., Mattern et al., 1998; Schneider et al., 2003). More recent research on ophiolites and magmatic rocks, coupled with detrital-zircon geochronology and paleomagnetic data, suggest that the BNS was a relic of a wide ocean consumed by northward subduction underneath the South Qiangtang continental margin (Zeng et al., 2016; Li et al., 2019b). Zhu et al. (2016), however, envisaged a transient southward subduction of the Bangong-Nujiang Ocean during the Early Cretaceous and proposed that the Bangong-Nujiang Ocean closed by double-sided subduction. The initiation of sea-floor spreading, subduction polarity, and closure timing of the Bangong-Nujiang Ocean have consequently become crucial issues in geological studies of the Tibetan Plateau.

The many controversies that exist in the study of the BNS depend on its complex geological phenomena (see Li et al., 2019b; Shi et al., 2020; Peng et al., 2020; Jiang et al., 2021 and references therein). Several characteristics are difficult to explain by current geological models: (1) BNS ophiolites do not follow a simple linear pattern but are discontinuously distributed in several lenticular belts, which leads to question whether the BNS is a single suture or contains multiple sutures (Mate et al., 1996; Wang et al., 2020; Tang et al., 2020); (2) tectonic deformation after ophiolite obduction makes it difficult to reconstruct the original geometries and paleogeography of the Bangong-Nujiang Ocean (Girardeau et al., 1984; Kapp et al., 2003); (3) there is a general scarcity of oceanic subduction-related magmatism in both South Qiangtang and North Lhasa blocks (Fig. 1b), whereas extensive syncollisional magmatism occurred in the BNS at 120-110 Ma (including the Baingoin granite and Qushenla volcanic rocks; Zhu et al., 2016; Li et al., 2018); (4) the typical profile of an arc-trench system including a subduction-related accretionary complex was seemingly not well developed in the BNS, although some studies interpreted the Mugagangri Complex as an accretionary prism and the Quse-Sewa-Buqu deposits as a forearc basin (Ma et al., 2017a, b; Li S. et al., 2017b); (5) there are few metamorphic rocks in the BNS, and collision-related molasse-type sediments are not recognized, whereas tectonic mélange is widespread (Zeng et al., 2016; Li et al., 2017b; Ma et al., 2020b); (6) sedimentary successions identifying the continental margins of the collided North Lhasa and South Qiangtang blocks mainly consist of deep-water to shallow-marine strata of Jurassic age (Ma et al., 2017a); (7) numerous porphyry-type ores dated as 120-110 Ma in the Duolong area (Lin et al., 2019; Yang et al., 2020) and orogenic gold deposits dated as 136 Ma in the Shangxu area (Fang et al., 2020) occur in the western part of the BNS, but it is unclear whether they are subduction-related or developed during syncollisional to post-collisional stages, which has major implications for future ore exploration. All these features are quite different from other better studied suture zones, such as the Yarlung-Zangbo suture between Tibet and India in the south, which explains why the evolution of the BNS remains so controversial.

This review article defines the boundaries and summarizes the structure and main characteristics of sedimentary, ophiolitic, magmatic and metamorphic rocks contained in the BNS, and presents a compilation and re-analysis of stratigraphic, petrological, paleobiogeographic, and paleomagnetic data. Based on such a wide range of observations, the hotly debated paleogeographic and paleogeodynamic issues concerning the opening and closure of the Bangong-Nujiang Ocean, the nature of microcontinents and seamounts, and the initiation and polarity of subduction are thoroughly reviewed and discussed. A comprehensive working model for the evolution of the Bangong-Nujiang Ocean will be finally proposed.

2. Boundaries of the Bangong-Nujiang suture zone

Any geologist who visits the Nima-Dongqiao-Amdo-Nagqu area (Fig. 2) may feel confused: where is the boundary of the BNS? The BNS does not appear as the Yarlung-Zangbo suture zone in the south, the orientation and boundaries of which are clearly outlined by the linear distribution of ophiolites, ophiolitic mélange, forearc basin, and continental arc (Hu et al., 2016). The BNS, instead, is only roughly defined by the irregular spatial distribution of ophiolites and siliciclastic mélange (Mugagangri Complex).

The northern boundary of the BNS could thus be traced along the northern boundary of the ophiolites and Mugagangri Complex, which corresponds to the fault contacts between Jurassic strata of South Qiangtang with the ophiolite in the Amdo and Dongqiao-Gaize areas, and with the Mugagangri Complex in the Dongqiao-Nima area (Fig. 2, Fig. 3). In areas where ophiolites are not exposed (e.g., near Nima County), the suture zone could be traced based on the distribution of the Mugagangri Complex.

The southern boundary of the BNS is disputed. Some researchers consider it as corresponding to the Shiquanhe-Namucuo ophiolite belt (Zhang et al., 2014a; Li et al., 2019; Tang et al., 2020), whereas others envisage the Shiquanhe-Yongzhu-Namucuo ophiolite as representing an oceanic basin distinct from the Bangong-Nujiang Ocean to the north (Matte et al., 1996; Zeng et al., 2018; Wang et al., 2020). According to the latter view, we consider the Shiquanhe-Yongzhu-Namucuo suture zone as representing a separate embryonic seaway formed in the early stage of continental rifting (Zeng et al., 2018). Supporting evidence includes: (1) the Shiquanhe-Namucuo ophiolitic complex is Middle-Late Jurassic in age (178~147 Ma; Zeng et al., 2018; Wang et al., 2020; Tang et al., 2020), which is younger than the age of the Bangong-Nujiang ophiolites; (2) the Upper Jurassic shallow-water carbonates of the Rila Formation developed along both sides of the Yongzhu ophiolites (Qu et al., 2013) and the Suor suite of siliciclastic rocks stratigraphically overlying the Yongzhu ophiolites indicate that they were generated in the Late Jurassic; (3) no large southward thrust displacement and nappe structure is observed between the two suture zones (Zeng et al., 2018). This considered, we trace the southern boundary of the BNS along the southern boundary of the Mugagangri Complex and ophiolite outcrops (Fig. 1a, Fig. 2). In the Nagqu-Beila-Selincuo area (Fig. 2), the BNS also includes the Amdo and Dongkacuo microcontinents, thus reaching a maximum width of ~100 km. The oceanic branches to the north and to the south of the Amdo-Dongkacuo microcontinents were named “Dongqiao-Amdo” and “Beila-Nagqu” oceans, respectively.

In this article, we informally divided the Bangong-Nujiang suture zone into three segments: the western Rutog-Gaize segment, the central Nima-Nagqu segment, and the eastern Dingqing-Qamdo segment. Geological data will be compiled only for the western and central segments of the Bangong-Nujiang suture zone.

3. Stratigraphy of the Bangong-Nujiang suture zone and adjacent areas

3.1 Stratigraphy of the Bangong-Nujiang suture zone

In the Nima-Nagqu area, the BNS consists of numerous mappable geological units of diverse origin, including Paleozoic strata, ophiolites, Triassic (?) strata (Quehala Group), Mugagangri Complex and deep-water Jurassic sediments (Jienu and Xihu groups), Jurassic volcanic rocks, Upper Jurassic Shamuluo Formation, Lower Cretaceous volcanic rocks (Qushenla Formation) and continental red beds, Lower Cretaceous granite, the Paleogene Niubao Formation, the late Paleogene-early Neogene Dingqinghu Formation, and Quaternary sediments (Wang et al., 2006; Chen et al., 2002; Li et al., 2019b; Ma et al., 2020b). In the Rutog-Gaize area, the BNS comprises a similar rock assemblage, including an ophiolitic suite (ultramafic rocks, basalt, chert, and seamounts), the Mugagangri Complex, the Upper Jurassic to Lower Cretaceous Shamuluo Formation, the Lower Cretaceous Qushenla Formation volcanic rocks and continental red beds, the Cenozoic Dingqinghu and Niubao formations, and Quaternary sediments (Zeng et al., 2006; Zeng et al., 2016a; Li et al., 2017b, 2019b; Sun et al., 2019; Luo et al., 2019). In addition, the Gamulong and Yaduo formations (Sun et al., 2019 and this study, respectively) are here distinguished from the Mugagangri Complex along its southern boundary. The present article focuses specifically on Mesozoic strata, whereas Cenozoic strata are not relevant to the aims of this study.

(1) Triassic (?) Quehala Group

The Quehala Group, consisting of locally metamorphosed quartzose sandstone, siltstone, and conglomerate in the Dongqiao-Beila area, lies with angular unconformity onto basaltic rocks possibly belonging to an ophiolite sequence and is conformably overlain by the Xihu Group (Chen et al., 2002). During geological mapping at the 1:250,000 scale, the unit was assigned a Late Triassic age based on bivalve assemblages including *Myophoria (Elegantinia)* sp., *Myophoricardium tulongense*, *Prorotrigonia* sp., *Schafhaeutlia* cf. *subastartifomis, Protocardia* cf. *contusa, Yunnanophorus boulei, Pomarangina haydeni* (Chen et al., 2002). In strata assigned to the Quehala Group, however, detrital zircons yielded U–Pb ages as young as 176 Ma west of Selincuo (Wang et al., 2016) and as young as 125 Ma east of Nima County (Kapp et al., 2007), which indicates that strata mapped as Quehala Group in these areas are considerably younger than the Triassic. More extensive regional studies are needed to better define the stratigraphy of the Quehala Group.

（2） Mesozoic Mugagangri Complex

The Mugagangri Complex mainly consists of deep-marine turbidites and siliciclastic mélange (Ma et al., 2020b). Its poorly constrained depositional age may include much of the Jurassic and even a part of the Triassic (Zeng et al., 2016; Huang et al., 2017b; Li et al., 2017b; Li et al., 2020a; Li et al., 2020c) and/or of the Cretaceous (as in Li et al., 2017b). Former studies in the Gaize, Nima, Selincuo, and Dongqiao-Beila areas, show that Mugagangri sandstones were derived from the Qiangtang Block (Zeng et al., 2016; Huang et al., 2017b; Li et al., 2017b, 2020a, 2020c). The Mugagangri Complex was envisaged as deposited in forearc or trench basins associated with the northward subduction of Bangong-Nujiang oceanic lithosphere, but deposition may have occurred along a passive continental margin during the Triassic and in collisional settings only subsequently in the latest Jurassic to Early Cretaceous (Li et al., 2017b; Ma et al., 2020b).

（3） Jurassic/Lower Cretaceous deep-water deposits (Xihu and Jienu groups, Gamulong, Wuga, and Yaduo formations)

Deep-water siliciclastic rocks widely occur as tectonic slices in the BNS. Regional correlations are hampered by poorly constrained depositional ages, and diverse lithostratigraphic names have thus been proposed.

Nima-Nagqu area (Fig. 2)**:** The Xihu Group is exposed from the Dongqiao area in the north to the Beila area in the south, where it lies in fault contact onto the Quehala Group and is conformably overlain by the Jienu Group. It consists of locally anchimetamorphic mudrocks and sandstones with a few conglomerate beds (Chen et al., 2002). During geological mapping at the 1:250,000 scale, the unit was assigned an Early to Middle Jurassic age based on a coral assemblage (Chen et al., 2002). More detailed studies focusing on the provenance and depositional environment of the Xihu Group have not been carried out so far.

The Jienu Group, exposed in the Dongqiao-Beila area but with only scattered outcrops west of Baingoin, mainly consists of mudrock, sandstone and slate, with andesitic tuffs reported in the Beila area (Chen et al., 2002). The Jienu Group conformably overlies the Xihu Group and is overlain with angular unconformity by the Qushenla Formation (Chen et al., 2002). During geological mapping at the 1:250,000 scale, a Middle to Late Jurassic age was assigned to the Jienu Group based on bivalves, corals, gastropods, bryozoans (Chen et al., 2002). The bivalve assemblage indicates a Middle Jurassic (Bajocian-Bathonian) age. The coral assemblage *Stylosmilia michelini*-*Epistreptophyllum giganteum* indicates a Late Jurassic (Oxfordian-Kimmeridgian) age. A Middle-Late Jurassic age is consistent with a youngest detrital-zircon age YC1σ(2+) of 169.5 ± 0.7 Ma (n = 2) (Table 1; Li et al., 2020c). The terrigenous fraction of this unit was most likely derived from South Qiangtang based on U–Pb age spectra of detrital zircons (Li et al., 2020c). The depositional environment of the Jienu Group remains poorly constrained due to the lack of accurate sedimentological studies.

Rutog-Gaize area (Fig. 3)**:** The more than 240 m thick Gamulong Formation lies in fault contact with the Mugagangri Complex or Dongcuo ophiolite and is interpreted as a trench deposit (Sun et al., 2019). It mainly consists of conglomerate and sandstone deposited in a deep-sea fan and containing abundant sedimentary clasts sourced from the Mugagangri Complex and Jurassic strata of South Qiangtang. A Late Jurassic stratigraphic age is indicated by a youngest detrital-zircon age YC1σ(2+) of 165±1.7 Ma (n=3).

The Wuga Formation exposed along the southern side of the Mugagangri Complex dominantly consists of sandy slate interbedded with limestone, chert, and conglomerate originally assigned to the Late Triassic (Zeng et al., 2006). A youngest detrital-zircon age YC1σ(2+) of 147.7 ± 0.6 Ma (n = 4), however, indicates a latest Jurassic or younger age (Table 1; Li et al., 2017c). Provenance analysis indicates South Qiangtang as the source area (Li et al., 2017c) and the depositional environment is considered to be hemipelagic to deep marine (Zeng, 2006; Li et al., 2017c).

More than 1-km-thick turbidites exposed to the south of the Mugagangri Complex and to the west of the Wuga Formation in the Gaize area (Zeng et al., 2006) were assigned to the Mugagangri Complex during geological mapping at the 1:250,000 scale. However, this stratigraphic unit is well defined and distinct from the Mugagangri Complex, and hence newly defined here as Yaduo Formation with type section exposed near Yaduo village to the south of Gaize. These sandstones and mudrocks deposited on a deep-sea fan (Yu et al., 1991) received detritus from South Qiangtang (Luo et al., 2019; Chen et al., 2020). The youngest detrital-zircon age YC1σ(2+) of 144 ± 1 Ma (n = 8) indicates a depositional age not older than the earliest Cretaceous (Table 1; Luo et al., 2019).

(4) Upper Jurassic Shamuluo and Dongqiao Formations

The Shamuluo Formation unconformably overlies the Mugagangri Complex, whereas the Dongqiao Formation was non-conformably deposited onto the BNS ophiolite. Both units consist of clastic rocks and tuffs (Girardeau et al., 1984; Chen et al., 2002; Wang et al., 2006; Zhu et al., 2016; Deng et al., 2017; Li et al. al., 2017b; Ma et al., 2018; 2020a). The Shamuluo and Dongqiao formations contain abundant corals, stromatopora, bivalves, foraminifera and algae, pointing at a Late Jurassic age (Ma et al., 2018; 2020a). Provenance analysis indicates that the Shamuluo Formation was sourced from South Qiangtang (Ma et al., 2018), whereas the Dongqiao Formation contains detritus of Lhasa affinity (Ma et al., 2020a). The Shamuluo Formation yielded no detrital zircon younger than 210 Ma north of Selincuo, where the unit is widely exposed (Table 1; Ma et al., 2018), and no zircon younger than ~160 Ma in the Gaize area (Table 1; Li et al., 2017b).

(5) Lower Cretaceous Qushenla Formation

The Qushenla Formation includes volcaniclastic strata deposited in a continental fluvio-lacustrine environment (Zheng, 2017), as well as andesites with some basalt and rhyolite (Kang et al., 2010; Wu et al., 2019). The unit is patchily exposed within the BNS, where it unconformably overlies the Mugagangri Complex and the Shamuluo Formation (Zhu, 2016; Zheng, 2017; Deng et al., 2020). Volcanic activity started by 136 Ma and peaked at ~115-105 Ma (Wu et al., 2013, 2014b; Zhu, 2016; Li et al., 2018; Mai et al., 2018; Deng et al., 2020).

(6) Cretaceous continental red beds

Lower Cretaceous red sandstones, conglomerates, and mudrocks deposited in alluvial fans, rivers, and lakes include the Qushenla Formation newly identified during geological mapping at the 1:250,000 scale (Zeng et al., 2006, Chen et al., 2017), the Kangtuo Formation exposed in the North Nima Basin (Kapp et al., 2007) and east of Selincuo (Hu et al., 2020), and the Jingzhushan Formation of the Beila-Dongqiao area (Zhu et al., 2019b). Deposition began at 118 Ma in the North Nima Basin (DeCelles et al., 2007). Provenance analysis documents diverse source areas, including South Qiangtang in the north for the North Nima basin (unit Kvc), and ophiolites, Mugagangri Complex, and Lower Cretaceous volcanic rocks for the Beila-Dongqiao area of the BNS (Zhu et al., 2019b). Widespread deposition of continental red beds indicates that the BNS became a continental basin long after the closure of the Bangong-Nujiang Ocean.

3.2 Mesozoic strata of South Qiangtang

Because of extensive oil and gas investigations and geological mapping, a bounty of stratigraphic, paleontological, and sedimentological data have been recently published from South Qiangtang. The Jurassic–Cretaceous lithostratigraphic framework is illustrated in Xue et al. (2020), who analysed and reconstructed the sedimentary history, provenance, and paleogeographic evolution of the South Qiangtang continental margin, as summarized below.

（1） Upper Triassic Nadigangri and Riganpeicuo formations

The Nadigangri Formation, exposed from east to west in central to northern Qiangtang where it unconformably overlies the Upper Triassic Xiaochaka Formation, consists of tuff and tuffaceous sandstone interbedded with andesite, rhyolite, and minor basalt in the lower and middle parts, and of coarse-grained sandstone, siltstone, and bioclastic marl in the upper part (Li, 2019). Zircon U–Pb data indicate an age of 221-201 Ma (Norian-Rhaetian) for this unit (Li, 2019), suggesting that the boundary with underlying strata corresponds to a hiatus of >2 Ma (Fu et al., 2007). Diverse continental-eruption and marine sedimentary facies have been identified in the Nadigangri Formation, including overflow, eruptive, eruptive-sedimentary, subvolcanic, deltaic, tidal flat, fluvial, and lacustrine deposits (Li, 2019). The bimodal basalt-rhyolite character of volcanic rocks suggestive of rift-related activity was emphasized by Fu et al. (2010), whereas a subduction-related volcanic-arc setting was favored by Zhai and Li (2007).

The Riganpeicuo Formation, mainly exposed in South Qiangtang, consists of shallow-marine carbonate interbedded with sandstone and shale. Bivalves, corals, and brachiopods indicate deposition in the Late Triassic. In the Gaize area, gray, gray-black and purple-red, medium- to thin-bedded micritic or oolitic limestone interbedded with reef limestone, sandy limestone, rudstone, and bioclastic limestone yielded rich fossil assemblages, including bivalves, crinoid stems, algae, corals, and sponges (Hou et al., 2014). In the Nagqu area, the Riganpeicuo Formation is dominated by sandstones and mudrocks transitionally overlain by the Suobucha Formation, composed of bioclastic limestone and mudstone and newly distinguished from the Riganpeicuo Formation by Wang and Zheng (2007).

(2) Lower to Middle Jurassic Quse, Sewa, and Buqu Formations

The > 600-m-thick Quse Formation mainly consists of dark gray mudrocks with limestones deposited on a shallow shelf (Wang and Zheng, 2007). The stratigraphic contact with underlying Triassic strata is unclear. Ammonites indicate a Toarcian-Aalenian (Early/Middle Jurassic) age (Chen et al., 2007; Ma et al., 2017a). The Sewa Formation, conformably overlying the Quse Formation, comprises a lower member of gray marl, a middle member of gray limestone and marl, and an upper member of dark gray shale interbedded with marl. The Sewa Formation was deposited in shallow shelf, deltaic, tidal flat, and lagoonal environments and yielded Aalenian-Bajocian ammonites (Yin and Chandler, 2016; Ma et al., 2017a). Its sandstones contain abundant volcanic rock fragments, pointing to provenance from the magmatic arc grown during subduction of Bangong-Nujiang oceanic lithosphere (Ma et al., 2017a).

The widely distributed Buqu Formation, conformably overlying the Sewa Formation, consists of medium/thick-bedded micritic or bioclastic limestone with minor gypsum (Yang et al., 2017). Dolostones occur in the Andaercuo and Biluoco areas, where they represent important oil and gas reservoirs (Wang et al., 2004). The Buqu Formation was deposited in tidal flat, shoal, lagoon, and platform environments (Ma et al., 2017a) and yielded bivalves, brachiopods, and ammonites indicating a Bathonian age (Yao et al., 2011).

(3) Middle-Upper Jurassic Xiali, Biluoco, 114 Daoban, and Suowa formations

The Xiali Formation, widely distributed in the Qiangtang Basin, is dominated by fine-grained red–green sandstone, siltstone, and claystone interbedded with shell beds and gypsum (Song et al., 2017a).

The unit, lying conformably onto the Buqu Formation and passing upwards conformably to the Suowa Formation, was deposited in tidal flat, lagoonal, and deltaic environments. Fossil assemblages, including plants, bivalves, brachiopods, and dinoflagellates indicate a Bathonian to early Oxfordian age (Song et al., 2016; Yao et al., 2011).

The Biluoco Formation, established by Ma et al. (2017) in the eastern Biluoco area of South Qiangtang, overlies the Buqu Formation unconformably and can be subdivided into upper and lower members. The 240-m-thick lower member is dominated by conglomerate commonly displaying graded bedding, whereas the upper member is dominated by light gray or reddish sandstone with parallel and trough laminations passing upwards conformably to the Suowa Formation. The Biluoco Formation was deposited in a fan-delta environment at late Bathonian to early Callovian times (Ma et al., 2017a). Detritus was largely generated by recycling of the older Buqu Formation and pre-Jurassic sedimentary rocks of South Qiangtang (Ma et al., 2017a).

The 114 Daoban Formation, mainly exposed in the northern Amdo area, consists of conglomerate, sandstone, siltstone, and micritic limestone, and contains numerous ammonites and nannofossils indicating a Bathonian-early Callovian age (Yin, 2005; Chen et al., 2019).

The Suowa Formation, widely distributed in South Qiangtang, consists of limestone interbedded with shell beds and includes a few coral reefs (Wang et al., 2010). The unit was deposited in a shallow-marine environment and yielded ammonites pointing at an early-middle Callovian age (Ma et al., 2017a).

(4) Upper Cretaceous Abushan Formation

These continental red beds overlying Jurassic marine strata with angular unconformity are widely distributed in South Qiangtang. Several hundred meters of red sandstone containing mainly limestone and sandstone pebbles pass upwards to sandstone and mudrock. A Late Cretaceous age is indicated by pollen assemblages, youngest detrital zircons, and magnetostratigraphy (Wu et al., 1986; Zhu et al., 2005; Ma et al., 2017a; Meng et al., 2018). Volcanic rocks dated as 80-102 Ma are intercalated in the Biluoco area (Li et al., 2013; Wu et al., 2014c; He et al., 2018).

3.3 Mesozoic stratigraphy of North Lhasa

Mesozoic strata exposed in the northern part of the Lhasa Block include the Upper Triassic Duoburi Formation, the Upper Jurassic-Lower Cretaceous Lagongtang Formation, the Lower Cretaceous Duoni and Duba formations, the mid-Cretaceous Langshan Formation, and the Upper Cretaceous Jingzhushan Formation.

(1) Upper Triassic Duoburi Formation

The Duoburi Formation, exposed in the Xianzha area of North Lhasa southwest of Baingoin, unconformably overlies the Upper Permian dolostone of the Mujiucuo Formation and mainly consists of sandstone, mudrock, and limestone, with limestone increasing up-section (Qu et al., 2003). Deposition took place in continental to transitional environments passing to shallow marine up-section. Corals, algae, gastropods, and pollen indicate a Late Triassic age (Qu et al., 2003). Age spectra of detrital zircons are similar as in Paleozoic strata of the Lhasa Block, and reworking of Paleozoic strata has been suggested based on the youngest zircon-age peak at 470–550 Ma (Fan et al., 2017b).

(2) Upper Jurassic-Lower Cretaceous Lagongtang Formation

The Lagongtang Formation, mainly exposed from east of Baingoin to west of Nagqu in the northernmost part of the Lhasa Block (Fig. 2), consists of gray to dark gray shale, siltstone, and sandstone intercalated with lenticular limestone yielding corals, ammonites, bryozoans, brachiopods, bivalves, foraminifera, and crinoids (Lai et al., 2022). The unit was considered as Middle-Late Jurassic in age until Lai et al. (2022) found detrital zircons yielding Early Cretaceous U-Pb ages in the Nagqu Basin, indicating that the unit extends into the Early Cretaceous. Deposition took place in a deep shelf environment. Sandstone petrography, paleocurrents, and U–Pb ages and Hf isotopes of detrital zircons indicate recycling of quartz-rich sandstones and supply from Middle Triassic to Lower Cretaceous magmatic rocks of the central-southern Lhasa Block (Lai et al., 2022). An alternative foreland-basin setting related to the Lhasa-Qiangtang collision was proposed based on a different provenance interpretation of the Lagongtang Formation (Li et al., 2022).

(3) Lower Cretaceous Duba Formation

The Duba Formation consists of siliciclastic rocks exposed in the Baingoin Basin and included in the Duoni Formation (Xia et al., 1997) until Lai et al. (2019b) documented that the two units have different detrital sources. Moreover, the Duba Formation crops out closer to the BNS to the north, whereas the Duoni Formation is exposed closer to Central Lhasa. The Duba Formation includes a > 250-m-thick lower member dominated by dark gray mudrock deposited on a shallow-shelf, a > 550-m-thick middle member dominated by gray-green sandstone and shale deposited in a deltaic environment, and a > 90-m-thick upper member dominated by red shale and siltstone deposited in a floodplain environment (Lai et al., 2019b). Depositional age is constrained as between 122 and 110 Ma by dating of volcanic ash and youngest detrital zircons (Lai et al., 2019b). Sandstone petrography, age spectra of detrital zircons, and geochemistry of detrital Cr-spinel indicate provenance from the BNS and South Qiangtang farther north (Lai et al., 2019b).

(4) Lower Cretaceous Duoni Formation

The Duoni Formation, widely distributed in North Lhasa from Nagqu in the east to Bangong Lake, mainly comprises siliciclastic rocks. In the Baingoin Basin, the lower member consists of black shales deposited in delta-front to shelf settings, the middle member of fan-delta deposits, and the upper member of meandering-river sediments (Leier et al., 2007; Lai et al., 2019b). In the southern Coqen area, the Duoni Formation consists of ≤ 1.2-km-thick fluvial deposits, whereas in the northern Coqen area it consists of 900-m-thick shelfal sandstones and mudrocks indicating northward-increasing paleo-water depths (Sun et al., 2017; Li et al., 2020b). U-Pb dating of zircon in interlayered tuffs yielded ages of 123-108 Ma (Zhang et al., 2011; Sun et al., 2017; Lai et al., 2019b). Paleocurrents, sandstone petrography, and age spectra of detrital zircons point at provenance from Lower Cretaceous Zenong Group volcanic rocks and pre-Jurassic strata of Central Lhasa (Zhang et al., 2011; Sun et al., 2017; Lai et al., 2019b).

(5) Mid-Cretaceous Langshan Formation

The Langshan Formation, widely distributed in North Lhasa with a stratigraphic thickness ranging from several meters to more than 1 km, represents the youngest marine strata described in this article. Fossil assemblages including orbitolinids, planktonic foraminifera, oysters, calcareous green algae, and rudists indicate a late Aptian-early Cenomanian (116-99 Ma) depositional age (Zhang, 1981;

Scott et al., 2010; Rao et al., 2015, 2020; BouDagher-Fadel, 2017; Xu et al., 2020). The shallow-marine Langshan Formation documents an evolution from carbonate ramps (116-107 Ma) to rimmed platforms (107-100 Ma), and again to carbonate ramps (100-99 Ma) (Xu et al., 2020), controlled by the interplay between tectonic subsidence and eustasy.

（6） Upper Cretaceous Jingzhushan Formation

The **Jingzhushan Formation**, exposed in a narrow belt from Biru in the east to Bangong Lake in the west, is separated from the Langshan Formation in the south by the north-vergent Gaize-Selincuo Thrust (Xia et al., 1997; Kapp et al., 2007; Ye et al., 2019; Lai et al., 2019a). This 2-km-thick unit consists of purplish-red conglomerate with minor sandstone and siltstone deposited in alluvial-fan to braided-river environments (Xia et al., 1997; Lai et al., 2019a). Pebbles are mainly derived from Langshan limestones exposed and eroded in the south, as indicated by their fossil content commonly including *Orbitolina*, rudists, and planktonic foraminifera. The depositional age is constrained as ~92 Ma by U-Pb dating of intercalated tuffs and youngest detrital zircons (Lai et al., 2019a).

4. Sandstone provenance in the Bangong-Nujiang suture zone

Provenance studies based on framework petrography (Table S1) coupled with detrital-zircon U–Pb geochronology (Table S2) are essential to unravel the tectonic evolution of the BNS.

(1) Nima-Nagqu area

In the Nima-Nagqu area, three units (Mugagangri Complex, Jienu Group, and Shamuluo Formation) are extensively distributed in the BNS. Sandstones of the Mugagangri Complex can be subdivided into three groups (Fig. 5) (Ma et al., 2020b). Group 1 is distinguished by high proportions of feldspar (23%) and felsic volcanic lithics (33%) and by an Early to Middle Jurassic (170-180 Ma) zircon-age cluster. Group 2 consists of mainly litho-quartzose sandstone, with ~27% lithics (mainly felsic volcanic, chert, and low-grade metamorphic types) and a wide age distribution of detrital-zircon ages between 200 and 2500 Ma. Group 3 consists of mainly litho-quartzose sandstone, with ~29% lithics (mainly sedimentary types) and three main clusters of zircon ages at 250-1200 Ma, 1600-1800 Ma, and 2500 Ma. The detrital zircon distribution of the Jienu Group and Shamuluo Formation is similar to Group 2 of the Mugagangri Complex.

Based on Multidimensional Scaling analysis (MDS; Vermeesch, 2013), Mesozoic sandstones of the Nima-Nagqu area in South Qiangtang and North Lhasa can be subdivided into three classes (Fig. 5a and b). Class 1 comprises sandstones of the Duoni, Duba, and Lagongtang formations in North Lhasa and Group 1 sandstones of the Mugagangri Complex in the BNS. Provenance analysis indicates that the Duoni and Lagongtang formations are derived from the Lhasa Block (Lai et al., 2019, 2022). Group 1 sandstones in the Mugagangri Complex also yielded age spectra of detrital zircons similar as those in the Lagongtang Formation (both classified as Class 1 in the MDS map; Fig. 5), but the former are mainly feldspatho-litho-quartzose (Q:F:L=44:23:33), whereas the latter are litho-quartzose with much lower feldspar content (Q:F:L=76:8:16) (Fig. 6). Therefore, Group 1 sandstones of the Mugagangri Complex are not derived from the Lhasa Block. They are characterized by an 170-180 Ma age cluster, as feldspatho-lithic sandstones in the Sewa Formation (Fig. 6), reflecting extensive volcanism along the southern margin of South Qiangtang at the time of deposition (Ma et al., 2017).

Class 2 comprises sandstones of the Upper Triassic Riganpeicuo and Jurassic Biluoco and Sewa formations in South Qiangtang, and of the Jienu and Shamuluo formations plus Group 2 sandstones of the Mugagangri Complex in the BNS. All these units were derived from recycling of pre-Jurassic strata and erosion of the Jurassic continental arc on South Qiangtang (Ma et al., 2017, 2018).

Class 3 comprises Group 3 sandstones of the Mugagangri Complex, which have similar detrital zircon signatures as pre-Jurassic sandstones in Central Lhasa (Fig. 5b). Group 3 sandstones yielded a zircon-age cluster at ~1200 Ma indicative of provenance from the Lhasa Block but also an 1800 Ma zircon-age peak (Fig. 5a and 6b), and are dominated by sedimentary lithics thus displaying remarkable similarities with sandstones from the Riganpeicuo and Biluoco formations in South Qiangtang (Fig. 5a). This led Ma et al. (2020b) to infer that Group 3 sandstones were sourced from both South Qiangtang and the Lhasa Block.

In summary, Upper Triassic to Jurassic siliciclastic units of the BNS in the Nima-Nagqu area are mainly derived from recycling of pre-Jurassic strata and erosion of the Jurassic continental arc in South Qiangtang, with the only exception of Group 3 sandstones of the Mugagangri Complex that may have received detritus from both Qiangtang and Lhasa Blocks at the same time.

(2) Rutog-Gaize area

In the Rutog-Gaize area, five stratigraphic units (Mugagangri Complex, Yaduo, Shamuluo, Gamulong, and Wuga formations) were distinguished in the BNS. The Mugagangri Complex was divided into three groups, named Trma, Trmb, and TrJmc by Zeng et al. (2016a), which correspond to the three groups (Group 3, Group 2 and Group 1) identified in the Nima-Nagqu area based on detrital-zircon age spectra (Figs. 4 and 5; Ma et al., 2020b; Li et al., 2021). Based on Multidimensional Scaling analysis (Fig. 5c and d), detrital-zircon age spectra of Mesozoic sandstones can also be subdivided into three classes, which correspond to the three classes identified in the Nima-Nagqu area. Sandstone composition is also similar as in the Nima-Naqu area (Fig. 5): Trma sandstones are dominated by sedimentary lithics (77%) and are classified as Class 3, whereas Trmb and TrJmc sandstones, which contain abundant felsic volcanic fragments (52% and 43% on average, respectively), are classified as Class 2 and Class 1, respectively (Fig. 6). These observations underscore the regional consistency of provenance features of the Mugagangri Complex from the Nagqu area in the east to the Gaize area in the west (Zeng et al., 2016a; Li et al., 2017b; Huang et al., 2017b). Combined information from framework petrography and detrital-zircon age spectra indicates that the Shamuluo, Yaduo, Wuga, Gamulong formations and the Mugagangri Complex (Trmb, TrJmc) are similar to the Upper Triassic Riganpeicuo and Jurassic Sewa formations mainly sourced from South Qiangtang (Li et al., 2017b; Chen et al., 2021). Although the Trma and pre-Jurassic strata of Central Lhasa are classified as Class 3, the general absence of the ~1200 Ma peak in Trma sandstones indicate provenance from Qiangtang pre-Jurassic strata rather than from the Lhasa Block (Chen et al., 2021).

5. Mesozoic sedimentary evolution of the Bangong-Nujiang suture zone and adjacent areas

5.1 South Qiangtang

The Upper Triassic volcano-sedimentary Nadigangri Formation in northern to central Qiangtang document magmatic activity followed by deposition in marine environments in the Jurassic (Fu et al., 2010b). At that time, sandstones and limestones of the Riganpeicuo Formation were deposited in South Qiangtang, indicating northward encroaching seas (Wang et al., 2006; Ma et al., 2017a).

Lower Jurassic strata are lacking in northern to central Qiangtang, whereas the Quse and Sewa formations were deposited in marine, coastal, and shelfal environments in South Qiangtang (Xue et al., 2020). In the late Middle Jurassic, Buqu limestones were extensively deposited across the Qiangtang

Basin, documenting a major transgression (Xue et al., 2020). The Baingoin-Shuanghu area of South Qiangtang was next affected by compressional tectonics, with basin inversion testified by the unconformity at the base of the Biluoco Formation (Ma et al., 2017a, 2018), while fine-grained siliciclastic sediments of the 114 Daoban Formation continued to be deposited in the Amdo area.

During the Late Jurassic, the shallow-marine limestones of the Suowa Formation were deposited across the Qiangtang Basin, documenting a second major transgression followed by progressive seaway retreat (Wang and Fu, 2019; Xue et al., 2020).

5.2 North Lhasa

Triassic strata are poorly exposed in North Lhasa, where limited information on their paleogeographic significance is available. During the Jurassic, the Lagongtang Formation was deposited in shelf environments, documenting a northward increase of water depth across the North Lhasa continental margin facing the Bangong-Nujiang Ocean (Lai et al., 2022).

During the Early Cretaceous, the Zenong Group volcanic rocks covered a large part of Central Lhasa. In the Coqen area, the Duoni Formation was deposited in a northward-deepening marine environment between 125 and 110 Ma (Sun et al., 2015). Detritus was mainly sourced from Zenong Group volcanic rocks and Central Lhasa basement. In the Baingoin area, the Duoni Formation documents a shallowing-upward sequence, finally passing upwards to fluvial environments. During the same period, the Duba Formation was deposited in deltaic to fluvial environments to the north closer to the BNS, indicating provenance from the already uplifted BNS and South Qiangtang (Lai et al., 2019b).

In the latest Early Cretaceous (113-99 Ma), shallow-marine carbonates of the Langshan Formation document a major transgression across North Lhasa, with seaways reaching as far north as the BNS (Xu et al., 2020). At ~92-90 Ma, large-scale tectonic shortening affected North Lhasa, compressed between the north-vergent Gaize-Selincuo Thrust along the northern side (Kapp et al., 2007) and the south-vergent Gugula Thrust along the southern side (Murphy et al., 1997). The initial rock and surface uplift of North Lhasa is testified by the Jingzhushan and Daxiong formations deposited on the thrust footwall (Sun et al., 2015; Lai et al., 2019a).

5.3 Bangong-Nujiang suture zone

The Triassic configuration of microcontinents and seaways in the study area is unclear. Deep-water strata include the Triassic part of the Mugagangri Complex, characterized by provenance signatures similar as those of sandstones in the Riganpeicuo Formation of South Qiangtang and thus considered as equivalent to the Riganpeicuo Formation (Zeng et al., 2016a; Li et al., 2017b; Ma et al., 2020b). The Quehala Group, deposited in coastal to shelf environments along the margin of the Dongkacuo microcontinent (Chen, 2002), extends eastward to the Dingqing area and is considered to contain detritus derived from the Lhasa Block in the Late Triassic (Chen et al., 2020). Further research on the Mugagangri and Quehala groups are required to clarify their paleogeographic significance.

During the Early-Middle Jurassic, the Xihu and Jienu groups document extensive siliciclastic deep-sea-fan deposition. The Jienu Group exposed in the Beila area received detritus from the Qiangtang Block (Li et al., 2020c), whereas the Xihu Group in the Dingqing area to the east was fed from the Lhasa Block (Chen et al., 2020).

In the latest Jurassic, the Shamuluo and Dongqiao formations were deposited in marine to paralic environments, indicating that deep-water sedimentation had ceased along the northern margin of the BNS. The Gamulong, Wuga, and Yaduo formations, fed from South Qiangtang, were still deposited in deep-water environments in the western BNS (Rutog-Gaize area) and a deep-water trough may have persisted to the south. The Mugagangri Complex formed mainly at this time, and ophiolite obduction has been reported from the Beila and Zhonggang areas (see Section 7).

In the Early Cretaceous, continental red beds became widespread, including the Qushenla Formation in Gaize (Chen et al., 2017), the Kvc unit in North Nima (Kapp et al., 2007), and the Upper Cretaceous Jingzhushan Formation in the eastern Selincuo (Hu et al., 2020) and Beila-Dongqiao areas (Zhu et al., 2019b; Lai et al., 2019), testifying to a complete demise of seaways.

6. Paleobiogeographic evolution of Lhasa and South Qiangtang

Zhang et al. (2013) systematically reviewed the Permian paleobiogeography of the Tibetan Plateau and summarized the biogeographic evolution of both South Qiangtang and Lhasa blocks. Permian marine faunas of the Tibetan Plateau can be assigned to four biotic provinces (Cathaysian, Indoralian, Cimmerian, and Himalayan) with a broad South Transition Zone for parts of the Permian in the south. Tethys Himalayan fauna belong to the Himalayan Province, whereas North Qiangtang faunas belong to the Cathaysian Province. The paleobiogeography of South Qiangtang and Lhasa blocks is more complex. During the Asselian (earliest Permian), South Qiangtang, Lhasa, and Tethys Himalayan faunas all belonged to the Himalayan Province, and glacigenic diamictites occurred in all these domains which were all parts of Gondwana at that time (Sun, 1993; Garzanti and Sciunnach, 1997). During the Sakmarian-Kungurian (middle-late Early Permian), after the onset of sea-floor spreading in Neo-Tethys (Sciunnach and Garzanti, 2012), the Lhasa Block and South Qiangtang gradually passed into the South Transition Zone (Shi et al., 1995), as indicated by the appearance of the brachiopods *Cimmeriella* and *Bandoproductus* and of the bivalve *Eurydesma*. In the Middle Permian, South Qiangtang and the Lhasa Block shifted to the Cimmerian biotic province, identified by mixed warm-water Cathaysian and cold-water Gondwanan faunas, such as the *Shanita-Hemigordiopsis* foraminiferal assemblage and the *Thomasiphyllum* coral assemblage. During the Late Permian, both Lhasa and South Qiangtang belonged to the Cathaysian Province, as indicated by South China-type warm-water brachiopod and conodont assemblages (Xu et al., 2019; Yuan et al., 2014; Wu et al., 2014a), although with significant variability in foraminifera (Qiao et al., 2019).

Zhang et al. (2013) underscored the paleobiogeographic differences between the Lhasa Block and South Qiangtang during the Late Permian. Warm-water assemblages, including the fusulind *Parafusulina*, *Wutuella*, and *Monodiexodina* (Nie and Song, 1983), and the corals *Polythecalis*, *Chusenophyllum*, and *Wentzellophyllum*, first appeared in South Qiangtang during the late Early Permian (He et al., 1990), while the Lhasa Block and the Tethys Himalaya remained dominated by cold-water biota including the conodont *Vjalovognathus* (Nicora and Garzanti, 1997; Zheng et al., 2007; Yuan et al., 2016) and the *Spiriferella-Costiferina* brachiopod assemblage (Sciunnach and Garzanti, 1996; Zheng et al., 2005). Warm-water organisms appeared in the Lhasa Block only during the Wordian (Middle Permian), significantly later than in South Qiangtang. In the Middle Permian, the *Nankinella-Chusenella* fusulinid assemblage appeared in the Lhasa Block, while the *Eopolydiexodina* and *Jinzhangia* assemblage appeared in South Qiangtang (Zhang et al., 2019). In the Late Permian, South Qiangtang was characterized by *Palaeofusulina*, while *Colaniella* and *Reichelina* occurred in the Lhasa Block at that time. Such faunal differences can be explained by initial separation of South Qiangtang from the Lhasa Block in the Middle Permian, followed by the rapid northward drift of South Qiangtang during the Late Permian, resulting in a significant paleogeographic isolation of the two blocks.

Although limited information is available on fossil distribution from poorly exposed Triassic strata of the Lhasa Block, quantitative statistical analysis of bivalve assemblages indicate that the Lhasa and South Qiangtang blocks were wide apart at Triassic time (Niu et al., 2011).

7. Age of Bangong-Nujiang ophiolites

Mantle serpentinite, cumulate, gabbro, diabase, basalt, and chert representing oceanic lithosphere are widely distributed in the BNS and document the existence and evolution of the Bangong-Nujiang Ocean (Girardeau et al., 1984; Shi et al., 2012; Wang et al., 2016). Recent research has produced a bounty of data on formation and emplacement of BNS ophiolites, using different geochronological methods (e.g., K-Ar and Ar-Ar dating of K-bearing minerals, U–Pb zircon dating of plagiogranite, Re-Os isochron ages) and radiolarian biostratigraphy. Not all dating methods are however equally robust, and criteria for the selection of most reliable ages must thus be defined.

We gave preference to published ages from rocks belonging to a complete ophiolite sequence rather than from sparse outcrops. Geochemical signatures were used to differentiate among OIB-, MORB-, and SSZ-type rocks with enriched and depleted isotopic signals. Because of the low closure temperature of the K-Ar system (< 500°C), K-Ar and Ar-Ar ages may be reset by later thermal events (e.g., magmatism, faulting, burial). Although zircon U–Pb ages are widely considered as robust, they require special care when used to date ophiolite sequences that contain very little zircon, because contamination from country rocks may occur (Huang et al., 2021). The reliability of zircon U–Pb ages can be judged from: (1) cathodo-luminescence images of zircons from ophiolites show unconfined, broad-ring zoning features, fan-like structures, or homogeneous distribution (Lissenberg et al., 2009); (2) zircons from ophiolites usually display a single U–Pb age peak, whereas inherited or contaminated zircons are usually characterized by multiple peaks; (3) zircons from ophiolites are identified by specific geochemical fingerprints (e.g., U and Y content, or Hf and O isotopes; Grimes et al., 2007).

The published zircon-age data for the BNS ophiolite selected according to the criteria illustrated above are summarized in Table S4 and Fig. 7. K-Ar and Ar-Ar ages are compiled (Table S5) and plotted for comparison (Fig. 7). The selected U–Pb zircon ages are mostly Jurassic, subordinately Early

Cretaceous, and sporadically Triassic. Jurassic ages range between 190 and 164 Ma in the eastern Nima-Nagqu area, and between 184 and 156 Ma in the western Kangqiong-Gaize area (Table S4). Especially along the Dongqiao-Amdo branch, ages cluster between 190 and 180 Ma (Table S4). Early Cretaceous ages between 141 and 133 Ma characterize igneous rocks (trachyandesite, troctolite, gabbro, and basalt) in the western Zhonggang-Kangqiong area near Dongcuo (Fig. 3), which show mainly OIB and some MORB features (Fan et al., 2021a; Zeng et al., 2021). In the east, Early Cretaceous ages (133-134 Ma; Zhong et al., 2018) were reported in the Yilashan area near Nagqu (Fig. 2), whereas rocks plausibly representing oceanic crust in the Beila area yielded Late Jurassic ages (148-149 Ma; Zhong et al., 2017), which suggests that the Beila-Nagqu oceanic branch may have remained partially open until the Early Cretaceous. Triassic ophiolite ages were sporadically reported from both eastern and western areas (Qin et al., 2017; Zhong et al., 2017; Wu, 2018). Ar-Ar and K-Ar ages range between 127-114 Ma, but for one age at 184.5 Ma. The much younger Ar-Ar and K-Ar ages may suggest alteration by later thermal events, as discussed in Huang et al. (2017a).

Re-Os isochron ages were obtained from six cumulate rocks in the Dongqiao area (251 ± 65 Ma, MSWD = 55; Shi et al., 2012) and from nine harzburgites from the Bangong Lake area (254 ± 28 Ma; Huang et al., 2012). These Permian/Triassic ages are interpreted to date the formation of Bangong-Nujiang oceanic crust.

Only a few biostratigraphic data have been obtained on chert exposed in the BNS, including Anisian (Middle Triassic) to Carnian (Late Triassic) ages from the Dingqing-Nagqu area. Carnian radiolarians are reported from chert of the Dingqing ophiolite suite (Wang et al., 2002), and Anisian radiolaria from the Gaga mélange in the Nagqu area (Nima and Xie, 2005). Radiolarians of Pliensbachian (Early Jurassic) age were retrieved near Zongbai town in Dingqing (Li, 1988). Li (1986) described Tithonian (Late Jurassic) radiolarians from chert overlying volcanic rocks and tuffs in Rutog County.

These observations allow only a sketchy reconstruction of the history of the Bangong-Nujiang Ocean. Radiolarian biostratigraphy coupled with Re-Os isochron ages of mafic rocks testify to active sea-floor spreading in the Bangong-Nujiang Ocean during much of the Triassic (since 245 Ma at least). Abundant ages indicate extensive formation of oceanic crust through the Early and Middle Jurassic, when deep-water sedimentation was widespread within the BNS. Early Cretaceous ages suggest that oceanic crust may have continued to form until as late as 133 Ma, representing the youngest age reported from BNS ophiolites.

8. Magmatic rocks in the Bangong-Nujiang suture zone and adjacent areas

Mesozoic magmatism is widely testified in South Qiangtang, BNS, and Lhasa Block (Figs. 1b and 8). Here we summarize the distribution of igneous rocks between South Qiangtang and Central Lhasa, and emphasize the limited areal extent but notable variability along strike of South Qiangtang magmatic rocks (Table S3; Figs. 1b and 8). Such features are unlike those of large-scale magmatic arcs, such as the Gangdese-Ladakh Transhimalayan Arc or the Andean Cordillera.

8.1 South Qiangtang

Igneous rocks in South Qiangtang include Early Permian and Middle Triassic mafic dikes, minor Late Triassic volcanic rocks, Jurassic intermediate- felsic intrusive rocks, and Early Cretaceous and minor Late Cretaceous intrusive and volcanic rocks.

The E/W trending mafic dike swarms exposed in western South Qiangtang were dated formerly as ~320-280 Ma by LA-ICP-MS U–Pb on zircon (Zhai et al., 2013a; Wang et al., 2019) and more recently as 291–283 Ma with peaks at ~290 Ma and ~285 Ma by SIMS and SHRIMP U–Pb on zircon (Dan et al., 2021a). The ~290 Ma rocks are low-Ti tholeiitic basalts with minor high-Ti alkaline basalts, whereas the widespread ~285 Ma rocks are mostly low-Ti tholeiitic basalts (Wang et al., 2019; Dan et al., 2021a). Based on age, spatial distribution and petrogenesis, these rocks are considered to represent part of the Qiangtang-Panjal Large Igneous Province (Dan et al., 2021a), which is linked to initial rifting of South Qiangtang and possibly of the Lhasa Block from India (Sciunnach and Garzanti, 2012).

Mafic dike swarms exposed near the Longmuco-Shuanghu suture zone yielded Middle/Late Triassic U–Pb zircon ages between 247 and 232 Ma (average 239 Ma; Dan et al., 2021b) and were thus distinguished from Early Permian dikes as previously mapped. These tholeiitic basalts display enrichment in light rare earth elements (LREE), moderate depletion in Nb and Ta, and evolved isotopic signatures, and were considered to document the magmatic response to collision between South and

North Qiangtang along the Longmucuo-Shuanghu suture zone (Dan et al., 2021b).

Upper Triassic intrusive and volcanic rocks of the Nadigangri Formation are exposed in central Qiangtang (Wu et al., 2015), yielding U–Pb zircon ages between 222 and 201 Ma (Li, 2019). Intrusive rocks are mainly I-type and S-type granites (Li et al., 2015a), whereas volcanic rocks range from andesite to rhyolite with minor OIB-type basalt and adakite (Fu et al., 2010a, b; Zhai et al., 2013; Li et al., 2015a; Wu et al., 2015; Li, 2019). Their geodynamic significance remains controversial, and both subduction- or collision-related (Zhai and Li, 2007; Zhai et al., 2013) and rift settings (Fu et al., 2010b) have been proposed.

Middle-Late Jurassic granites with minor diorite and andesite-rhyolite are exposed for ~500 km from east to west along the southwestern margin of South Qiangtang (Fig. 8). Three magmatic stages were identified (Li et al., 2020), and all are widely attributed to northward subduction of the Bangong-Nujiang oceanic lithosphere. Stage 1 is represented by plutonic rocks exposed at Larelaxin near Rutog (168–161 Ma; Li et al., 2014b), and in the Duobuzha, Qingcaoshan, and Liqunshan areas (170–154 Ma; Li et al., 2014a; Zhang et al., 2017b). These high-K calc-alkaline and highly fractionated I-type granites with associated high-alumina basaltic dikes and mafic enclaves were interpreted to indicate melting, assimilation, storage, and homogenization above a subduction zone.

Stage 2 is represented by medium-K adakitic dacites exposed in the Gaize-Rena Tso (~160–154 Ma; Fan et al., 2016; Li et al., 2016a) and Kangqiong areas (~148 Ma; Li et al., 2016b), and by OIB-type basalts near Gaize (~158 Ma; Li et al., 2016a). The adakites display high Sr/Y, low Y, high MgO and Mg#, small negative to positive $\varepsilon_{Nd}(t)$, and positive zircon $\varepsilon_{Hf}(t)$, indicating an oceanic-crust (Li et al., 2016a) or eroded arc-crust origin (Yang et al., 2021). The OIB-type rocks are enriched in LREE and Nb-Ta and have positive $\varepsilon_{Nd}(t)$, suggesting a sub-slab asthenospheric source (Li et al., 2016a).

Stage 3 is represented by adakitic diorites and granodiorites (~153–148 Ma) exposed in the Gaize-Rena Tso area. These intrusive rocks belong to the high-K series (Hao et al., 2016a) and have high Sr/Y and La/Yb, and negative $\varepsilon_{Nd}(t)$ and zircon $\varepsilon_{Hf}(t)$ values similar as high-K I-type granites of Stage 1. They are thus inferred to indicate crustal thickening (Hao et al., 2016a).

Early Cretaceous (123-106 Ma) magmatic rocks widely exposed in the Rutog-Gaize areas of South Qiangtang (J.X. Li et al., 2014a; Hao et al., 2016b; Liu et al., 2017b; Fig. 8) include the Xiabie batholith in central South Qiangtang (Yang et al., 2018), and are best studied around Duolong in South Qiangtang where Cu–Au porphyry ores occur (Li et al., 2016a). These rocks are mainly high-K calc-alkaline diorite and granite dated between ~125 and ~100 Ma (Li et al., 2018), inferred to have been generated during collision between the Lhasa and Qiangtang Blocks (Zhu et al., 2016). The widespread distribution of Lower Cretaceous continental red beds and Upper Jurassic shallow-marine deposits in the BNS (see Section 5) indicates that these Early Cretaceous magmatic rocks cannot be the product of northward subduction of Bangong-Nujiang lithosphere (as suggested by J.X. Li et al., 2014a).

Volumetrically minor Late Cretaceous magmatic rocks include the Mg-rich Biluoco andesite (~95 Ma; He et al., 2018), the high-silica, I-type Amdo granite (~80 Ma; He et al., 2019), the K-rich Amdo alkaline andesite (~ 80 Ma; Chen et al., 2017), and the Abushan trachyandesite (80–76 Ma; Li et al., 2013). Most of these rocks belong to the alkaline series and are interpreted as products of lithospheric thickening and foundering after the Lhasa-Qiangtang collision.

8.2 Bangong-Nujiang suture zone

Intermediate- felsic intrusive rocks of Early Jurassic age (~194–173 Ma) are exposed in the Amdo microcontinent (Zhu et al., 2011; Liu, 2012; Yan et al., 2016; Liu et al., 2017a) and can be subdivided into two phases based on rock type and composition. The early phase (~194–180 Ma) is represented by diorite, granodiorite, monzogranite, and syenogranite belonging to the calc-alkaline series and ranging from medium-K to shoshonitic (Liu, 2012). The late phase is represented by calc-alkaline gabbro, diorite, granodiorite, alkaline monzodiorite, monzonite, and syenite. These rocks were generally interpreted as related to subduction of Bangong-Nujiang lithosphere and assembly of the Amdo microcontinent to South Qiangtang, but the geodynamic process remains controversial.

In the Middle-Late Jurassic (166–160 Ma) (Fig. 8), magmatism mainly developed in the Dongkacuo microcontinent in the eastern part of the BNS (Li et al., 2015c; Zeng et al., 2016b; Li, 2019a; Li et al., 2020c) and in the Shiquanhe area in the western part of the BNS (Liu et al., 2018). These Mg-rich andesites and rhyolites are interpreted as products of partial melting of the mantle wedge modified by sediment-derived melt and are hypothesized to indicate either an initial subduction event during the long-term evolution of the Bangong-Nujiang Ocean (Zeng et al., 2016b) or an oceanic ridge-trench collision (Li et al., 2020c).

Early Cretaceous (118-110 Ma) magmatism (Fig. 8), widely documented in the BNS by intermediate- felsic rocks with minor OIB-type alkaline basalt and gabbro (Zhu et al., 2016), may represent syncollisional magmatism in the BNS.

8.3 Central and North Lhasa

Early Cretaceous magmatism is much more extensively documented in North Lhasa than in South Qiangtang or BNS, as testified by the Baingoin batholith in the east and by basalts and andesites of the Qushenla Formation in central and western regions. The Baingoin batholith (139–105 Ma; Zhu et al., 2016) consists of calc-alkaline metaluminous to strongly peraluminous granite. Zircon crystals dated between 139 and 125 Ma yield mostly positive ε_{Hf}(t) values (–1.9 to +11.0), whereas zircon crystals dated between 125 and 110 Ma yield negative ε_{Hf}(t) values (–7.0 to –2.1), features interpreted as the result of hypothetical slab rollback and break-off (Zhu et al., 2016). The Qushenla Formation volcanic rocks (Li et al., 2018) document two stages: Stage 1 (131–116 Ma) is characterized by medium-K calc-alkaline basalt and andesite, whereas Stage 2 (116–105 Ma) is characterized by high-K basalt and andesite, suggesting a lower degree of partial melting possibly in an extensional setting. A bimodal volcanic suite dated at ~110 Ma near Yanhu (Sui et al., 2013), and a belt of A-type granite and rhyolite exposed from Rutog and Gaize in the west, across the northern Xainza region, and to the Baingoin areas in the east, were also related to an extensional setting (Qu et al., 2012; Ma et al., 2020c).

Middle-Late Jurassic to Early Cretaceous rocks with typical magmatic-arc signatures are widespread in Central and North Lhasa (Li et al., 2018), and especially extensive in the western part. Whether these calc-alkaline rocks are related to northward subduction of Neo-Tethyan lithosphere or to southward subduction of the Bangong-Nujiang lithosphere remains highly controversial (e.g., Zhu et al., 2013; Cao et al, 2016; Li et al., 2018).

9. Metamorphic rocks in the Bangong-Nujiang suture zone

In the BNS, only a few metamorphic rocks are exposed in the Dongcuo, Amdo, and Basu areas (Li et al., 2017a). In the Dongcuo-Gaize area, high-pressure rocks within ophiolitic mélange include eclogite, granulite, amphibolite, greenschist, metadiorite, and metasedimentary rocks (e.g., Wang et al., 2008; Wang et al., 2015; Dong et al., 2016; Zhang et al. al., 2017b). Amphibolites were dated by $^{40}Ar/^{39}Ar$ as ca. 177-170 Ma (Wang et al., 2008). The lenticular, laminar or massive granulites associated with plagioclase amphibolite and metagabbro in the Shemala valley to the northwest of Dongcuo yielded U–Pb zircon ages of 254 ± 2 Ma and 176.9 ± 2.7 Ma, interpreted as the formation age of the basaltic protolith and of high-pressure metamorphism, respectively (Wang et al., 2015; Zhang et al., 2017a). The Dongcuo eclogites in the Shemala valley are divided into two types (Dong et al., 2016; Zhang et al., 2016; Zhang et al., 2017a). The first eclogite type, containing a peak-metamorphic paragenesis including garnet and monazite, was dated as ~260 Ma and considered to represent a mid-ocean ridge basaltic protolith. The second type, including garnet, monazite, and rutile, was dated as 242 Ma and considered to represent an OIB-type protolith (Zhang et al., 2016). SIM zircon ages from these eclogites indicate a protolith age of 250.7 ± 3.7 Ma (Zhang et al., 2017a). Minerals from the metamorphic aureole, instead, yielded a SIM zircon age of 176.9 ± 2.7 (Zhang et al., 2017a) and a U–Pb rutile age of 166.7 ± 3.9 Ma (Zhang et al., 2017a), suggesting garnet growth at ~177 Ma during peak metamorphism (T = 610-630°C, P = 2.4-2.6 GPa) followed by retrometamorphic rutile growth at ~167 Ma (Zhang et al., 2017a). The reconstructed P-T-t path points at subduction to a depth ≥ 85 km (Zhang et al., 2016).

The 8-m-thick metamorphic sole in amphibolite to greenschist facies found at the base of the Dongqiao ophiolite (Zhou et al., 1997) yielded Ar-Ar hornblende ages of 175-180 Ma. This age constrains the timing of obduction onset, whereas the Oxfordian-Kimmeridgian age of the Dongqiao Formation stratigraphically overlying the ophiolite indicates that ophiolite obduction terminated by ~163 Ma (Ma et al., 2020a).

Metamorphic rocks, mainly including orthogneiss, amphibolite, and minor paragneiss, marble, and quartzite, are common in the Amdo microcontinent, where they were intruded by two generations of granite yielding Early/Middle Jurassic (185-170) and Early Cretaceous ages (~112 Ma) (Guynn et al., 2006). The granitic protoliths of Amdo orthogneisses were formed in two episodes, between 915 and 840 Ma and between 530 and 470 Ma (Guynn et al., 2012). The age spectra of detrital zircons from the other metamorphic rocks are similar as those in Paleozoic strata of South Qiangtang. Although earlier studies associated metamorphism with Cambrian magmatic intrusion (Xu et al., 1985; Coward et al., 1988), modern studies demonstrated that peak metamorphism of Amdo metamorphic rocks took place in the latest Early Jurassic (~178 Ma; Guynn et al., 2006, 2013). Zircons with positive Eu anomalies from gneisses yielded older Early Jurassic U–Pb ages (~191 Ma), interpreted as peak metamorphic ages, whereas zircons with negative Eu anomalies yielded U–Pb ages of ~181 Ma, interpreted as retrograde metamorphic ages (Zhang et al., 2014).

This complex magmatic and metamorphic record indicates that the Amdo microcontinent was originally part of Pan-African Gondwana in the Paleozoic but was already a detached independent microcontinent situated between the South Qiangtang and Lhasa blocks and surrounded by oceanic branches during the Triassic. Mostly high K and high Ca type-I alkaline granites were generated between ca. 185 and 170 Ma during subduction of the Beila-Nagqu Ocean along the southern side of the Amdo microcontinent (Liu et al., 2017), which was also responsible for subduction-related high-pressure metamorphism.

10. Paleomagnetic constraints on the evolution of the Bangong-Nujiang Ocean

Paleomagnetic data can provide quantitative constraints on the relative position and motion of microcontinents on both sides of the BNS from the Permian to the Cretaceous and consequently important information on the opening, evolution, and closure of the Bangong-Nujiang Ocean. Notwithstanding numerous paleolatitude data have been provided (Table S6), large uncertainties remain in the paleopositions of the South Qiangtang and Lhasa blocks. As done above for geochronological data, we chose to select and consider only the most reliable paleomagnetic pieces of information based on criteria proposed by Meert et al. (2020) and using only data with R-value ≥ 5.

Because various regions of the central Tibetan Plateau have undergone rotation and strike-slip faulting following the middle Paleocene India-Asia collision (Lippert et al., 2011; Tong et al., 2015, 2017; Yang et al, 2015; Cao et al., 2017; Chen et al., 2017; Ma et al., 2017b; Meng et al., 2018), paleomagnetic data from the South Qiangtang and Lhasa blocks cannot be used directly to constrain the paleolatitudes of other areas. Based on a statistical comparison of data from the central and western parts of the South Qiangtang and Lhasa blocks, the paleolatitude of the two blocks was calculated using as reference points 32.5°N/83°E for the western part of the BNS and 32.5°N/92°E for the central part of the BNS (Fig. 9).

Selected paleomagnetic data from the central part of South Qiangtang indicate paleolatitudes of 12.0 ± 10.6°S during the Early Triassic (Zhou et al., 2019), of 28.2 ± 3.7°N during the Late Triassic (Song et al., 2012), of 32.8 ± 4.1°N during the Middle Jurassic (Cao et al., 2019), and of 23.1 ± 3.9°N during the Late Cretaceous (Meng et al., 2018). Paleomagnetic data from the western part of South Qiangtang indicate paleolatitudes of 27.0 ± 5.0°N at ~120-115 Ma (Cao et al., 2020), of 24.5 ± 5.1°N at ~110-100 Ma (Chen et al., 2017), and of 19.4 ± 3.5°N during the Late Cretaceous (Chen et al., 2017). These data imply that South Qiangtang was situated at subequatorial latitudes in the Southern Hemisphere during the Early Triassic and moved rapidly northwards across the Equator for over 4000 km in the Middle Triassic to reach subtropical latitudes of the Northern Hemisphere in the Late Triassic (Fig. 9a).

Paleomagnetic data from the central part of the Lhasa Block indicate paleolatitudes of 14.0 ± 9.8°S in the Early Permian (Ran et al., 2012), of 0.9 ± 2.4°S at ~180 Ma (ZY Li et al., 2016c), of 9.6 ± 8.1°N at ~120 Ma (Li et al, 2017d), of 16.4 ± 8.0°N at ~114 Ma (Sun et al., 2008), and of 15.5 ± 3.3°N in the Late Cretaceous (Achache et al., 1984; Tan et al., 2010; Sun et al., 2012; Cao et al., 2017). Paleomagnetic data from the western part of the Lhasa Block indicate paleolatitudes of 16.7 ± 4.7°S in the Early-Middle Triassic (Zhou et al., 2016), of 18.5 ± 12.4°S in the Late Triassic (Zhou et al., 2016), of 20.6 ± 5.0°N at ~132-106 Ma (Chen et al., 2012; Ma et al., 2014; Yang et al., 2015; Bian et al., 2017; Wang et al., 2021), and of 16.7 ± 3.0° N in the Late Cretaceous (Tang et al., 2013; Yang et al., 2015; Yi et al., 2015; Ma et al., 2017b; Ma et al., 2019; Bian et al., 2020). These data imply that the Lhasa Block remained at subequatorial latitudes in the Southern Hemisphere from Permian to Triassic times, moving rapidly northwards away from Gondwana and across the Equator during the Jurassic to reach a paleolatitude of 10-20°N in the Cretaceous (Fig. 9).

The Bangong-Nujiang Ocean, therefore, continued to expand during the Triassic north of the relative fixed Lhasa Block while South Qiangtang was rapidly moving northwards, reaching a maximum width of 4800 ± 900 km by the Late Triassic. After the Triassic, the Lhasa Block started to move rapidly northward towards South Qiangtang, while the Bangong-Nujiang Ocean was being consumed. The paleolatitudes of South Qiangtang and Lhasa blocks overlap at ~120-110 Ma and are undistinguished since then, indicating that no Bangong-Nujiang Ocean existed after the late Early

Cretaceous.

11.Microcontinents and seamounts within the Bangong-Nujiang suture zone

11.1 Microcontinents

The terms “terrane”, “block” or “microcontinent” are generally used rather loosely in the scientific literature to designate an independent geological entity containing arc and/or continental crust that testifies to an evolution distinct from neighboring arc or continental domains. The Amdo microcontinent is composed of a varied rock assemblage including gneiss, schist, quartzite, dacite, and igneous rocks of Jurassic–Cretaceous age, bounded by suture zones to the north and south (Bai et al., 2005; Sun et al., 2011; Guynn et al., 2006). Considering affinities of detrital-zircon U–Pb age spectra with South Qiangtang (Guynn et al., 2013), the Amdo microcontinent was envisaged as rifted originally from South Qiangtang, then collisionally assembled to South Qiangtang, and eventually collided with the Lhasa Block together with South Qiangtang (Guynn et al., 2006; Guynn et al., 2013; Zhu et al., 2013; Zhang et al., 2014b; Chen et al., 2015). Virtually identical Early Jurassic zircon ages were obtained from ophiolite-like sequences in both suture zones delimiting the Amdo microcontinent: 184 ± 2 Ma in the northern Dongqiao-Amdo suture (Wang et al., 2016), and 184 ± 1 Ma in the southern Nagqu (or Yilashan) suture (Huang et al., 2013). Guynn et al. (2006, 2013) suggested that granitoid intrusions in the Amdo microcontinent were generated by northward subduction of the Early-Middle Jurassic Beila-Nagqu Ocean. Based on Early Jurassic zircon ages from ophiolitic sequences, other researchers suggested instead that Jurassic oceanic crust newly formed in a back-arc basin between South Qiangtang and the Amdo microcontinent during northward subduction in the south, and that this back-arc basin closed in the Middle Jurassic (Kapp and DeCelles et al, 2019). Nearly 500 km along strike to the southeast of Amdo, the Tongka microcontinent is bounded by ophiolites on both sides and contains rock assemblages similar to those in the Amdo microcontinent. Basement rocks with crystallization ages of 500–492 Ma, were intruded by 186–174 Ma granitoid rocks and display metamorphic overprint at ~173 Ma (Li et al., 2017a).

A Dongkacuo microcontinent was also identified to the west of the Amdo microcontinent in the Dongqiao-Beila area, mainly based on the occurrence of two ophiolite belts occurring to the north (Dongqiao ophiolite) and to the south (Beila-Nagqu ophiolite), with other ophiolite slivers exposed in-between (Chen et al., 2002; Zeng et al., 2016b). The pioneering Sino-French study (Girardeau et al., 1984) suggested that all oceanic rocks between Dongqiao and Beila were nappes generated by southward thrusting from a single suture zone in the north, the southern Beila ophiolite being thus considered as allochthonous. The Dongqiao ophiolite in the north, however, appears to be older than the Beila ophiolite in the south (Table S4), and Paleozoic strata sandwiched between these two ophiolites show a stratigraphy similar as that of the Lhasa Block (Chen et al., 2002), suggesting that arc or continental basement may be present underneath. Considering that stratigraphic and paleontological similarities with North Lhasa during the Palaeozoic (Chen et al., 2002), the Dongkacuo microcontinent was generally considered as originally attached to North Lhasa and subsequently rifted northward possibly during the Triassic. Between 166 and 160 Ma, the Dongkacuo microcontinent collided with South Qiangtang, was overthusted by the Dongqiao ophiolite while northward subduction of the Beila-Nagqu oceanic branch was active along its south side (Li et al., 2015c; Zeng et al., 2016b; Li, 2019a; Li et al., 2020c).

11.2 Seamounts

Pillow basalts with alkaline intraplate geochemical signature associated with chert and limestone occur widely along the BNS and are commonly interpreted as seamounts (Zhu D.C. et al., 2006; Fan et al., 2014, 2021a; Wang et al., 2016) or oceanic plateaus within the Bangong-Nujiang Ocean (Zhang et al., 2014a; Zeng et al, 2021). These seamounts formed at different times. Around Gaize, one Middle Triassic, one Upper Triassic, and one Middle Jurassic seamount have been identified, together with OIB-type mafic rocks of Triassic to Middle Jurassic age (Table S4). The Middle Triassic seamount to the east of Gaize, termed Nare Island, includes phonolites yielding zircons with U–Pb ages of 242 and 239 Ma (Fan et al., 2017a). The Upper Triassic seamount in the northern part of the Gaize area, termed Gufeng Island, consists of basaltic basement of both MORB and OIB type, overlain by chert and limestone yielding conodonts of Norian (Late Triassic) age (Fan et al., 2017a). The Middle Jurassic seamount in the eastern part of Gaize, termed Nadong Island and lying in contact with the Mugagangri

Complex, contains gabbro, basalt, tuff, conglomerate, and carbonate layers yielding the coral *Cladophyllia* sp. (Xu et al., 2014; Fan et al., 2014).

Rock assemblages interpreted as remnants of Cretaceous oceanic islands are common in the BNS, with geochronological evidence (U–Pb zircon and whole-rock or single-mineral ^{40}Ar-^{39}Ar ages) indicating that OIB basalts formed between ~141 and 108 Ma (Zhu et al., 2006; Bao et al., 2007; Fan et al., 2014). Because of the low closure temperature of the ^{40}Ar-^{39}Ar system and widespread Early Cretaceous magmatism in North Lhasa, BNS, and South Qiangtang (Zhu et al., 2016), however, these Ar-Ar ages may have been reset. Even several U–Pb zircon ages failed to meet the requirements for reliability defined in Section 6. The most reliable ages from the Zhonggang and Zhongchang OIB rocks cluster between 141 and 135 Ma, but it is unclear whether these lavas were generated in oceanic or continental settings (Zhu et al., 2016).

Some criteria were proposed for the identification of intraplate oceanic islands (Fan et al., 2021a, c): (i) stratigraphy including basaltic basement and sedimentary cover; (ii) presence of debris-flow “collapse” conglomerates; (iii) lack of terrigenous contamination in limestone and other sedimentary and volcaniclastic rocks; (iv) OIB-type basaltic geochemistry; and (v) "blocks -in-matrix" facies. Although own field observations indicate that all these criteria are met for the Zhonggang Island, it must still be determined whether Zhonggang rocks truly document an oceanic seamount or were formed in a continental setting.

12. The opening of the Bangong-Nujiang Ocean

Major issues concerning the initial history of the Bangong-Nujiang Ocean remain unclear and controversial. When did break-up occur and sea-floor spreading began? There is general agreement that South Qiangtang lay to the north of this ocean, but what continental block lay to the south of it? One view, supported by Sino-French, Sino-British, and Sino-US research cooperation (Allègre et al., 1984; Yin and Harrison, 2000; Gehrels et al., 2011; Ali et al., 2013) is that South Qiangtang and Lhasa were both originally attached to the northern margin of India before South Qiangtang separated from the Lhasa Block (Fan et al., 2017b; Zeng et al., 2019). Another view is that South Qiangtang rifted away directly from India, while the Lhasa block was attached to the northern margin of Australia to the east of South Qiantang (Zhu et al., 2011; Wang et al., 2021) or perhaps between the northwestern corner of

India and Arabia to the west of South Qiangtang (e.g., Zhang et al., 2012; Hu et al., 2018). This latter view was based on zircon affinity of Upper Paleozoic sandstones and diamictites (Zhu et al., 2011; Wang et al., 2021). Although conclusive evidence is wanting, we favor the first viewpoint for the following reasons: (1) the Carboniferous-Lower Permian stratigraphy and fossil assemblages in the Lhasa Block and South Qiangtang are very similar (Smith and Xu, 1988; Sun, 1993; Zhang et al., 2019); (2) the Qiangtang-Panjal Large Igneous Province (290-285 Ma) extended from the northern margin of South Qiangtang (Zhai et al., 2013; Dan et al., 2021a) to the Tethys Himalaya (Garzanti et al., 1999), indicating that South Qiantang, Lhasa, and India were all still part of Gondwana in the Early Permian; (3) Middle Permian (~262 Ma) amphibole-rich, mantle-derived Yawa basalts in the Lhasa Block further support Permian rifting (Zeng et al., 2019); (4) age spectra of detrital zircons contained in Paleozoic to Triassic sandstones of the Lhasa Block (Xainza area) bear strong similarities with both South Qiangtang and the Tethys Himalaya but are sharply distinct from those in coeval sandstones from the northern margin of Australia (Fan et al., 2017b).

Regarding the timing of rifting and onset of sea-floor spreading in the Bangong-Nujiang Ocean, the available stratigraphic, paleontological, and geochronological evidence indicates that the Bangong-Nujiang Ocean existed between South Qiangtang and Lhasa at least since the Early Triassic (250-240 Ma) (Fig. 10). This is based on: (1) radiolarian cherts overlying oceanic crust dated as Anisian to Carnian (Wang et al., 2002), fixing a minimum age limit for generation of oceanic crust; (2) geochronological data on ophiolites including Re-Os isotope ages confirm that sea-floor spreading was ongoing since the earliest Triassic at least (260-220 Ma); (3) paleomagnetic data indicate that the Lhasa and Qiangtang blocks were still attached at Early Permian times, whereas a significant paleolatitude difference became manifest after the Middle Permian (Fig. 8). This is independently supported by the Qiangtang-Panjal large igneous province (290-285 Ma) extending from the northern margin of South Qiangtang (Zhai et al., 2013; Dan et al., 2021a) to India (Garzanti et al., 1999); (4) in the western part of South Qiangtang, the Lower Permian Tunlong Gongba Formation is unconformably overlain by the Upper Permian Jipu Ri'a Formation, and the Middle Permian is missing (Zhang et al., 2019). Such a stratigraphic change marked by a prolonged hiatus was interpreted as the result of continental rifting; (5) provenance analysis indicates that the Jipu Ri'a Formation contains basaltic and tuffaceous clasts and numerous Phanerozoic and ~260 Ma zircons, whereas the underlying passive-margin sandstones in the Lower Permian Tunlong Gongba

Formation contain mainly older zircon grains (Fan et al., 2021b); (6) both Middle Permian *Eopolydiexodina*-like and Late Permian warm-water *Palaeofusulina*-like faunas of South Qiangtang are significantly different from coeval assemblages in the Lhasa Block (Zhang et al., 2019).

These pieces of evidence combined indicate that the Bangong-Nujiang Ocean opened during the Permian. Early Permian rifting and break-up associated with massive outburst of Panjal-Qiangtang lavas was followed by a phase of slow (Red Sea and Gulf of Aden type) spreading in the Middle and Late Permian, and eventually by rapid sea-floor spreading in the Triassic.

13. Polarity of Bangong-Nujiang Ocean subduction

The subduction polarity of the Bangong-Nujiang Ocean has been the object of hot debate, especially concerning the existence of southward subduction (Hao et al., 2016b; Zhu et al., 2016; Li et al., 2018; Kapp and DeCelles, 2019). In our preferred scenario, subduction occurred in one stage: early oceanic northward subduction (~190-140 Ma) followed by continental collision neither northwards beneath South Qiangtang nor southwards beneath North Lhasa during the Early Cretaceous (~140-120 Ma) (Fig. 10).

13.1 Jurassic northward subduction

In the western segment of the BNS (Gaize area), geochronological data indicate that the oceanic-crust protoliths of eclogitic rocks with MORB and OIB characteristics were generated by sea-floor spreading at ~250 Ma and underwent subduction-related high-pressure metamorphism at ~177 Ma (Zhang et al., 2017a). This evidence of northward subduction of the Bangong-Nujiang Ocean is consistent with the presence of arc magmatism north of the Gaize-Rutog area between 170 and 148 Ma. During this period, numerous U–Pb zircon ages clustering between 170 and 160 Ma obtained from diabase and gabbro exposed in the Gaize-Rutog area indicate a period of extensive formation of oceanic crust. These ophiolitic rocks mainly display supra-subduction-zone (SSZ) geochemical features (Fig. 7), indicating that they are part of either forearc or back-arc ophiolitic sequences. All pieces of evidence combined indicate that northward subduction of Bangong-Nujiang oceanic lithosphere occurred in the western segment of the Rutog- Gaize area between the latest Early Jurassic and the close of the Jurassic (177-148 Ma).

The widespread Mugagangri Complex in the BNS was fed from South Qiangtang in the north and contains youngest detrital zircons of mostly Middle Jurassic ages, suggesting that the Mugagangri Complex is part of the accretionary complex grown during northward subduction of the Bangong-Nujiang Ocean (Zeng et al., 2016; Li et al., 2017b, 2019b; Sun et al., 2019; Ma et al., 2020a).

In the central segment of the BNS (Nima-Nagqu area), Jurassic arc magmatism is documented only sparsely. In the Amdo region, arc magmatism was dated as between 185 and 170 Ma, and subduction-related high-pressure metamorphism as between ~191 and 178 Ma (Guynn et al., 2006, 2013; Zhang et al., 2014b). In the southwestern Jiangcuo region, and locally farther to the west (Fig. 1b), arc-related rocks were dated as between 166 and 160 Ma, suggesting that oceanic subduction and arc magmatism may have taken place earlier in the east and later in the west and south. Northward subduction of the Bangong-Nujiang oceanic lithosphere occurred between the Early Jurassic and the earliest Late Jurassic (191-160 Ma) in the Nima-Nagqu area, and thus started 14 Ma earlier and ended 12 Ma earlier than in the Rutog-Gaize area to the west.

Arc magmatism along the southern margin of South Qiangtang is also testified by detrital zircons contained in Jurassic sandstones of the South Qiangtang Basin and BNS (i.e., Sewa Formation and Group 1 sandstones of the Mugagangri Complex; n = 132), yielding U–Pb ages between 193 and 162 Ma (Fig. 11). It is noteworthy that shallow-marine and deep-water Jurassic sedimentary facies in South Qiangtang and the BNS appear as more characteristic of a stable continental margin rather than of a forearc basin (Ma et al., 2020b), mainly because of limited magmatism associated with the Jurassic oceanic subduction.

13.2 Is there Early Cretaceous subduction: northward, southward, double-side or none?

The available data from North Lhasa do not support the existence of southward subduction of the Bangong-Nujiang Ocean during the Triassic-Jurassic. The Gaga mélange in the Nagqu area, suggested by provenance analysis to have been fed from the Lhasa Block, may represent the remnants of an accretionary wedge grown during southward subduction of the Bangong-Nujiang Ocean beneath the Lhasa Block (Lai et al., 2017). The depositional age of the Gaga mélange, however, is poorly constrained, and this unit may not be distinct from the Mugagangri Complex, as suggested by compositional, provenance, and structural similarities.

Based on magmatic, metamorphic, and stratigraphic data from the BNS, Qiangtang, and Lhasa domains, Zhu et al. (2009, 2016) documented the existence of the Caima-Duobuza-Rongma-Kangqiong-Amdo magmatic arc in western Qiangtang and of the Alongcuo-Yanhu-Daguo-Baingoin magmatic belt in North Lhasa, both active between 140 and 120 Ma and characterized by subduction-related geochemical features. Although the Alongcuo-Yanhu-Daguo-Baingoin magmatic belt may be explained by northward subduction of Neo-Tethyan lithosphere (e.g., Zhang et al., 2012), Zhu et al. (2009) and Li et al. (2018) considered that southward subduction of Bangong-Nujiang lithosphere better explains the spatial and temporal distribution of magmatic rocks in Central and North Lhasa. Double-sided subduction of Bangong-Nujiang Ocean lithosphere was thus proposed and envisaged to have been followed by slab break-off at 120-110 Ma based on geochemical characteristics of the Lower Cretaceous Qushenla Formation (Zhu et al., 2016). Further information is offered by the Zenong Group, which unconformably overlies Permian limestones documenting the onset of a new tectono-magmatic regime in Central and North Lhasa. These volcanic rocks, loosely constrained as Early Cretaceous in age (140-110 Ma), display enrichment in LREE and large ionic lithophile elements (LILE) such as Rb and Ba, and depletion in high field strength elements (HFSE) such as Nb, Ta and Ti, indicating a subduction-related arc origin. Negative zircon εHf(t) values (from -12.0 to -1.6) and εNd(t) values (from -10.6 to -7.1) suggest that the magma originated from melting of Palaeoproterozoic-Mesoproterozoic Lhasa basement with addition of mantle components. Southward subduction of Bangong-Nujiang oceanic lithosphere was thus indicated as the most plausible cause for Zenong Group magmatism (Zhu et al., 2009), although low-angle northward subduction of Neo-Tethyan lithosphere cannot be ruled out (Coulon et al., 1986; Kapp et al., 2005).

It must be pointed out that Early Cretaceous southward subduction of the Bangong-Nujiang Ocean was mainly proposed based on petrological and geochemical studies of both Zenong volcanic rocks in Central Lhasa and Alongcuo-Yanhu-Daguo-Baingoin magmatic rocks in North Lhasa (Zhu et al., 2009, 2016; Li et al., 2018). Other supporting pieces of evidence are however lacking, including: (1) no trench-arc system has been identified yet between these arc-type magmatic rocks and the Bangong-Nujiang ophiolites; (2) the Upper Jurassic-Lower Cretaceous Lagongtang Formation was sourced from

Central and South Lhasa (Lai et al., 2022), and thus cannot represent forearc sediments fed from such a hypothetic volcanic arc; (3) no sedimentary unit in the Mugagangri Complex was sourced from Lower Cretaceous arc-type rocks in Central and North Lhasa (see Section 4).

These various pieces of evidence can be explained in two ways. In the first scenario, the Bangong-Nujiang Ocean was finally consumed by double-sided subduction beneath the Lhasa Block in the south and beneath South Qiangtang in the north, and its closure was completed by ~120 Ma. In the second scenario, the Caima-Duobuza-Rongma-Kangqiong-Amdo magmatic arc in western Qiangtang and the Alongcuo-Yanhu-Daguo-Baingoin magmatic belt in North Lhasa, both active between 140 and 120 Ma, are considered as syncollisional, as Linzizong volcanic rock continued to be emplaced in South Lhasa well after the India-Asia collision onset (Mo et al., 2008; Zhu et al., 2019a). If so, then closure of the Bangong-Nujiang Ocean was already complete by 140 Ma and followed by widespread post-collisional Early Cretaceous magmatism. In this paper, the second scenario is preferred when considering sedimentological and stratigraphical data (see discussion below).

14. Timing of Lhasa-Qiangtang collision onset

The timing of initial collision between the Lhasa and Qiangtang Blocks is hotly debated (see Ma et al., 2017b; Li et al., 2019b; Shi et al., 2020). Initial continental collision is here defined as the time when oceanic lithosphere is eventually consumed at a point where the two opposite continental margins come into direct contact and continental subduction therefore begins (Hu et al., 2016; 2017).

In the Nima-Nagqu area, the Amdo and Dongkacuo microcontinents began to collide with South Qiangtang at 166-163 Ma (Callovian, Middle Jurassic) resulting in the closure of the Dongqiao-Amdo oceanic seaway. Supporting geological evidence includes: (1) the upper Bathonian (~166 Ma) Biluoco Formation unconformably overlies the Buqu Formation, testifying to folding and thrusting in South Qiangtang; (2) the Upper Jurassic (Oxfordian to Kimmeridgian, 163-152 Ma) sandstones of the Shamuluo Formation were deposited in shallow-water environments on top of the Mugagangri Complex within the BNS, indicating that the Dongqiao-Amdo oceanic seaway was closed by that time; (3) Group 2 sandstones of the Mugagangri Complex in the BNS, and the Biluoco Formation in South Qiangtang contain abundant sedimentary clasts, indicating tectonic inversion, uplift, and erosion of South Qiangtang Basin strata; (4) the Dongqiao Formation non conformably overlies the ophiolite, indicating that obduction of the Dongqiao Ophiolite was completed by ~163 Ma (Ma et al., 2020a). Geological information is insufficient to equally robustly constrain the closure time of the Beila-Nagqu southern oceanic branch in the Nima-Nagqu area of the BNS.

In North Lhasa, the Lower Cretaceous (~120 Ma) shallow-marine clastic deposits of the and Duba and Duoni formations were fed from both South Qiangtang and Lhasa blocks (Lai et al., 2019b), which indicates that collision between North Lhasa and South Qiangtang was already completed. This is confirmed by paleomagnetic data from the Nima-Nagqu area (Fig. 10).

In the Rutog-Gaize area of the BNS, where no continent existed between North Lhasa and South Qiangtang, collision onset is constrained to have occurred at latest Jurassic times (150-145 Ma), based on the following lines of evidence: (1) the uppermost Jurassic to lowermost Cretaceous Yaduo Formation exposed in the Gaize area and deposited on a deep-sea fan adjacent to the southern part of the Mugagangri Complex was sourced from South Qiangtang, and is interpreted to represent trench deposits in the initial stage of the Lhasa-South Qiangtang collision; (2) Latest Jurassic-Early Cretaceous tectonic shortening is documented in the Duoma area of South Qiangtang (Raterman et al., 2014); (3) Upper Jurassic sandstones of the Gamulong, Shamuluo, and Yaduo formations, together with Group 2 sandstones of the Mugagangri Complex in the BNS, contain abundant sedimentary clasts sourced from South Qiangtang.

All data considered, the initial collision between North Lhasa and South Qiangtang most plausibly took place at the close of the Jurassic (150-145 Ma). In the central segment of the Nima-Nagqu area, the Dongqiao-Amdo oceanic seaway closed in the latest Middle Jurassic (166-163 Ma), a few million years earlier than the Beila-Nagqu oceanic seaway. In this framework, the widespread Early Cretaceous (140-120 Ma) Caima-Duobuza-Rongma-Kangqiong-Amdo arc magmatism in western Qiangtang, the Qushenla Formation in the BNS, and the Alongcuo-Yanhu-Daguo-Baingoin magmatic belt in North Lhasa are all considered the products of syn-collisional magmatism associated with the Lhasa-Qiangtang collision.

15. The history of the Bangong-Nujiang Ocean

An evolutionary model for the Bangong-Nujiang Ocean is outlined here based on the geological evidence summarized above (Figs. 12, 13).

Faunal assemblages in Lhasa and South Qiangtang started to diverge since the late Early Permian, indicating that breakup between the Lhasa Block and South Qiangtang took place around mid-Early Permian times (Zhang et al., 2019). It must be noted that, within the limits of biostratigraphic and radiometric methods, this age coincides with the age of break-up between India and a northern peri-Gondwanian microcontinent (Garzanti et al., 1996; Sciunnach and Garzanti, 2012). Early Permian rifting is supported by the occurrence of a major stratigraphic hiatus between the Lower Permian Tunlong Gongba and the Upper Permian Jipu Ri'a Formation in the western part of South Qiangtang, which plausibly corresponds to the break-up unconformity consistently with the provenance change documented by the Jipu Ri'a Formation (Fan et al., 2021b). Mafic dykes are widely developed in northern South Qiangtang (Zhai et al., 2013), as part of the large Qiangtang-Panjal volcanic province affecting a vast region all the way to northern India (Vannay and Spring, 1993; Dan et al., 2021a).

Sea-floor spreading was fully active throughout the Triassic, as indicated by Re-Os ages from ophiolites, by radiolarian ages of the overlying cherts, and by widely diverging paleolatitudes (up to 40° degrees) between the Lhasa Block and South Qiangtang. Triassic paleogeography, however, is poorly constrained. A ≥ 4000 km-wide Bangong-Nujiang Ocean expanded during this period, between the Lhasa Block that remained close to 10°S while South Qiangtang drifted rapidly towards tropical northern latitudes (Fig. 9). No firm evidence has been provided so far to locate the Amdo and Dongkacuo microcontinents within this vast oceanic domain. In a speculative reconstruction partly based on Guynn et al. (2006) and Zhang et al. (2014b), the Amdo microcontinent is envisaged to have been separated from South Qiangtang in the Early Jurassic by back-arc rifting, resulting in the formation of the Amdo oceanic branch, whereas the Dongkacuo microcontinent may have rifted away from North Lhasa in the Triassic.

The Bangong-Nujiang oceanic lithosphere began to subduct northward beneath the Amdo microcontinent around 190 Ma, as well documented by the age and character of arc-related magmatic and high-pressure metamorphic rocks (Guynn et al., 2006; Zhang et al., 2014b; Wang et al., 2016; Kapp and DeCelles, 2019). The Dongqiao-Amdo oceanic seaway separating the Amdo and South Qiangtang may have been a back-arc basin. The Dongqiao ophiolite was obducted southward onto the Dongkacuo microcontinent at ~163 Ma. and the Biluoco conglomerates accumulated in South Qiangtang around 166 Ma (Ma et al., 2017a, 2020a). The Dongkacuo arc-related magmatic rocks dated as 166-160 Ma were generated by northward subduction of the Beila-Nagqu oceanic seaway, envisaged here to represent the main Bangong-Nujiang Ocean (Fig. 13). In the Middle-Late Jurassic, South Qiantang was affected by intense structural deformation, while the Mugagangri Complex started to grow by subduction accretion. In the south, the northward subduction of the Beila- Nagqu oceanic branch continued possibly until the latest Jurassic, as indicated by the youngest ophiolite radiometric ages (Zhong et al., 2017, 2018). The Mugagangri Complex and Gajia mélange may have grown further during this stage, when deposition of the Suowa Formation documented the cessation of marine sedimentation in South Qiangtang. In the Late Jurassic, the Dongqiao and Shamuluo formations were deposited on top of the Dongqiao ophiolite and Mugagangri Complex, respectively, thus sealing the stage of subduction-accretion, while the deep-sea-fan turbidites of the Gamulong Formation were deposited.

In the Rutog-Gaize area (western segment of the BNS), a slightly younger episode of oceanic subduction followed by the exhumation of high-pressure rocks between ~170 Ma and 150 Ma is testified by the Dongcuo eclogite and granulite (Zhang et al., 2016; Zhang et al., 2017a) and by calc-alkaline magmatism generated by northward subduction of Bangong-Nujiang oceanic lithosphere (Fig. 1). The magmatic gap between 150 and 140 Ma, together with sedimentation of the Upper Jurassic-Lower Cretaceous Shamuluo Formation to the south of the Zhonggang oceanic island (Li et al., 2017b, 2019b), marked the end of this oceanic subduction stage.

Collision between North Lhasa and South Qiangtang began most probably at the close of the Jurassic (150-145 Ma). In the Late Jurassic-Early Cretaceous, deep-water sediments continued to accumulate in the BNS (Yaduo and Wuga formations; Li et al., 2017c; Luo et al., 2019), which are envisaged as syncollisional trench deposits. At this time, shallow-marine shelf sedimentation characterized the northern margin of the Lhasa Block, when the Lagongtang Formation was fed from erosion of the Yeba arc and of pre-Jurassic sedimentary rocks to the south (Lai et al., 2022).

In the Early Cretaceous, volcanic rocks of the Qushenla Formation were widely emplaced across the BNS, where marine seaways disappeared by 120 Ma, as documented in the Beila-Maqian (Zhu et al., 2019b), eastern Selincuo (Hu et al., 2020), northern Nima (Kapp et al., 2007), and Gaize (Chen et al, 2017) areas. A shallow-marine environment persisted longer in North Lhasa, where the Duoni and Duba formations were sourced from the conjugate Lhasa and Qiangtang Blocks, respectively. The residual sea retreated by ~113 Ma (Lai et al., 2019b), but renewed widespread marine transgression is documented by the thick Langshan limestones accumulated on North Lhasa between 113 and 99 Ma (Xu et al., 2020, 2022).

Igneous rocks were emplaced on both sides of the BNS between ~140 and 110 Ma, including the Zenong Group widely exposed in Central Lhasa and the Baingoin granites, documenting a phase of extensive magmatism in the region (Zhu et al., 2016). These orogenic igneous rocks are considered as the product of syncollisional to post-collisional processes generated after the transition from oceanic subduction to intracontinental convergence. Many economic ores were formed in the western part of the BNS at this time, followed by tectonic uplift starting at ~92 Ma (Sun et al., 2015; Lai et al., 2019a). If the Lhasa-Qiangtang collision indeed began close to the Jurassic/Cretaceous boundary, then porphyry-type deposits in the western BNS (Duolong ore, 120-110 Ma, Lin et al., 2019; Yang et al., 2020) and orogenic gold deposits (Shangxu ore, 136 Ma, Fang et al., 2020) were all formed during the syncollisional stage rather than during the oceanic-subduction stage. Extensive syncollisional magmatism on both sides of, and inside the BNS created the conditions for extensive mineralization.

16. Conclusions and Perspectives

A major and still largely unexplained feature of the Tethyan realm is the multistep rifting from the northern part of the Gondwana Supercontinent of ribbon-like microcontinental blocks of various sizes that drifted rapidly northward to converge and be eventually accreted in succession to Eurasia, the final one being India (Şengör, 1979; Dercourt and Vrielynck, 1993; Wan et al., 2019; Wu et al., 2020). During multiple rifting episodes, not only a larger and persistent ocean such as Neo-Tethys but also a series of smaller oceanic seaways were generated and consumed. Some of these seaways were short-lived, and the reconstruction of their geometry, location, and origin (i.e., mid-ocean ridge or supra-subduction) represents a hard geological challenge. We faced this challenge by summarizing and discussing all available geological evidence, including stratigraphic, paleontological, sedimentological, petrological, structural, paleomagnetic, and geochronological data from any type of rocks exposed in the BNS and adjacent regions, with the final goal to clarify as far as possible the history of the Bangong-Nujiang Ocean from its birth to its growth and final closure. These are our main conclusions:

(1) based on stratigraphic, paleontological, sedimentological and paleomagnetic evidence,

rifting between the Lhasa Block and South Qiangtang took place during the Early Permian, roughly at the same time of break-up and opening of Neo-Tethys north of India;

(2) paleomagnetic data suggest that the Bangong-Nujiang Ocean was still a narrow proto-oceanic basin in the Middle and Late Permian. As two continental ribbons similar perhaps to the Agulhas Plateau off the southern margin of Africa (Ben-Avraham et al., 1995), the Amdo and Dongkacuo microcontinents may have detached at this early rifting stage, most probably from South Qiangtang and North Lhasa, respectively;

(3) the Triassic was a period of rapid sea-floor spreading in the Bangong-Nujiang Ocean. The Lhasa Block remained at low southern latitudes, whereas South Qiangtang drifted rapidly away reaching tropical northern latitudes during the Triassic. The north–south width of the Bangong-Nujiang Ocean then reached 4000 km according to paleomagnetic data.

(4) the northward subduction of the Bangong-Nujiang Ocean began in the Early Jurassic, earlier in the eastern Amdo region (~190 Ma) than in the western Gaize region (~170 Ma). This phase of oceanic subduction lasted between 30 and 40 Ma, as documented by Amdo and Dongkacuo arc magmatism, Amdo and Dongcuo metamorphic rocks, and growth of the Mugagangri Complex;

(5) the Dongqiao-Amdo oceanic seaway, representing the northern branch of the Bangong-Nujiang Ocean, closed when the Amdo and Dongkacuo microcontinents collided with South Qiangtang in the latest Middle Jurassic (166-163 Ma). The Beila-Nagqu oceanic seaway, representing the main southern branch of the Bangong-Nujiang Ocean, closed when the Lhasa and Qiangtang Blocks collided in the latest Jurassic (150-145 Ma). Syncollisional sediments were incorporated into the Mugagangri Complex;

(6) the Early Cretaceous (140-120 Ma) arc-type igneous rocks widely distributed across the Lhasa-Qiangtang collisional zone document large-scale syncollisional to post-collisional magmatism;

(7) in the late Early Cretaceous (120-100 Ma), the disappearance of marine seaways is testified by widespread deposition of continental red beds across the BNS, where a suite of volcanic rocks (Qushenla Formation) was emplaced. The Langshan Formation documents the last marine

ingression on North Lhasa between 113 and 99 Ma, followed by a stage of intracontinental convergence that led to tectonic inversion and initial surface uplift of the Tibetan Plateau.

The efforts made to unravel the paleogeographic evolution of the Bangong-Nujiang Ocean and surrounding landmasses indicated criteria that may turn out to be useful when similar geological problems are tackled:

（1） How can the birth of an ancient ocean be most accurately dated?

Theoretically, this question can be answered by finding and dating the oldest piece of oceanic crust. Oceanic lithosphere, however, is generally and even completely consumed by subduction (Stern, 2004). Moreover, obtaining radiometric ages from ultramafic and mafic rocks is challenging. Both Re-Os ages of peridotites and cumulates and biostratigraphic ages of cherts overlying the ophiolitic sequence were obtained from the BNS, but they can only fix a minimum age for the initiation of sea-floor spreading. A more profitable, although indirect approach, is the detailed stratigraphic study of the two conjugate rifted margins, where the break-up unconformity can be detected and dated (e.g., Sciunnach and Garzanti, 2012 and references therein). In the case of active rifting associated with the eruption of a "mantle plume" (White and McKenzie, 1989), the age of continental flood basalts provides a further constraint on the geological evolution from the rift stage to the break-up stage. This is the case of the Qiangtang-Panjal large igneous province (Garzanti et al., 1999; Dan et al., 2021a).

（2） How can the timing of subduction initiation be effectively determined?

Arc magmatism and high-pressure metamorphic rocks provide the key evidence of oceanic subduction. The significance of mélange units (e.g., Mugagangri Complex) is more difficult to understand, because of undetermined effects of tectonic erosion, disruption by tectonic deformation, difficulties in dating sedimentation and accretion episodes, and continuing growth during the early syncollisional stage.

（3） How can the timing of collision onset be effectively determined?

Arc magmatism may continue for long, and even reach climax well after the onset of continent-continent or arc-continent collision (e.g., Zhu et al., 2019b). Cessation of arc magmatism, therefore, cannot be used for an accurate determination of collision onset. The same is true for the cessation of marine sedimentation in the intervening seaways, which can persist for tens of million years after the first continent-continent or arc-continent contact, as seen for instance in the Taiwan Strait, Timor Sea, or Persian Gulf. Paleomagnetic data provide useful constraints, but are seldom precise enough (e.g., Hu et al., 2016). The best criterion proves to be the combination of biostratigraphic and detrital-radiometric dating of siliciclastic deposits fed from both colliding margin at the same time (e.g., DeCelles et al., 2014). This is the case of the Yaduo Formation in the BNS, which is adjacent to North Lhasa but sourced from South Qiangtang (Hu et al., 2017). Interfingering of strata fed from both colliding continental margins, however, may occur somewhat earlier than actual collision onset if the trench is overfilled and bypassed by turbiditic flows that may spread oceanward onto the abyssal plain for some hundreds of kilometers (e.g., Contreras-Reyes et al., 2010).

Looking ahead, there are still a number of major unsolved issues related to the evolution of the Bangong-Nujiang Ocean:

(1) much has still to be discovered concerning rifting and opening of the Bangong-Nujiang Ocean, and its relationships with the coeval opening of Neo-Tethys in the south. The Lhasa Block and South Qiangtang are narrow, ribbon-like microcontinents detached in succession from the northern margin of Gondwana, thus replicating through time a plate-tectonic process that remains unclear (Gaetani et al., 2003). Zhu et al. (2013) suggested that southward subduction of the Bangong-Nujiang Ocean led to the separation of Lhasa from Australia. Gaina et al. (2003) called upon the interaction between a mantle plume and an oceanic ridge and Schneider et al. (2003) proposed a pull-apart mechanism for the initial formation of the Bangong-Nujiang Ocean. These theories, however, remain speculative and not firmly grounded on stratigraphic, petrological, and structural evidence. One fruitful way to better understand the complexities of the rifting process that gave rise to the Bangong-Nujiang Ocean is the comparison with modern examples of microcontinents, such as the Agulhas Plateau, the Seychelles, or the Elan Blank in the Indian Ocean;

(2) the nature and origin of rock assemblages inferred to represent seamounts and consisting of basalt with intraplate-type geochemical features, limestone without terrigenous contamination, and slumped breccia, is unclear. For instance, the Zhonggang-Kangqiong oceanic island, dated as 141-135

Ma (Fan et al., 2021a; Zeng et al., 2021), satisfies all criteria to be identified as a seamount. Geological evidence, however, suggests that the earliest Cretaceous was the time of double-sided subduction and final closure of the Bangong-Nujiang Ocean rather than a period of open-ocean subduction when trench-seamount collisions would be expected to occur;

(3) the variability of the Bangong-Nujiang suture along strike, and especially its western and eastern terminations, are poorly documented. Triassic-Jurassic paleomagnetic data for the western Lhasa Block are also wanting;

(4) the configuration of the Bangong-Nujiang Ocean and of its distinct branches (e.g., did the Dongqiao-Amdo oceanic seaway in the north or the Beila-Nagqu oceanic seaway in the south represent the main Bangong-Nujiang Ocean?), the origin and location of small microcontinents (i.e., Amdo and Dongkacuo), and the possible occurrence of back-arc basin remain poorly understood and lively debated.

Declaration of Competing Interest

The authors declare that they have no known competing financial interests or personal relationships that could have appeared to influence the work reported in this paper.

Acknowledgements

This research was supported by the National Natural Science Foundation of China (Grant No. 91755209 and 41888101). We are very grateful to Chengshan Wang, Fuyuan Wu, Juxing Tang, Qiang Wang, Ling Chen, Dicheng Zhu, Yalin Li, Qinggao Zeng, Rendeng Shi, Qingguo Zhai, Yichun Zhang, Tiangen Dai, Jianjun Fan, and Jiangang Wang for beneficial discussions, and warmly thank Lin Li (University of Arizona, USA) and Shun Li (China) for their very careful constructive comments.

References

Achache, J., Courtillot, V. and Xiu, Z.Y., 1984. Paleogeographic and tectonic evolution of southern Tibet since Middle Cretaceous time: New paleomagnetic data and synthesis. Journal of Geophysical Research: Solid Earth, 89(B12): 10311-10339.

Ali, J.R., Cheung, H.M., Aitchison, J.C. and Sun, Y., 2013. Palaeomagnetic re-investigation of Early Permian rift basalts from the Baoshan Block, SW China: constraints on the site-of-origin of the Gondwana-derived eastern Cimmerian terranes. Geophysical Journal International, 193(2): 650-663.

Allègre, C.J., Courtillot, V., Tapponnier, P., Hirn, A., Mattauer, M., Coulon, C., Jaeger, J.J., Achache, J., Scharer, U., Marcoux, J., Burg, J.P., Girardeau, J., Armijo, R., Gariepy, C., Gopel, C., Li, T.D., Xiao, X.C., Chang, C.F., Li, G.Q., Lin, B.Y., Teng, J.W., Wang, N.W., Chen, G.M., Han, T.L., Wang, X.B., Den, W.M., Sheng, H.B., Cao, Y.G., Zhou, J., Qiu, H.R., Bao, P.S., Wang, S.C., Wang, B.X., Zhou, Y.X. and Xu, R.H., 1984. Structure and evolution of the Himalaya-Tibet orogenic belt. Nature, 307(5946): 17-22.

Bai, Z., Xu, D., Zhang, X., Zhu, G. and Sun, L., 2005. Geological report of the 1:250, 000 regional geological survey in Amdo area (in Chinese).

Bao, P., Xiao, X., Su, L. and Wang, J., 2007. Petrological, geochemical and chronological constraints for the tectonic setting of the Dongco ophiolite in Tibet. Science in China Series D: Earth Sciences, 50(5): 660-671.

Ben-Avraham, Z., Hartnady, C. and Le Roex, A., 1995. Neotectonic activity on continental fragments in the southwest Indian Ocean: Agulhas Plateau and Mozambique Ridge. Journal of Geophysical Research: Solid Earth, 100(B4): 6199-6211.

Bian, W., Yang, T., Ma, Y., Jin, J., Gao, F., Zhang, S., Wu, H. and Li, H., 2017. New Early Cretaceous palaeomagnetic and geochronological results from the far western Lhasa terrane: Contributions to the Lhasa-Qiangtang collision. Scientific Reports, 7(1): 1-14.

BouDagher-Fadel, M.K., Hu, X., Price, G.D., Sun, G., Wang, J.-G. and An, W., 2017. Foraminiferal biostratigraphy and palaeoenvironmental analysis of the mid-cretaceous limestones in the southern Tibetan Plateau. Journal of Foraminiferal Research, 47(2): 188-207.

Cao, M., Qin, K., Li, G., Li, J., Zhao, J., Evans, N.J. and Hollings, P., 2016. Tectono-magmatic evolution of Late Jurassic to Early Cretaceous granitoids in the west central Lhasa subterrane, Tibet. Gondwana Research, 39: 386-400.

Cao, Y., Sun, Z., Li, H., Pei, J., Jiang, W., Xu, W., Zhao, L., Wang, L., Li, C., Ye, X. and Zhang, L., 2017. New Late Cretaceous paleomagnetic data from volcanic rocks and red beds from the Lhasa terrane and its implications for the paleolatitude of the southern margin of Asia prior to the collision with India. Gondwana Research, 41: 337-351.

Cao, Y., Sun, Z., Li, H., Pei, J., Liu, D., Zhang, L., Ye, X., Zheng, Y., He, X., Ge, C. and Jiang, W., 2019. New paleomagnetic results from Middle Jurassic limestones of the Qiangtang terrane, Tibet: constraints on the evolution of the Bangong-Nujiang Ocean. Tectonics, 38(1): 215-232.

Cao, Y., Sun, Z., Li, H., Ye, X., Pan, J., Liu, D., Zhang, L., Wu, B., Cao, X., Liu, C. and Yang, Z., 2020. Paleomagnetism and U-Pb geochronology of Early Cretaceous volcanic rocks from the Qiangtang block, Tibetan Plateau: Implications for the Qiangtang-Lhasa collision. Tectonophysics, 789: 228500.

Chang, C.F. and Zheng, X., 1973. Discussion on the geological structural features of the Mt. Everest area in southern Tibet of China and the formation of the east-west mountain series of the Qinghai-Tibet Plateau. Geological Journal, 8(1): 1-12.

Chen, L., Mattioli, E., Da, X., Jenkyns, H.C., Zhu, Z., Xu, G. and Yi, H., 2019. Calcareous nannofossils from the Jurassic black shales in the Qiangtang basin, northern Tibet (China): New records of stratigraphic ages and palaeoceanography. Newsletters on Stratigraphy, 52: 55-72.

Chen, S.S., Shi, R.D., Zou, H.B., Huang, Q.S., Liu, D.L., Gong, X.H., Yi, G.D. and Wu, K., 2015. Late Triassic island-arc–back-arc basin development along the Bangong–Nujiang suture zone (central Tibet): Geological, geochemical and chronological evidence from volcanic rocks. Lithos, 230: 30-45.

Chen, W., Yang, T., Zhang, S., Yang, Z., Li, H., Wu, H., Zhang, J., Ma, Y. and Cai, F., 2012. Paleomagnetic results from the Early Cretaceous Zenong Group volcanic rocks, Cuoqin, Tibet, and their paleogeographic implications. Gondwana Research, 22(2): 461-469.

Chen, W., Zhang, S., Ding, J., Zhang, J., Zhao, X., Zhu, L., Yang, W., Yang, T., Li, H. and Wu, H., 2017. Combined paleomagnetic and geochronological study on Cretaceous strata of the Qiangtang terrane, central Tibet. Gondwana Research, 41: 373-389.

Chen, Y., Chen, G., Zhang, K., Zhao, S., Liu, B. and Suolang, G., 2002. Geological report of the 1:250, 000 regional geological survey in Baingoin area (in Chinese).

Chen, Y., Ding, L., Li, Z., Laskowski, A.K., Li, J., Baral, U., Qasim, M. and Yue, Y., 2020. Provenance analysis of Cretaceous peripheral foreland basin in central Tibet: Implications to precise timing on the initial Lhasa-Qiangtang collision. Tectonophysics, 775: 228311.

Cheng, X., Wu, H., Guo, Q., Hou, B., Xia, L., Wang, H., Diao, Z., Huo, F., Ji, W., Li, R., Chen, S., Zhao, Z. and Liu, X., 2012. Paleomagnetic results of Late Paleozoic rocks from northern Qiangtang Block in Qinghai-Tibet Plateau, China. Science China Earth Sciences, 55(1): 67-75.

Contreras-Reyes, E., Flueh, E.R. and Grevemeyer, I., 2010. Tectonic control on sediment accretion and subduction off south central Chile: Implications for coseismic rupture processes of the 1960 and 2010 megathrust earthquakes. Tectonics, 29(6).

Coward, M.P., Kidd, W., Yun, P., Shackleton, R.M. and Hu, Z., 1988. The structure of the 1985 Tibet geotraverse, Lhasa to Golmud. Philosophical Transactions of the Royal Society of London. Series A, Mathematical and Physical Sciences, 327(1594): 307-333.

Dan, W., Wang, Q., Murphy, J.B., Zhang, X.-Z., Xu, Y.-G., White, W.M., Jiang, Z.-Q., Ou, Q., Hao, L.-L. and Qi, Y., 2021a. Short duration of Early Permian Qiangtang-Panjal large igneous province: Implications for origin of the Neo-Tethys Ocean. Earth and Planetary Science Letters, 568: 117054.

Dan, W., Wang, Q., White, W.M., Li, X.-H., Zhang, X.-Z., Tang, G.-J., Ou, Q., Hao, L.-L. and Qi, Y., 2021b. Passive-margin magmatism caused by enhanced slab-pull forces in central Tibet. Geology, 49(2): 130-134.

DeCelles, P.G., Kapp, P., Gehrels, G.E. and Ding, L., 2014. Paleocene- Eocene foreland basin evolution in the Himalaya of southern Tibet and Nepal: Implications for the age of initial India- Asia collision. Tectonics, 33(5): 824-849.

Deng, J., Yuan, Z., Yu, J., Du, C., Tang, Z., Sun, S., Lv, X., Zhong, W., Wan, C. and Zhong, J., 2017. New discovery of the basal conglomerate in the Upper Jurassic—Lower Cretaceous Shamuluo Formation in western part of Bangong Lake—Nujiang River Suture Zone and its geological significance. Geol. Rev., 63(2).

Deng, S., Lin, B., Zhang, H., Wang, T. and Hu, Z., 2020. Geochronology and Ore Prospecting Potential of Qushenla Formation in Middle Segment of Bangong Co-Nujiang Suture Zone, Tibet. Earth Science, 45(3): 776-788. [in Chinese with English abstract]

Dercourt, J. and Vrielynck, B., 1993. Atlas Tethys paleoenvironmental maps. Gauthier-Villars.

Dewey, J.F., Shackleton, R.M., Chang, C. and Sun, Y., 1988. The tectonic evolution of the Tibetan Plateau. Philosophical Transactions of the Royal Society of London A: Mathematical, Physical and Engineering Sciences, 327(1594): 379-413.

Dong, Y.-L., Wang, B.-D., Zhao, W.-X., Yang, T.-N. and Xu, J.-F., 2016. Discovery of eclogite in the Bangong Co–Nujiang ophiolitic mélange, central Tibet, and tectonic implications. Gondwana Research, 35: 115-123.

Fan, J.-J., Li, C., Wang, M., Liu, Y.-M. and Xie, C.-M., 2017a. Remnants of a Late Triassic ocean island in the Gufeng area, northern Tibet: Implications for the opening and early evolution of the Bangong–Nujiang Tethyan Ocean. Journal of Asian Earth Sciences, 135: 35-50.

Fan, J.-J., Li, C., Xie, C.-M. and Wang, M., 2014. Petrology, geochemistry, and geochronology of the Zhonggang ocean island, northern Tibet: implications for the evolution of the Banggongco–Nujiang oceanic arm of the Neo-Tethys. International Geology Review, 56(12): 1504-1520.

Fan, J.-J., Niu, Y., Liu, Y.-M. and Hao, Y.-J., 2021a. Timing of closure of the Meso-Tethys Ocean: Constraints from remnants of a 141–135 Ma ocean island within the Bangong–Nujiang Suture Zone, Tibetan Plateau. Geological Society of America Bulletin, 133(9-10): 1875-1889.

Fan, J.-J., Niu, Y., Luo, A.-B., Xie, C.-M., Hao, Y.-J. and Liu, H.-Y., 2021b. Timing of the Meso-Tethys Ocean opening: Evidence from Permian sedimentary provenance changes in the South Qiangtang Terrane, Tibetan Plateau. Palaeogeography, Palaeoclimatology, Palaeoecology, 567: 110265.

Fan, J.J., Li, C., Niu, Y., Xie, C.M. and Wang, M., 2021c. Identification method and geological significance of intraplate ocean island seamount fragments in orogenic belt. Earth Science, 46(2): 381–404. [in Chinese with English abstract]

Fan, J.J., Li, C., Wu, H., Zhang, T., Wang, M., Chen, J.W. and Xu, J.X., 2016. Late Jurassic adakitic granodiorite in the Dong Co area, northern Tibet: Implications for subduction of the Bangong–Nujiang oceanic lithosphere and related accretion of the Southern Qiangtang terrane. Tectonophysics, S0040195116304796.

Fan, S., Ding, L., Murphy, M.A., Yao, W. and Yin, A., 2017b. Late Paleozoic and Mesozoic evolution of the Lhasa Terrane in the Xainza area of southern Tibet. Tectonophysics, 721: 415-434.

Fang, X., Tang, J., Song, Y., Beaudoin, G., Yang, C. and Huang, X., 2020. Genesis of the Shangxu orogenic gold deposit, Bangong-Nujiang suture belt, central Tibet, China: Constraints from H, O, C, Si, He and Ar isotopes. Ore Geology Reviews, 103810.

Fu, X., Wang, J., Chen, W. and Feng, X., 2010a. Age and tectonic implications of the Late Triassic Nadi Kangri volcanic rocks in the Qiangtang basin, northern Tibet. Journal of Chengdu University of Technology, 37: 605-615. [in Chinese with English abstract]

Fu, X., Wang, J., Wang, Z. and Chen, W., 2007. Identification of sedimentary gap between the Late Triassic Nadi kangri Formation and its underlying strata in the Qiangtang basin, northern Tibet and its geological significance. Geological Review, 53(3): 329-336. [in Chinese with English abstract]

Fu, X.G., Wang, J., Tan, F.W., Chen, M. and Chen, W.B., 2010b. The Late Triassic rift-related volcanic rocks from eastern Qiangtang, northern Tibet (China): age and tectonic implications. Gondwana Research, 17(1): 135-144.

Gaetani, M., Dercourt, J. and Vrielynck, B., 2003. The Peri-Tethys programme: achievements and results. Episodes, 26(2): 79-93.

Gaina, C., Mller, R.D., Brown, B.J. and Ishihara, T., 2003. Microcontinent formation around Australia. Special Paper of the Geological Society of America, 372: 405-416.

Garzanti, E., Angiolini, L. and Sciunnach, D., 1996. The Mid-Carboniferous to Lowermost Permian succession of Spiti (Po Group and Ganmachidam Formation; Tethys Himalaya, Northern India): Gondwana glaciation and rifting of Neo-Tethys. Geodinamica Acta, 9(2-3): 78-100.

Garzanti, E., Le Fort, P. and Sciunnach, D., 1999. First report of Lower Permian basalts in South Tibet: tholeiitic magmatism during break-up and incipient opening of Neotethys. Journal of Asian Earth Sciences, 17(4): 533-546.

Garzanti, E. and Sciunnach, D., 1997. Early Carboniferous onset of Gondwanian glaciation and Neo-tethyan rifting in South Tibet. Earth and Planetary Science Letters, 148(1-2): 359-365.

Garzanti, E., 2019. Petrographic classification of sand and sandstone. Earth-Science Reviews, 192: 545-563.

Gehrels, G., Kapp, P., DeCelles, P.G., Pullen, A., Blakey, R., Weislogel, A., Ding, L., Guynn, J., Martin, A., McQuarrie, N. and Yin, A., 2011. Detrital zircon geochronology of pre-Tertiary strata in the Tibetan-Himalayan orogen. Tectonics, 30: TC5016.

Girardeau, J., Marcoux, J., Allegre, C.J., Bassoullet, J.P., Tang, Y.K., Xiao, X.C., Zao, Y.G. and Wang, X.B., 1984. Tectonic environment and geodynamic significance of the Neo-Cimmerian Donqiao ophiolite, Bangong-Nujiang suture zone, Tibet. Nature, 307(5946): 27-31.

Grimes, C.B., John, B.E., Kelemen, P., Mazdab, F., Wooden, J., Cheadle, M.J., Hanghøj, K. and Schwartz, J., 2007. Trace element chemistry of zircons from oceanic crust: A method for distinguishing detrital zircon provenance. Geology, 35(7): 643-646.

Guynn, J., Kapp, P., Pullen, A., Heizler, M., Gehrels, G. and Ding, L., 2006. Tibetan basement rocks near Amdo reveal “missing” Mesozoic tectonism along the Bangong suture, central Tibet. Geology, 34(6): 505-508.

Guynn, J., Tropper, P., Kapp, P. and Gehrels, G.E., 2013. Metamorphism of the Amdo metamorphic complex, Tibet: implications for the Jurassic tectonic evolution of the Bangong suture zone. Journal of Metamorphic Geology, 31(7): 705-727.

Hao, L.L., Wang, Q., Wyman, D.A., Ou, Q., Dan, W., Jiang, Z.Q., Wu, F.Y., Yang, J.H., Long, X.P. and Li, J., 2016a. Underplating of basaltic magmas and crustal growth in a continental arc: Evidence from Late Mesozoic intermediate–felsic intrusive rocks in southern Qiangtang, central Tibet. Lithos, 245: 223-242.

Hao, L.L., Wang, Q., Wyman, D.A., Ou, Q., Dan, W., Jiang, Z.Q., Yang, J.H., Li, J. and Long, X.P., 2016b. Andesitic crustal growth via mélange partial melting: Evidence from Early Cretaceous arc dioritic/andesitic rocks in southern Qiangtang, central Tibet. Geochemistry, Geophysics, Geosystems, 17(5): 1641-1659.

He, H., Li, Y., Wang, C., Zhou, A., Qian, X., Zhang, J., Du, L. and Bi, W., 2018. Late Cretaceous (ca. 95 Ma) magnesian andesites in the Biluoco area, southern Qiangtang subterrane, central Tibet: Petrogenetic and tectonic implications. Lithos, 302: 389-404.

He, X., Yang, Z. and Nie, Z., 1990. Carboniferous and Permian rugose corals and tabulates of the Ngari area, Tibet (Xizang). China University of Geosciences Press, Wuhan, 76-79 pp. [in Chinese with English abstract]

Hu, X., Garzanti, E., Wang, J., Huang, W., An, W. and Webb, A., 2016. The timing of India-Asia collision onset–Facts, theories, controversies. Earth-Science Reviews, 160: 264-299.

Hu, X., Wang, J., An, W., Garzanti, E. and Li, J., 2017. Constraining the timing of the India-Asia continental collision by the sedimentary record. Science China Earth Sciences, 60: 603-625.

Hu, Y., Liu, Z.B., Wang, G., Gao, J., Song, Y., Zheng, M. and Li, D., 2020. Study of molasse within the middle segment of the Bangong- Nujiang suture zone, central Tibet: Constraints of ocean–continent transform. Geological Journal, 55(10): 6625-6641.

Huang, B., Fu, D., Zhou, W. and Wenbin, N., 2021. Complexity of zircon ages of mafic rocks in ophiolitic mélanges: A case from the Hegenshan ophiolite, Inner Mongolia. Scientia Geologica Sinica, 56(2): 596-614. [in Chinese with English abstract]

Huang, Q.-t., Liu, W.-l., Xia, B., Cai, Z.-r., Chen, W.-y., Li, J.-f. and Yin, Z.-x., 2017a. Petrogenesis of the Majiari ophiolite (western Tibet, China): Implications for intra-oceanic subduction in the Bangong–Nujiang Tethys. Journal of Asian Earth Sciences, 146: 337-351.

Huang, Q.S., Shi, R.D. and Ding, B.H., 2012. Re-Os isotopic evidence of MOR-type ophiolite from the Bangong Co for the opening of Bangong-Nujiang Tethys Ocean. Acta Mineralogica et Petrologica, 31(4): 465-478. [in Chinese with English abstract]

Huang, T.-T., Xu, J.-F., Chen, J.-L., Wu, J.-b. and Zeng, Y.-C., 2017b. Sedimentary record of Jurassic northward subduction of the Bangong–Nujiang Ocean: insights from detrital zircons. International Geology Review, 59(2): 166-184.

Ingersoll, R.V., Bullard, T.F., Ford, R.L., Grimm, J.P., Pickle, J.D. and Sares, S.W., 1984. The effect of grain size on detrital modes: a test of the Gazzi-Dickinson point-counting method. Journal of Sedimentary Research, 54(1): 103-116.

Jiang, S., Jiang, Y., Liu, Y., Li, S., Zhang, W., Wang, G., Lu, L. and Somerville, I., 2021. The Bangong-Nujiang Suture Zone, Tibet Plateau: Its role in the tectonic evolution of the eastern Tethys Ocean. Earth-Science Reviews, 218: 103656.

Kang, Z., Xu, J., Wang, B. and Chen, J., 2010. Qushenla Formation volcanic rocks in north Lhasa block: Products of Bangong Co-Nujiang Tethy's southward subduction. Acta Petrologica Sinica, 26(10): 3106-3116. [in Chinese with English abstract]

Kapp, P. and DeCelles, P.G., 2019. Mesozoic–Cenozoic geological evolution of the Himalayan-Tibetan orogen and working tectonic hypotheses. American Journal of Science, 319(3): 159-254.

Kapp, P., DeCelles, P.G., Gehrels, G.E., Heizier, M. and Ding, L., 2007. Geological records of the Lhasa-Qiangtang and Indo-Asian collisions in the Nima area of central Tibet. Geological Society of America Bulletin, 119(7-8): 917-932.

Kapp, P., Murphy, M.A., Yin, A., Harrison, T.M., Ding, L. and Guo, J., 2003. Mesozoic and Cenozoic tectonic evolution of the Shiquanhe area of western Tibet. Tectonics, 22(4). DOI: 10.1029/2001TC001332

Kidd, W.S.F., Yusheng, P., Chengfa, C., Coward, M.P., Dewey, J.F., Gansser, A., Molnar, P., Shackleton, R.M., Yiyin, S., Chengfa, C., Shackleton, R.M., Dewey, J.F. and Jixiang, Y., 1988. Geological mapping of the 1985 Chinese-British Tibetan (Xizang-Qinghai) Plateau Geotraverse route. Philosophical Transactions of the Royal Society of London. Series A, Mathematical and Physical Sciences, 327(1594): 287-305.

Lai, W., Hu, X., Garzanti, E., Sun, G., Garzione, C.N., BouDagher Fadel, M. and Ma, A., 2019. Initial growth of the Northern Lhasaplano, Tibetan Plateau in the early Late Cretaceous (ca. 92 Ma). Geological Society of America Bulletin, 131(11-12): 1823-1836.

Lai, W., Hu, X., Ma, A., Garzanti, E. and Xu, Y., 2022. From the southern Gangdese Yeba arc to the Bangong-Nujiang Ocean: Provenance of the Upper Jurassic-Lower Cretaceous Lagongtang Formation (northern Lhasa, Tibet). Palaeogeography, Palaeoclimatology, Palaeoecology, 588:

110837.

Lai, W., Hu, X., Zhu, D., An, W. and Ma, A., 2017. Discovery of the early Jurassic Gajia mélange in the Bangong–Nujiang suture zone: Southward subduction of the Bangong–Nujiang Ocean? International Journal of Earth Sciences, 106(4): 1277-1288.

Leier, A.L., DeCelles, P.G., Kapp, P. and Gehrels, G.E., 2007. Lower Cretaceous Strata in the Lhasa Terrane, Tibet, with Implications for Understanding the Early Tectonic History of the Tibetan Plateau. Journal of Sedimentary Research, 77(10): 809-825.

Li, C., Wang, G.H., Zhao, Z.B., Du, J.X., Ma, X.X. and Zheng, Y.L., 2020a. Late Mesozoic tectonic evolution of the central Bangong–Nujiang Suture Zone, central Tibetan Plateau. International Geology Review, 62(18): 2300-2323.

Li, F., Zhang, S., Li, J., Liu, H. and Qin, Y., 2022. Definition of Mid-Late Jurassic peripheral foreland basin in the northern margin of Lhasa block. Earth Science, DOI: 10.3799/dqkx.2021.047 [in Chinese with English abstract]

Li, G.-M., Li, J.-X., Zhao, J.-X., Qin, K.-Z., Cao, M.-J. and Evans, N.J., 2015a. Petrogenesis and tectonic setting of Triassic granitoids in the Qiangtang terrane, central Tibet: Evidence from U-Pb ages, petrochemistry and Sr-Nd-Hf isotopes. Journal of Asian Earth Sciences, 105: 443-455.

Li, H.-Q., Xu, Z.-Q., Webb, A.A.G., Li, T.-F., Ma, S.-W. and Huang, X.-M., 2017a. Early Jurassic tectonism occurred within the Basu metamorphic complex, eastern central Tibet: Implications for an archipelago-accretion orogenic model. Tectonophysics, 702: 29-41.

Li, H.S., 1986. Upper Jurassic (early Tithonian) radiolarians from southern Bangong Lake, Xizang. Acta Micropalaeontologica Sinica, 3(3): 297-316. [in Chinese with English abstract]

Li, H., 1988. Early Jurassic (Late Pliensbachian) radiolaria from the Dengqen area, Xizang (Tibet). Acta Micropalaeontologica Sinica, 5(3): 323-330. [in Chinese with English abstract]

Li, H., Liu, Z., Chen, W., Wang, N., Wang, J., Zhang, K., Li, F. and Wang, C., 2019a. The discovery of high-Mg rhyolitic rocks in Peng Tso area, Tibet and its significance for evolution of Bangong-Nujiang Ocean. Acta Petrologica Sinica, 35(3): 799-815. [in Chinese with English abstract]

Li, J., Zhang, H. and Li, H., 2015b. The tectonic setting and evolution of Indian Ocean research progress of tectonic map of Indian Ocean. Acta Oceanologica Sinica, 37(7): 1-14. [in Chinese with English abstract]

Li, J.X., Qin, K.Z., Li, G.M., Richards, J.P., Zhao, J.X. and Cao, M.J., 2014a. Geochronology, geochemistry, and zircon Hf isotopic compositions of Mesozoic intermediate–felsic intrusions in central Tibet: Petrogenetic and tectonic implications. Lithos, 198: 77-91.

Li, J.X., Qin, K.Z., Li, G.M., Xiao, B., Zhao, J.X. and Chen, L., 2016a. Petrogenesis of Cretaceous igneous rocks from the Duolong porphyry Cu–Au deposit, central Tibet: evidence from zircon U–Pb geochronology, petrochemistry and Sr–Nd–Pb–Hf isotope characteristics. Geological Journal, 51(2): 285-307.

Li, S., Ding, L., Guilmette, C., Fu, J.J., Xu, Q., Yue, Y.H. and Pinto, R.H., 2017b. The subduction-accretion history of the Bangong-Nujiang Ocean: Constraints from provenance and geochronology of the Mesozoic strata near Gaize, central Tibet. Tectonophysics, 702: 42-60.

Li, S., Guilmette, C., Ding, L., Xu, Q., Fu, J.-J. and Yue, Y.-H., 2017c. Provenance of Mesozoic clastic rocks within the Bangong-Nujiang suture zone, central Tibet: Implications for the age of the initial Lhasa-Qiangtang collision. Journal of Asian Earth Sciences, 147: 469-484.

Li, S., Yin, C., Ding, L., Guilmette, C., Zhang, J., Yue, Y. and Baral, U., 2020b. Provenance of Lower Cretaceous sedimentary rocks in the northern margin of the Lhasa terrane, Tibet: Implications for the timing of the Lhasa-Qiangtang collision. Journal of Asian Earth Sciences, 190: 104162.

Li, S., Yin, C., Guilmette, C., Ding, L. and Zhang, J., 2019b. Birth and demise of the Bangong-Nujiang Tethyan Ocean: A review from the Gerze area of central Tibet. Earth-Science Reviews, 198: 102907.

Li, S.M., Wang, Q., Zhu, D.C., Cawood, P.A., Stern, R.J., Weinberg, R., Zhao, Z. and Mo, X.X., 2020c. Reconciling orogenic drivers for the evolution of the Bangong- Nujiang Tethys during Middle-Late Jurassic. Tectonics, 32(2).

Li, S.M., Wang, Q., Zhu, D.C., Stern, R.J., Cawood, P.A., Sui, Q.L. and Zhao, Z., 2018. One or two Early Cretaceous arc systems in the Lhasa Terrane, southern Tibet. Journal of Geophysical Research: Solid Earth, 123(5): 3391-3413.

Li, S.M., Zhu, D.C., Wang, Q., Zhao, Z., Zhang, L.L., Liu, S.A., Chang, Q.S., Lu, Y.H., Dai, J.G. and Zheng, Y.C., 2016b. Slab-derived adakites and subslab asthenosphere-derived OIB-type rocks at 156 ± 2 Ma from the north of Gerze, central Tibet: Records of the Bangong–Nujiang oceanic ridge subduction during the Late Jurassic. Lithos, 262: 456-469.

Li, S.M., Zhu, D.C., Wang, Q., Zhao, Z.D., Sui, Q.L., Liu, S.A., Liu, D. and Mo, X.X., 2014b. Northward subduction of Bangong-Nujiang Tethys: Insight from Late Jurassic intrusive rocks from Bangong Tso in western Tibet. Lithos, 205: 284-297.

Li, X., 2019. Volcanic-sedimentary petrological characteristics and tectonic: Attribute of Nadigangri Formation in Qiangtang Basin. Ph. D thesis, China University of Geosciences (Beijing), Beijing, 1-144 pp. [in Chinese with English abstract]

Li, X., Wang, B., Liu, H., Wang, L. and Chen, L., 2015c. The Late Jurassic high-Mg andesites in the Daru Tso area, Tibet: Evidence for the subduction of the Bangong Co-Nujiang River oceanic lithosphere. Geological Bulletin of China, 34(2/3): 251-261. [in Chinese with English abstract]

Li, Y., He, J., Wang, C., Santosh, M., Dai, J., Zhang, Y., Wei, Y. and Wang, J., 2013. Late Cretaceous K-rich magmatism in central Tibet: Evidence for early elevation of the Tibetan plateau? Lithos, 160-161: 1-13.

Li, Z., Ding, L., Lippert, P.C., Song, P., Yue, Y. and van Hinsbergen, D.J., 2016c. Paleomagnetic constraints on the Mesozoic drift of the Lhasa terrane (Tibet) from Gondwana to Eurasia. Geology, 44(9): 727-730.

Li, Z., Ding, L., Song, P., Fu, J. and Yue, Y., 2017d. Paleomagnetic constraints on the paleolatitude of the Lhasa block during the Early Cretaceous: implications for the onset of India–Asia collision and latitudinal shortening estimates across Tibet and stable Asia. Gondwana Research, 41: 352-372.

Lin, B., Fang, X., Wang, Y., Yang, H. and He, W., 2019. Petrologic genesis of ore-bearing porphyries in Tiegelongnan giant Cu (Au, Ag) deposit, Tibet and its implications for the dynamic of Cretaceous mineralization, Duolong. Acta Petrologica Sinica, 35(3): 642-664. [in Chinese with English abstract]

Lippert, P.C., Zhao, X., Coe, R.S. and Lo, C.-H., 2011. Palaeomagnetism and 40Ar/39Ar geochronology of upper Palaeogene volcanic rocks from Central Tibet: implications for the Central Asia inclination anomaly, the palaeolatitude of Tibet and post-50 Ma shortening within Asia. Geophysical Journal International, 184(1): 131-161.

Lissenberg, C.J., Rioux, M., Shimizu, N., Bowring, S.A. and Mével, C., 2009. Zircon dating of oceanic crustal accretion. Science, 323(5917): 1048-1050.

Liu, D.-L., Shi, R.-D., Ding, L. and Zou, H.-B., 2017a. Late Cretaceous transition from subduction to collision along the Bangong-Nujiang Tethys: New volcanic constraints from central Tibet. Lithos, 296-299: 452-470.

Liu, D., Shi, R., Ding, L., Huang, Q., Zhang, X., Yue, Y. and Zhang, L., 2017b. Zircon U–Pb age and Hf isotopic compositions of Mesozoic granitoids in southern Qiangtang, Tibet: Implications for the subduction of the Bangong–Nujiang Tethyan Ocean. Gondwana Research, 41: 157-172.

Liu, W.-L., Huang, Q.-T., Gu, M., Zhong, Y., Zhou, R., Gu, X.-D., Zheng, H., Liu, J.-N., Lu, X.-X. and Xia, B., 2018. Origin and tectonic implications of the Shiquanhe high-Mg andesite, western Bangong suture, Tibet. Gondwana Research, 60: 1-14.

Luo, A.-B., Fan, J.-J., Hao, Y.-J., Li, H. and Zhang, B.-C., 2020. Aptian Flysch in Central Tibet: Constraints on the Timing of Closure of the Bangong-Nujiang Tethyan Ocean. Tectonics, 39(12): e2020TC006198.

Luo, A., Fan, J., Wang, M. and Zeng, X., 2019. Age of flysch in Bangong-Nujiang Ocean: constraints of detrital zircon from Yaduo village of Gerze County. Earth Science, 44(7): 2426-2440. [in Chinese with English abstract]

Ma, A., Hu, X., Garzanti, E., Han, Z. and Lai, W., 2017a. Sedimentary and tectonic evolution of the southern Qiangtang basin: Implications for the Lhasa-Qiangtang collision timing. Journal of Geophysical Research: Solid Earth, 122(7): 4790-4813.

Ma, A., Hu, X., Kapp, P., BouDagher- Fadel, M. and Lai, W., 2020a. Pre- Oxfordian (> 163 Ma) Ophiolite Obduction in Central Tibet. Geophysical Research Letters, 47(10): e2019GL086650.

Ma, A., Hu, X., Kapp, P., Han, Z., Lai, W. and BouDagher-Fadel, M., 2018. The disappearance of a Late Jurassic remnant sea in the southern Qiangtang Block (Shamuluo Formation, Najiangco area): Implications for the tectonic uplift of central Tibet. Palaeogeography, Palaeoclimatology, Palaeoecology, 506: 30-47.

Ma, A., Hu, X., Kapp, P., Lai, W., Han, Z. and Xue, W., 2020b. Mesozoic subduction accretion history in central Tibet: constrained from provenance analysis of the Mugagangri subduction complex in the Bangong-Nujiang suture zone. Tectonics, 39(9): e2020TC006144.

Ma, X., Song, Y., Tang, J. and Chen, W., 2020c. Newly identified rhyolite-biotite monzogranite (A2-type granite)-norite belt from the Bangong-Nujiang collision zone in Tibet Plateau: Evidence for the slab break-off beneath the Lhasa Terrane. Lithos, 366: 105565.

Ma, Y., Wang, Q., Wang, J., Yang, T., Tan, X., Dan, W., Zhang, X., Ma, L., Wang, Z., Hu, W., Zhang, S., Wu, H., Li, H. and Cao, L., 2019. Paleomagnetic Constraints on the Origin and Drift History of the North Qiangtang Terrane in the Late Paleozoic. Geophysical Research Letters, 46(2): 689-697.

Ma, Y., Yang, T., Bian, W., Jin, J., Wang, Q., Zhang, S., Wu, H., Li, H., Cao, L., Yuan, H. and Ding, J., 2017b. Paleomagnetic and geochronologic results of latest Cretaceous lava flows from the Lhasa terrane and their tectonic implications. Journal of Geophysical Research: Solid Earth, 122(11): 8786-8809.

Ma, Y., Yang, T., Yang, Z., Zhang, S., Wu, H., Li, H., Li, H., Chen, W., Zhang, J. and Ding, J., 2014. Paleomagnetism and U-Pb zircon geochronology of Lower Cretaceous lava flows from the western Lhasa terrane: New constraints on the India-Asia collision process and intracontinental deformation within Asia. Journal of Geophysical Research: Solid Earth, 119(10): 7404-7424.

Mai, Y., Yang, W., Zhu, L., Tao, G. and Lu, Z., 2018. Zircon U-Pb age and geochemistry of volcanic rocks from the Queshenla formation in the Chagelong area of southern margin of Qiangtang, Tibet—restriction on the evolution time limit of the Ban Gong Lake Nu River Ocean basin. Journal of Mineralogy and Petrology, 38(2): 70-79. [in Chinese with English abstract]

Matte, P., Tapponnier, P., Arnaud, N., Bourjot, L., Avouac, J., Vidal, P., Qing, L., Yusheng, P. and Yi, W.,

1996. Tectonics of Western Tibet, between the Tarim and the Indus. Earth and Planetary Science Letters, 142(3-4): 311-330.

Mattern, F., Schneider, W., Wang, P. and Li, C., 1998. Continental strike-slip rifts and their stratigraphic signature: application to the Bangong/Nujiang zone (Tibet) and the South Penninic zone (Alps). Geologische Rundschau, 87(2): 206-224.

Meert, J.G., Pivarunas, A.F., Evans, D.A.D., Pisarevsky, S.A., Pesonen, L.J., Li, Z.-X., Elming, S.-Å., Miller, S.R., Zhang, S. and Salminen, J.M., 2020. The magnificent seven: A proposal for modest revision of the Van der Voo (1990) quality index. Tectonophysics, 790: 228549.

Meng, J., Zhao, X., Wang, C., Liu, H., Li, Y., Han, Z., Liu, T. and Wang, M., 2018. Palaeomagnetism and detrital zircon U–Pb geochronology of Cretaceous redbeds from central Tibet and tectonic implications. Geological Journal, 53(5): 2315-2333.

Mo, X., Niu, Y., Dong, G., Zhao, Z., Hou, Z., Zhou, S. and Ke, S., 2008. Contribution of syncollisional felsic magmatism to continental crust growth: a case study of the Paleogene Linzizong volcanic succession in southern Tibet. Chemical Geology, 250(1-4): 49-67.

Murphy, M.A., Yin, A., Harrison, T.M., Dürr, S.B., Chen, Z., Ryerson, F.J., Kidd, W.S.F., Wang, X. and Zhou, X., 1997. Did the Indo-Asian collision alone create the Tibetan plateau? Geology, 25(8): 719-722.

Nicora, A. and Garzanti, E., 1997. The Permian/Triassic boundary in the central Himalaya. Albertiana, 19: 47-51.

Nie, Z. and Song, Z.M., 1983. Fusulinids of Lower Permian Tunlonggongba Formation from Rutong of Xizang (Tibet), China. Earth Science, 19(1): 43-55. [in Chinese with English abstract]

Nima, C. and Xie, R.W., 2005. Discovery of Middle Triassic strata in the Nagqu area, northern Tibet, China, and its geological implications. Geological Bulletin of China, 24: 1141-1149. [in Chinese with English abstract]

Nima, C., Xie, y., Sha, Z., Xiluo, L. and Qiangba, Z., 2005. Geological report of the 1:250, 000 regional geological survey in Nagqu area, 380pp (in Chinese).

Niu, Y., Jiang, B. and Huang, H., 2011. Triassic marine biogeography constrains the palaeogeographic reconstruction of Tibet and adjacent areas. Palaeogeography, Palaeoclimatology, Palaeoecology, 306(3-4): 160-175.

Pan, G., Zheng, H., Xu, Y., Wang, P. and Jiao, S., 1983. A preliminary study on Bangong Co–Nujiang suture. Contribution to the Geology of the Qinghai Xizang, 12: 229-242.

Pan, G., Ding, J., Yao, D., & Wang, L. (2004). The Guide Book of 1:1,500,000 Geologic Map of the Qinghai-Xizang (Tibet) Plateau and Adjacent Areas. Chengdu Map Publishing Company, Chengdu.

Peng, Y., Yu, S., Li, S., Liu, Y., Santosh, M., Lv, P., Li, Y., Xie, W. and Liu, Y., 2020. The odyssey of Tibetan Plateau accretion prior to Cenozoic India-Asia collision: probing the Mesozoic tectonic evolution of the Bangong-Nujiang Suture. Earth-Science Reviews, 211: 103376.

Qiao, F., Xu, H.-P. and Zhang, Y.-C., 2019. Changhsingian (Late Permian) foraminifers from the topmost part of the Xiala Formation in the Tsochen area, central Lhasa Block, Tibet and their geological implications. Palaeoworld, 28(3): 303-319.

Qin, Y., Li, D., Liu, D. and Li, H., 2017. Opening Time of Middle Tethys Oceanic Basin: Constrained from Zircon U–Pb Dating of MOR-type Gabbro in Bangong Lake Ophiolite. Geotecton. Metallog, 41: 1148-1157.

Qu, X.-M., Wang, R.-J., Xin, H.-B., Jiang, J.-H. and Chen, H., 2012. Age and petrogenesis of A-type granites in the middle segment of the Bangonghu–Nujiang suture, Tibetan plateau. Lithos, 146:

264-275.

Qu, Y., Wang, Y., Duan, J., Zhang, S., Wang, Z. and Lv, P., 2003. Geological report of the 1:250, 000 regional geological survey in Duoba area (in Chinese).

Qu, Y., Zhai, S., Zheng, C., Wang, Y., Lu, P., Wang, H., Li, X., Li, Q., 2013. The Late Jurassic-Early Cretaceous Rila Formation, Rila Formation Suor clastic rocks and characteristics of biotas in the Yunzhug ophiolite belt, northern Tibet. Geological Bulletin of China, 22: 959-963. (in Chinese with English abstract)

Ran, B., Wang, C., Zhao, X., Li, Y., He, M., Zhu, L. and Coe, R.S., 2012. New paleomagnetic results of the early Permian in the Xainza area, Tibetan Plateau and their paleogeographical implications. Gondwana Research, 22(2): 447-460.

Rao, X., Skelton, P., Sha, J., Cai, H. and Iba, Y., 2015a. Mid-Cretaceous rudists (Bivalvia: *Hippuritida*) from the Langshan Formation, Lhasa block, Tibet. Papers in Palaeontology, 1: 401–424.

Rao, X., Skelton, P.W., Sano, S.i., Zhang, Y., Zhang, Y., Pan, Y., Cai, H., Peng, B., Zhang, T. and Ma, Z., 2020. Shajia, a new genus of polyconitid rudist from the Langshan Formation of the Lhasa block, Tibet, and its palaeogeographical implications. Cretaceous Research, 105: 104151.

Rao, X., Skelton, P.W., Sha, J., Cai, H. and Iba, Y., 2015b. Mid- Cretaceous rudists (Bivalvia: *Hippuritida*) from the Langshan Formation, Lhasa block, Tibet. Papers in Palaeontology, 1(4): 401-424.

Raterman, N.S., Robinson, A.C. and Cowgill, E.S., 2014. Structure and detrital zircon geochronology of the Domar fold-thrust belt: Evidence of pre-Cenozoic crustal thickening of the western Tibetan Plateau. Geological Society of America Special Papers, 507: 89-104.

Schneider, W., Mattern, F., Wang, P. and Li, C., 2003. Tectonic and sedimentary basin evolution of the eastern Bangong–Nujiang zone (Tibet): a Reading cycle. International Journal of Earth Sciences, 92(2): 228-254.

Sciunnach, D. and Garzanti, E., 1996. Sedimentary record of Late Paleozoic rift and break-up in Northern Gondwana: a case history from the Thini Chu Group and Tamba-Kurkur Formation (Dolpo Tethys Himalaya, Nepal). Geodinamica Acta, 9(1): 41-56.

Sciunnach, D. and Garzanti, E., 2012. Subsidence history of the Tethys Himalaya. Earth-Science Reviews, 111(1-2): 179-198.

Scott, R.W., Wan, X., Sha, J. and Wen, S.-X., 2010. Rudists of Tibet and the Tarim Basin, China: significance to Requieniidae phylogeny. Journal of Paleontology, 84(3): 444-465.

Ṣengör, A.C., 1979. Tethys and its implications. Nature, 279(14): 590–593.

Shi, G., Archbold, N. and Zhan, L., 1995. Distribution and characteristics of mid-Permian (Late Artinskian-Ufimian) mixed/transitional marine faunas in the Asian region and their palaeogeographical implications. Palaeogeography, Palaeoclimatology, Palaeoecology, 114(2): 241-271.

Shi, L.-Z., Huang, J.-Y. and Chen, W., 2020. Birth and demise of the Bangong–Nujiang Tethyan Ocean: A review from the Gerze area of Central Tibet: Comment. Earth-Science Reviews, 208: 103209.

Shi, R., Griffin, W.L., O'Reilly, S.Y., Huang, Q., Zhang, X., Liu, D., Zhi, X., Xia, Q. and Ding, L., 2012. Melt/mantle mixing produces podiform chromite deposits in ophiolites: implications of Re–Os systematics in the Dongqiao Neo-tethyan ophiolite, northern Tibet. Gondwana Research, 21(1): 194-206.

Smith, A. and Xu, J., 1988. Palaeontology of the 1985 Tibet geotraverse, Lhasa to Golmud.

Philosophical Transactions of the Royal Society of London. Series A, Mathematical and Physical Sciences, 327(1594): 53-105.

Song, C., Wang, J., Fu, X., Feng, X., Chen, M. and He, L., 2012. Late Triassic paleomagnetic data from the Qiangtang terrane of Tibetan Plateau and their tectonic significances. Journal of Jilin University (Earth Science Edition), 42(2): 241-250. [in Chinese with English abstract]

Song, C., Zeng, Y., Yan, M., Fang, X., Feng, Y., Pan, J., Liu, X., Meng, Q., Hu, C. and Zhong, S., 2017a. Sedimentary conditions of evaporites in the Late Jurassic Xiali Formation, Qiangtang Basin: Evidence from Geochemistry Records. Acta Geologica Sinica-English Edition, 91(1): 156-174.

Song, C., Zeng, Y., Yan, M., Wu, S., Fang, X., Bao, J., Zan, J. and Liu, X., 2016. Magnetostratigraphy of the middle-upper Jurassic sedimentary sequences at Yanshiping, Qiangtang Basin, China. Geophysical Journal International, 206(3): 1847-1863.

Song, P., Ding, L., Li, Z., Lippert, P.C., Yang, T., Zhao, X., Fu, J. and Yue, Y., 2015. Late Triassic paleolatitude of the Qiangtang block: Implications for the closure of the Paleo-Tethys Ocean. Earth and Planetary Science Letters, 424: 69-83.

Song, P., Ding, L., Li, Z., Lippert, P.C. and Yue, Y., 2017b. An early bird from Gondwana: Paleomagnetism of Lower Permian lavas from northern Qiangtang (Tibet) and the geography of the Paleo-Tethys. Earth and Planetary Science Letters, 475: 119-133.

Song, P., Ding, L., Lippert, P.C., Li, Z., Zhang, L. and Xie, J., 2020. Paleomagnetism of Middle Triassic Lavas From Northern Qiangtang (Tibet): Constraints on the Closure of the Paleo-Tethys Ocean. Journal of Geophysical Research: Solid Earth, 125(2): e2019JB017804.

Sui, Q.-L., Wang, Q., Zhu, D.-C., Zhao, Z.-D., Chen, Y., Santosh, M., Hu, Z.-C., Yuan, H.-L. and Mo, X.-X., 2013. Compositional diversity of ca. 110 Ma magmatism in the northern Lhasa Terrane, Tibet: implications for the magmatic origin and crustal growth in a continent–continent collision zone. Lithos, 168: 144-159.

Sun, D., 1993. On the Permian biogeographic boundary between Gondwana and Eurasia in Tibet, China as the eastern section of the Tethys. Palaeogeography, Palaeoclimatology, Palaeoecology, 100(1-2): 59-77.

Sun, G., Hu, X., Sinclair, H.D., BouDagher-Fadel, M.K. and Wang, J., 2015. Late Cretaceous evolution of the Coqen Basin (Lhasa terrane) and implications for early topographic growth on the Tibetan Plateau. Geological Society of America Bulletin, 127(7-8): 1001-1020.

Sun, L., Bai, Z., Xun, D., Li, H. and Sun, B., 2011. Geological characteristics and zircon U-Pb SHRIMP dating of the plagiogranite in Amduo ophiolites, Tibet. Geological Survey and Research, 34(1): 10-15. [in Chinese with English abstract]

Sun, Z., Pei, J., Li, H., Xu, W., Jiang, W., Zhu, Z., Wang, X. and Yang, Z., 2012. Palaeomagnetism of late Cretaceous sediments from southern Tibet: Evidence for the consistent palaeolatitudes of the southern margin of Eurasia prior to the collision with India. Gondwana Research, 21(1): 53-63.

Sun, Z., Wan, J., Pei, J. and Li, H., 2008. New Early Cretaceous paleomagnetic data from volcanic of the eastern Lhasa Block and its tectonic implications. Acta Petrologica Sinica, 24(7): 1621-1626. [in Chinese with English abstract]

Tan, X., Gilder, S., Kodama, K.P., Jiang, W., Han, Y., Zhang, H., Xu, H. and Zhou, D., 2010. New paleomagnetic results from the Lhasa block: Revised estimation of latitudinal shortening across Tibet and implications for dating the India–Asia collision. Earth and Planetary Science Letters, 293(3): 396-404.

Tang, X.-D., Huang, B.-C., Yang, L.-K., Yi, Z.-Y., Qiao, Q.-Q. and Chen, L.-W., 2013. Paleomagnetism and Ar-Ar geochronology of Cretaceous volcanic rocks in the middle Lhasa terrane, China and tectonic implications. Chinese Journal of Geophysics, 56(1): 136-149.

Tang, Y., Zhai, Q.-G., Chung, S.-L., Hu, P.-Y., Wang, J., Xiao, X.-C., Song, B., Wang, H.-T. and Lee, H.-Y., 2020. First mid-ocean ridge-type ophiolite from the Meso-Tethys suture zone in the north-central Tibetan plateau. Geological Society of America Bulletin, 132(9-10): 2202-2220.

Tong, Y.-B., Yang, Z., Gao, L., Wang, H., Zhang, X.-D., An, C.-Z., Xu, Y.-C. and Han, Z.-R., 2015. Paleomagnetism of Upper Cretaceous red-beds from the eastern Qiangtang Block: Clockwise rotations and latitudinal translation during the India–Asia collision. Journal of Asian Earth Sciences, 114: 732-749.

Tong, Y., Yang, Z., Pei, J., Wang, H., Xu, Y. and Pu, Z., 2017. Paleomagnetism of the Upper Cretaceous red-beds from the eastern edge of the Lhasa Terrane: New constraints on the onset of the India-Eurasia collision and latitudinal crustal shortening in southern Eurasia. Gondwana Research, 48: 86-100.

Ueno, K., 2006. The Permian *antitropical fusulinoidean* genus Monodiexodina: Distribution, taxonomy, paleobiogeography and paleoecology. Journal of Asian Earth Sciences, 26(3-4): 380-404.

Vannay, J.C. and Spring, L., 1993. Geochemistry of the continental basalts within the Tethyan Himalaya of Lahul-Spiti and SE Zanskar, northwest India. Geological Society, London, Special Publications, 74(1): 237-249.

Vermeesch, P., 2013. Multi-sample comparison of detrital age distributions. Chemical Geology, 341: 140-146.

Wan, B., Wu, F., Chen, L., Zhao, L., Liang, X., Xiao, W. and Zhu, R., 2019. Cyclical one-way continental rupture-drift in the Tethyan evolution: Subduction-driven plate tectonics. Science China Earth Sciences, 62(12): 2005-2016.

Wang, B.-D., Wang, L.-Q., Chung, S.-L., Chen, J.-L., Yin, F.-G., Liu, H., Li, X.-B. and Chen, L.-K., 2016. Evolution of the Bangong–Nujiang Tethyan ocean: insights from the geochronology and geochemistry of mafic rocks within ophiolites. Lithos, 245: 18-33.

Wang, B., Liu, H. and Wang, L., 2020. Spatial-temporal framework of Shiquanhe-Laguoco-Yongzhu-Jiali ophiolite mélange zone, Qinghai-Tibet Plateau and its tectonic evolution. Earth Science, 45(8): 2764-2784. [in Chinese with English abstract]

Wang, B., Wang, L., Xu, J., Chen, L., Zhao, W., Liu, H., Peng, T. and Li, X., 2015. The discovery of high-pressure granulite at Shelama in Dongco area along the Bangong Co-Nujiang River suture zone and its tectonic significance. Geological Bulletin of China, 34(9): 1605-1616. [in Chinese with English abstract]

Wang, C., Yi, H., Liu, C., Li, Y.L., Zou, H., Wu, X., Deng, B. and Yang, X., 2004. Discovery of paleo-oil-reservoir in Qiangtang basin in Tibet and its geological significance. Oil & Gas Geology, 25(2): 139-143. [in Chinese with English abstract]

Wang, J., Fu, X., Tan, F., Chen, M. and He, J., 2010. A new sedimentary model for the Qiangtang Basin. Acta Sedimentologica Sinica, 28(5): 884-893. [in Chinese with English abstract]

Wang, J. G., Wu, F. Y., Garzanti, E., Hu, X., Ji, W. Q., Liu, Z. C. and Liu, X. C., 2016. Upper Triassic turbidites of the northern Tethyan Himalaya (Langjiexue group): the terminal of a sediment-routing system sourced in the gondwanide orogen. Gondwana Research, 34: 84-98.

Wang, M., Li, C., Zeng, X.-W., Li, H., Fan, J.-J., Xie, C.-M. and Hao, Y.-J., 2019. Petrogenesis of the southern Qiangtang mafic dykes, Tibet: Link to a late Paleozoic mantle plume on the northern margin of Gondwana? Geological Society of America Bulletin, 131(11-12): 1907-1919.

Wang, Q., Zhu, D.C., Cawood, P.A., Chung, S.L. and Zhao, Z.D., 2021. Resolving the paleogeographic puzzle of the Lhasa Terrane in southern Tibet. Geophysical Research Letters, 48(15): e2021GL094236.

Wang, W.-L., Aitchison, J.C., Lo, C.-H. and Zeng, Q.-G., 2008. Geochemistry and geochronology of the amphibolite blocks in ophiolitic mélanges along Bangong-Nujiang suture, central Tibet. Journal of Asian Earth Sciences, 33(1-2): 122-138.

Wang, Y., Zhang, S., Xie, Y., Li, C., Yu, X. and Zheng, C., 2006. Geological report of the 1:250, 000 regional geological survey in Angdaerco area (in Chinese).

Wang, Y. and Zheng, C., 2007. Lithostratigraphy, sequence stratigraphy, and biostratigraphy of the Suobucha and Quse Formations and the Triassic-Jurassic boundary in the Sewa area on the south margin of the Qiangtang basin, northern Tibet. Journal of Stratigraphy, 31(4): 377-384. [in Chinese with English abstract]

Wang, Y.J., Wang, J.P. and Pei, F., 2002. A late Triassic radiolarian fauna in the Dingqing ophiolite belt, Xizang (Tibet). Acta Micropalaeontologica Sinica, 19(4): 323- 336. [in Chinese with English abstract]

White, R. and McKenzie, D., 1989. Magmatism at rift zones: the generation of volcanic continental margins and flood basalts. Journal of Geophysical Research: Solid Earth, 94(B6): 7685-7729.

Wu, F., Wan, B., Zhao, L., Xiao, W. and Zhu, R., 2020. Tethyan geodynamics. Acta Petrologica Sinica, 36(6): 1627-1674. [in Chinese with English abstract]

Wu, G., Ji, Z., Trotter, J.A., Yao, J. and Zhou, L., 2014a. Conodont biostratigraphy of a new Permo-Triassic boundary section at Wenbudangsang, north Tibet. Palaeogeography, Palaeoclimatology, Palaeoecology, 411: 188-207.

Wu, H., Li, C., Chen, J. and Xie, C., 2015. Late Triassic tectonic framework and evolution of Central Qiangtang, Tibet, SW China. Lithosphere, 8(2): 141-149.

Wu, H., Li, C., Hu, P., Fan, J., Zhang, H. and Li, J., 2013. The discovery of Qushenla volcanic rocks in Tasepule area of Nyima Country, Tibet, and its geological significance. Geological Bulletin of China, 32(7): 1014-1026. [in Chinese with English abstract]

Wu, H., Li, C., Hu, P., Zhang, H. and Li, J., 2014b. The discovery of Early Cretaceous bimodal volcanic rocks in the Dachagou area of Tibet and its significance. Geological Bulletin of China, 33(11): 1804-1814. [in Chinese with English abstract]

Wu, J., Yin, X., Liu, W., Lei, C., Wang, B., Li, W., Pei, Y. and Zhang, W., 2019. The discovery of Nb-rich volcanic rock of the Qushenla Formation in Yema area of the western segment of Bangong Co-Nujiang suture in Tibet and its implications. Geological Bulletin of China, 38(4): 471-483. [in Chinese with English abstract]

Wu, R., Hu, C., Wang, C. and Chen, D., 1986. The stratigraphical system of Qiangtang district in northern Xizang (Tibet). Contribution to the Geology of the Qinghai-Xizang (TIBET) Plateau, 9(9): 7-38.

Wu, Y., Cheng, S.Y., Qin, M.K., Guo, D.F., Guo, G.L., Zhang, C. and Yang, J.S., 2018. Zircon U-Pb Ages of Dongcuo Ophiolite in Western Bangonghu-Nujiang Suture Zone and Their Geological Significance. Earth Science, 43(4): 147-164. [in Chinese with English abstract]

Wu, Z.H., Wu, X.W., Zhao, Z., Lu, L., Ye, P.S. and Zhang, Y.L., 2014c. SHRIMP U-Pb Isotopic Dating of the Late Cretaceous Volcanic Rocks and Its Chronological Constraint on the Red-beds in Southern Qiangtang Block. Acta Geoscientica Sinica, 35(5): 567-572. [in Chinese with English abstract]

Xia, D., Liu, S. and Teng, Y., 1997. Stratigraphy (Lithostratic) of Xizang Autonomous Region. China University of Geosciences Press, Beijing. [in Chinese with English abstract]

Xu, H., Zhang, Y., Qiao, F. and Shen, S., 2019. A new Changhsingian brachiopod fauna from the Xiala Formation at Tsochen in the central Lhasa Block and its paleogeographical implications. Journal of Paleontology, 93(5): 876-898.

Xu, J., Li, C., Fan, J., Basang, Y. and Xu, M., 2014. Jurassic oceanic island type rock association in the Bangong Co-Nujiang River suture zone: Evidence from petrology and geochemistry. Geological Bulletin of China, 11: 145-155. [in Chinese with English abstract]

Xu, R.H., Schärer, U. and Allègre, C.J., 1985. Magmatism and metamorphism in the Lhasa block (Tibet): a geochronological study. The Journal of Geology, 93: 41-57.

Xu, Y., Hu, X., BouDagher-Fadel, M.K., Sun, G., Lai, W., Li, J. and Zhang, S., 2020. The major Late Albian transgressive event recorded in the epeiric platform of the Langshan Formation in central Tibet. Geological Society, London, Special Publications, 498: 211-232.

Xu, Y., Hu, X., Garzanti, E., BouDagher-Fadel, M., Sun, G., Lai, W. and Zhang, S., 2022. Mid-Cretaceous thick carbonate accumulation in Northern Lhasa (Tibet): eustatic vs. tectonic control? Bulletin, 134(1-2): 389-404.

Xue, W., Hu, X., Ma, A., Garzanti, E. and Li, J., 2020a. Eustatic and tectonic control on the evolution of the Jurassic North Qiangtang Basin, northern Tibet, China: Impact on the petroleum system. Marine and Petroleum Geology, 120: 104558.

Xue, W., Ma, A. and Hu, X., 2020b. The redefinition of the Jurassic—Cretaceous lithostratigraphic framework in the Qiangtang Basin, Xizang Plateau. Geological Review, 66(5): 1114-1129.

Yan, M., Zhang, D., Fang, X., Ren, H., Zhang, W., Zan, J., Song, C. and Zhang, T., 2016. Paleomagnetic data bearing on the Mesozoic deformation of the Qiangtang Block: Implications for the evolution of the Paleo- and Meso-Tethys. Gondwana Research, 39: 292-316.

Yang, C., Beaudoin, G., Tang, J.-X., Song, Y. and Zhang, Z., 2020. Hydrothermal fluid evolution at the Tiegelongnan porphyry-epithermal Cu (Au) deposit, Tibet, China: Constraints from H and O stable isotope and in-situ S isotope. Ore Geology Reviews, 125: 103694.

Yang, T., Ma, Y., Zhang, S., Bian, W., Yang, Z., Wu, H., Li, H., Chen, W. and Ding, J., 2015. New insights into the India–Asia collision process from Cretaceous paleomagnetic and geochronologic results in the Lhasa terrane. Gondwana Research, 28(2): 625-641.

Yang, X., Fan, T., Tang, S., Li, J., Meng, M. and Hu, P., 2017. Sedimentology and sequence stratigraphy of evaporites in the Middle Jurassic Buqu Formation of the Qiangtang Basin, Tibet, China. Carbonates and Evaporites, 32(3): 379-390.

Yang, Z.-Y., Wang, Q., Zhang, C., Dan, W., Zhang, X.-Z., Qi, Y., Xia, X.-P. and Zhao, Z.-H., 2018. Rare earth element tetrad effect and negative Ce anomalies of the granite porphyries in southern Qiangtang Terrane, central Tibet: New insights into the genesis of highly evolved granites. Lithos, 312: 258-273.

Yao, H., Zhang, R., Duan, Q., Sheng, X., Niu, Z., Wang, J., Zeng, B. and Wu, J., 2011. Jurassic rocks, bivalves, and depositional environments of the source area of the Yangtze River, Qinghai Province, western China. Science China Earth Sciences, 54(8): 1136-1148.

Ye, J., Hu, X. and Sun, G., 2019. The disappearance of the Late Cretaceous Bangong-Nujiang residual seaway constrained by youngest marine strata in Geji area, Lhasa Terrane. Chinese Science Bulletin, 64(15): 1620-1636.

Yi, Z., Huang, B., Yang, L., Tang, X., Yan, Y., Qiao, Q., Zhao, J. and Chen, L., 2015. A quasi-linear structure of the southern margin of Eurasia prior to the India-Asia collision: First paleomagnetic constraints from Upper Cretaceous volcanic rocks near the western syntaxis of Tibet. Tectonics, 34(7): 1431-1451.

Yin, A. and Harrison, T.M., 2000. Geologic evolution of the Himalayan-Tibetan orogen. Annual Review of Earth and Planetary Sciences, 28(1): 211-280.

Yin, J., 2005. Middle Jurassic (Bathonian–Callovian) ammonites from the Amdo area, Northern Tibet. Acta Palaeontologica Sinica, 44: 1-16.

Yin, J. and Chandler, R.B., 2016. Aalenian to Lower Bajocian ammonites from the Qiangtang block (North Tibet). Proceedings of the Geologists' Association, 127(2): 172-188.

Yu, G., Wang, C. and Zhang, S., 1991. The characteristic of Jurassic sedimentary basin of Bangong Co-Dêngqên fault belt in Xizang. Bull Chengdu Inst Geol MR, Chinese Acad Geol Sci, 13: 33-44. [in Chinese]

Yuan, D.-x., Zhang, Y.-c., Shen, S.-z., Henderson, C.M., Zhang, Y.-j., Zhu, T.-x., An, X.-y. and Feng, H.-z., 2016. Early Permian conodonts from the Xainza area, central Lhasa Block, Tibet, and their palaeobiogeographical and palaeoclimatic implications. Journal of Systematic Palaeontology, 14(5): 365-383.

Yuan, D.-X., Zhang, Y.-C., Zhang, Y.-J., Zhu, T.-X. and Shen, S.-Z., 2014. First records of Wuchiapingian (Late Permian) conodonts in the Xainza area, Lhasa Block, Tibet, and their palaeobiogeographic implications. Alcheringa: An Australasian Journal of Palaeontology, 38(4): 546-556.

Zeng, M., Zhang, X., Cao, H., Ettensohn, F.R., Cheng, W. and Lang, X., 2016a. Late Triassic initial subduction of the Bangong- Nujiang Ocean beneath Qiangtang revealed: stratigraphic and geochronological evidence from Gaize, Tibet. Basin Research, 28(1): 147-157.

Zeng, Q., Mao, G., Wang, B. and Nima, C., 2006. Geological report of the 1:250, 000 regional geological survey in Gaize area (in Chinese).

Zeng, Y.C., Chen, J.L., Xu, J.F., Wang, B.D. and Huang, F., 2016b. Sediment melting during subduction initiation: Geochronological and geochemical evidence from the Darutso high- Mg andesites within ophiolite mélange, central Tibet. Geochemistry, Geophysics, Geosystems, 17(12): 4859-4877.

Zeng, Y.C., Xu, J.F., Chen, J.L., Wang, B.D., Huang, F., Xia, X.P. and Li, M.J., 2021. Early Cretaceous (~ 138–134 Ma) Forearc Ophiolite and Tectonomagmatic Patterns in Central Tibet: Subduction Termination and Re- initiation of Meso- Tethys Ocean Caused by Collision of an Oceanic Plateau at the Continental Margin? Tectonics, 40(3): e2020TC006423.

Zeng, Y.-C., Xu, J.-F., Chen, J.-L., Wang, B.-D., Kang, Z.-Q. and Huang, F., 2018. Geochronological and geochemical constraints on the origin of the Yunzhug ophiolite in the Shiquanhe–Yunzhug–Namu Tso ophiolite belt, Lhasa Terrane, Tibetan Plateau. Lithos, 300: 250-260.

Zeng, Y.C., Xu, J.F., Ducea, M.N., Chen, J.L., Huang, F. and Zhang, L., 2019. Initial rifting of the Lhasa Terrane from Gondwana: Insights from the Permian (~ 262 Ma) amphibole- rich lithospheric mantle- derived Yawa basanitic intrusions in southern Tibet. Journal of Geophysical Research: Solid Earth, 124(3): 2564-2581.

Zhai, Q. and Li, C., 2007. Zircon SHRIMP Dating of Volcanic Rock from the Nadigangri Formation in Juhuashan, Qiangtang, Northern Tibet and Its Geological Significance. Acta Geologica Sinica, 81(6): 795-800.

Zhai, Q.G., Jahn, B.M., Su, L., Ernst, R.E., Wang, K.L., Zhang, R.Y., Wang, J. and Tang, S.H., 2013.

SHRIMP zircon U–Pb geochronology, geochemistry and Sr–Nd–Hf isotopic compositions of a mafic dyke swarm in the Qiangtang terrane, northern Tibet and geodynamic implications. Lithos, 174: 28-43.

Zhang, K.-J., Xia, B., Zhang, Y.X., Liu, W.L., Zeng, L., Li, J.F. and Xu, L.F., 2014a. Central Tibetan Meso-Tethyan oceanic plateau. Lithos, 210: 278-288.

Zhang, Q.-H., Ding, L., Cai, F.-L., Xu, X.-X., Zhang, L.-Y., Xu, Q. and Willems, H., 2011. Early Cretaceous Gangdese retroarc foreland basin evolution in the Selin Co basin, central Tibet: evidence from sedimentology and detrital zircon geochronology. Geological Society, London, Special Publications, 353(1): 27-44.

Zhang, X.R., Shi, R.D., Huang, Q.S., Liu, D.L., Gong, X.H., Chen, S.S., Wu, K., Yi, G.D., Sun, Y.L. and Ding, L., 2014b. Early Jurassic high-pressure metamorphism of the Amdo terrane, Tibet: Constraints from zircon U–Pb geochronology of mafic granulites. Gondwana Research, 26(3-4): 975-985.

Zhang, X.Z., Wang, Q., Dong, Y.S., Zhang, C., Li, Q.Y., Xia, X.P. and Xu, W., 2017a. High- pressure granulite facies overprinting during the exhumation of eclogites in the Bangong- Nujiang suture zone, central Tibet: Link to flat- slab subduction. Tectonics, 36(12): 2918-2935.

Zhang, Y.-c., Shi, G. and Shen, S.-z., 2013. A review of Permian stratigraphy, palaeobiogeography and palaeogeography of the Qinghai–Tibet Plateau. Gondwana Research, 24(1): 55-76.

Zhang, Y.-X., Li, Z.-W., Yang, W.-G., Zhu, L.-D., Jin, X., Zhou, X.-Y., Tao, G. and Zhang, K.-J., 2017b. Late Jurassic–Early Cretaceous episodic development of the Bangong Meso-Tethyan subduction: Evidence from elemental and Sr–Nd isotopic geochemistry of arc magmatic rocks, Gaize region, central Tibet, China. Journal of Asian Earth Sciences, 135: 212-242.

Zhang, Y.-X., Li, Z.-W., Zhu, L.-D., Zhang, K.-J., Yang, W.-G. and Jin, X., 2016. Newly discovered eclogites from the Bangong Meso–Tethyan suture zone (Gaize, central Tibet, western China): Mineralogy, geochemistry, geochronology, and tectonic implications. International Geology Review, 58(5): 574-587.

Zhang, Y., Zhang, Y., Yuan, D., Xu, H. and Qiao, F., 2019. Stratigraphic and paleontological constraints on the opening time of the Bangong-Nujiang Ocean. Acta Petrologica Sinica, 35(10): 3083-3096. [in Chinese with English abstract]

Zhang, Z., Dong, X., Liu, F., Lin, Y., Yan, R., He, Z. and Santosh, M., 2012. The making of Gondwana: discovery of 650 Ma HP granulites from the North Lhasa, Tibet. Precambrian Research, 212: 107-116.

Zheng, C., Wang, Y. and Zhang, S., 2005. The Carboniferous-Permian biostratigraphic division of Deriangmato-Xialashan of the Xainza area, northern Tibet. Journal of Stratigraphy, 29: 520-528. [in Chinese with English abstract]

Zheng, M., 2017. Geochemical Characteristics and Petrogenesis of Tarenben basalt in the middle segment of Bangongco-Nujiang suture zone. Master-degree thesis, China University of Geosciences (Beijing), Beijing. [in Chinese with English abstract]

Zheng, Y., He, J., Li, W., Zou, G. and Zhao, P., 2003. Geological report of the 1:250, 000 regional geological survey in Zigetangco area (in Chinese).

Zheng, Y., Xu, R., Wang, C. and Ma, G., 2007. The first discovery of Permian conodont fauna from peri-Gondwana cool water facies in Tibet, China. Chinese Science Bulletin, 52(9): 1231-1237.

Zhong, Y., Hu, X.-C., Liu, W.-L., Xia, B., Zhang, X., Huang, W., Fu, Y.-B. and Wang, Y.-G., 2018. Age and nature of the Jurassic–Early Cretaceous mafic and ultramafic rocks from the Yilashan area, Bangong–Nujiang suture zone, central Tibet: implications for petrogenesis and tectonic Evolution. International Geology Review, 60(10): 1244-1266.

Zhong, Y., Liu, W.-L., Xia, B., Liu, J.-N., Guan, Y., Yin, Z.-X. and Huang, Q.-T., 2017. Geochemistry and geochronology of the Mesozoic Lanong ophiolitic mélange, northern Tibet: Implications for petrogenesis and tectonic evolution. Lithos, 292: 111-131.

Zhou, M.-F., Malpas, J., Robinson, P.T. and Reynolds, P.H., 1997. The dynamothermal aureole of the Donqiao ophiolite (northern Tibet). Canadian Journal of Earth Sciences, 34(1): 59-65.

Zhou, Y., Cheng, X., Wu, Y., Kravchinsky, V., Shao, R., Zhang, W., Wei, B., Zhang, R., Lu, F. and Wu, H., 2019. The northern Qiangtang Block rapid drift during the Triassic Period: Paleomagnetic evidence. Geoscience Frontiers, 10(6): 2313-2327.

Zhou, Y., Cheng, X., Yu, L., Yang, X., Su, H., Peng, X., Xue, Y., Li, Y., Ye, Y., Zhang, J., Li, Y. and Wu, H., 2016. Paleomagnetic study on the Triassic rocks from the Lhasa Terrane, Tibet, and its paleogeographic implications. Journal of Asian Earth Sciences, 121: 108-119.

Zhu, D.-C., Li, S.-M., Cawood, P.A., Wang, Q., Zhao, Z.-D., Liu, S.-A. and Wang, L.-Q., 2016. Assembly of the Lhasa and Qiangtang terranes in central Tibet by divergent double subduction. Lithos, 245: 7-17.

Zhu, D.-C., Pan, G., Mo, X., Wang, L., Zhao, Z., Liao, Z., Geng, Q. and Dong, G., 2006. Identification for the Mesozoic OIB-type basalts in central Qinghai-Tibetan Plateau: Geochronology, geochemistry and their tectonic setting. Acta Geologica Sinica, 80(9): 1312-1328. [in Chinese with English abstract]

Zhu, D.-C., Wang, Q., Chung, S.-L., Cawood, P.A. and Zhao, Z.-D., 2019a. Gangdese magmatism in southern Tibet and India–Asia convergence since 120 Ma. Geological Society, London, Special Publications, 483: 583-604.

Zhu, D.-C., Zhao, Z.D., Niu, Y., Dilek, Y. and Mo, X.X., 2011. Lhasa terrane in southern Tibet came from Australia. Geology, 39(8): 727-730.

Zhu, D.C., Zhao, Z.D., Niu, Y.L., Dilek, Y., Hou, Z.Q. and Mo, X.X., 2013. The origin and pre-Cenozoic evolution of the Tibetan Plateau. Gondwana Research, 23(4): 1429-1454.

Zhu, M., 2016. The characteristics of Qushenla group's volcanic rocks and tectonic significance in Zanzongcuo, Shuanghu county, Tibet. Master-degree thesis, China University of Geosciences (Beijing). [in Chinese with English abstract]

Zhu, T., Dong, H., Shi, W., Li, H. and Ou, C., 2005. Geological report of the 1:250, 000 regional geological survey in Tuco area (in Chinese). pp.300.

Zhu, Z., Zhai, Q., Hu, P., Chung, S., Tang, Y., Wang, H., Wu, H., Wang, W., Huang, Z. and Lee, H., 2019b. Closure of the Bangong–Nujiang Tethyan Ocean in the central Tibet: Results from the provenance of the Duoni Formation. Journal of Sedimentary Research, 89(10): 1039-1054.

Figure captions

Fig. 1 (a) Simplified geological map of the Bangong-Nujiang suture zone (revised from Pan et al., 2004). (b) Spatio-temporal distribution of magmatic rocks within and adjacent to the Bangong-Nujiang suture zone (modified from Zhu et al., 2016). Data sources provided in Supplementary Table S3. SNMZ = Shiquan River-Nam Tso Mélange Zone, NL= North Lhasa; CL = Central

Lhasa; SQ = South Qiangtang; BNS = Bangong-Nujiang suture zone; JSZ=Jingsha suture zone.

Fig. 2 Simplified geological map of the Nima-Nagqu area in the Bangong-Nujiang suture zone (modified from Chen et al., 2002; Qu et al., 2003; Zheng et al., 2003; Bai et al., 2005; Nima et al., 2005; Wang et al., 2006).

Fig. 3 Simplified geological map of the Gaize-Dongcuo area in the Bangong-Nujiang suture zone (modified from Zeng et al., 2006).

Fig. 4 Integrated stratigraphic framework of South Qiangtang, Bangong-Nujiang suture zone, and North Lhasa.

Fig. 5 Kernel density estimation (a, c) and MDS plots (b, d) based on age spectra of detrital zircons from Triassic to Jurassic strata in the Nima-Nagqu and Rutog-Gaize areas, Bangong-Nujiang suture zone, North Lhasa, and South Qiangtang.

Fig. 6 Petrographic composition of Mesozoic lithostratigraphic units in South Qiangtang, Bangong-Nujiang suture zone, and North Lhasa. The Rutog-Gaize and Nima-Nagqu areas (western and central segments of the BNS, respectively) are distinguished. Q = quartz; F= feldspars; L= lithic fragments (Lm = metamorphic; Lv = volcanic; Ls = sedimentary); parameters after Ingersoll et al. (1984) and compositional fields in the QFL plot after Garzanti (2019).

Fig. 7 Histograms of ophiolite ages in the Bangong-Nujiang suture zone (data sources provided in Supplementary Table S4). P_3 = Late Permian; T_1 = Early Triassic, T_2 = Middle Triassic, T_3 = Late Triassic, J_1 = Early Jurassic, J_2 = Middle Jurassic, J_3 = Late Jurassic, K_1 = Early Cretaceous.

Fig. 8 Histograms of the ages of Jurassic-Cretaceous magmatic rocks in South Qiangtang, Bangong-Nujiang suture zone, and North Lhasa. Data sources provided in Supplementary Table S3.

Fig. 9 Paleolatitude *versus* time plot for the South Qiangtang and Lhasa Block during the Permian to the Cretaceous: (a) Nima-Nagqu central segment of the BNS; (b) Rutog-Gaize western segment of the BNS). Data sources provided in Supplementary Table S5. P_1 = Early Permian, P_2 = Middle Permian, P_3 = Late Permian; T_1 = Early Triassic, T_2 = Middle Triassic, T_3 = Late Triassic, J_1 = Early Jurassic, J_2 = Middle Jurassic, J_3 = Late Jurassic, K_1 = Early Cretaceous, K_2 = Late Cretaceous.

Fig. 10 Summary chart indicating timing of magmatism, metamorphism, oceanic subduction, deep-marine sedimentation, formation of oceanic crust, key biota, stratigraphy, and paleomagnetic data for South Qiangtang, Bangong-Nujiang suture zone, and North Lhasa.

Fig. 11 Distribution of Jurassic detrital-zircon ages in the Mugagangri Complex and Sewa Formation of South Qiangtang. Data sources provided in Supplementary Table S2.

Fig. 12 Envisaged palaeogeographic evolution of the Bangong-Nujiang oceanic realm and inferred positions of microcontinents. AM = Amdo microcontinent, DKC = Dongkacuo microcontinent, SQ = South Qiangtang, NQ = North Qiangtang, LSSZ= Longmucuo-Shuanghu suture zone; JSZ=Jingsha suture zone.

Fig. 13 Cross-sections depicting the envisaged tectonic evolution of the Bangong-Nujiang Ocean from the Dongqiao to the Beila areas. DQ = Dongqiao, DKC = Dongkacuo microcontinent, QT = Qiangtang, LS = Lhasa.

Table 1 Stratigraphic units of South Qiangtang, Bangong-Nujiang suture zone, and North Lhasa considered for provenance analysis, including information on youngest detrital-zircon ages and data sources.

Supplementary Data

Table S1 Summary of petrographic data (point-counting according to the Gazzi-Dickinson method; Ingersoll et al., 1984) from sandstones in South Qiangtang, Bangong-Nujiang suture zone, and North Lhasa.

Table S2 Summary of detrital-zircon ages from sandstones in South Qiangtang, Bangong-Nujiang suture zone, and North Lhasa.

Table S3 Summary of geochronological data from magmatic rocks of South Qiangtang, Bangong-Nujiang suture zone, and North Lhasa.

Table S4 Summary of U-Pb zircon-age data from ophiolitic rocks in the Bangong-Nujiang suture zone.

Table S5 Summary of Ar-Ar/K-Ar age data from ophiolitic rocks in the Bangong-Nujiang suture zone.

Table S6 Permian-Cretaceous paleomagnetic data from the South Qiangtang and Lhasa blocks.